FEMTOSECOND LASER ASSISTED SYNTHESIS OF SILICATE-1 ZEOLITE

A THESIS SUBMITTED TO
THE GRADUATE SCHOOL OF ENGINEERING AND SCIENCE
OF BILKENT UNIVERSITY
IN PARTIAL FULFILLMENT OF THE REQUIREMENTS FOR
THE DEGREE OF
MASTER OF SCIENCE
IN
MATERIAL SCIENCE AND NANOTECHNOLOGY

BY

MEHDI HAGVERDIYEV

January 2022

FEMTOSECOND LASER ASSISTED SYNTHESIS OF SILICALITE-1 ZEOLITE

by Mehdi Hagverdiyev

January 2022

We certify that we have read the thesis and that in our opinion it is fully adequate, in scope and quality, as a thesis for the degree of Master of Science.

_____

Serim Kayacan İlday (Advisor)

_____

Sezin Galioğlu Özaltuğ (Co-Advisor)

_____

Burcu Akata Kurç

_____

Talip Serkan Kasırga

Approved for the Graduate School of Engineering and Science:

_____

Ezhan KARAŞAN

Director of the Graduate School

ABSTRACT

FEMTOSECOND LASER ASSISTED SYNTHESIS OF SILICALITE-1 ZEOLITE

Hagverdiyev, Mehdi
M.S. in Material Science and Nanotechnology Department
Supervisor: Asst. Prof. Dr. Serim Kayacan İlday
Co-advisor: Dr. Sezin Galioğlu Özaltuğ
January 2022,

Zeolites are microporous (pore sizes < 2 nm) inorganic aluminosilicate materials with well-defined molecular pores and high surface areas used widely for various chemical processes, primarily as catalysts, sorbents, and ion exchangers. Aside from 40 types of natural zeolite, 253 different synthetic zeolitic framework types are synthesized and recognized by the International Zeolite Association (IZA). Zeolite synthesis requires moderate temperatures between 50°C - 270°C and high pressures (up to 120 bar). A fundamental challenge in zeolite synthesis is to elucidate and control the nucleation and growth of the zeolite crystals. The main reason for this is the fast kinetics of zeolite synthesis and rapid conformational transitions between quasi-equilibrium phases. Zeolite synthesis is a complex process because more than 40 different types of silica polymerization and depolymerization reactions occur simultaneously in a reaction mixture (i.e., precursor suspension). Reaction time scales of the silica polymerization are within the range of picoseconds and femtoseconds. Using the traditional hydrothermal synthesis method, which is occurring near thermal equilibrium, it is impossible to control the system at the time scale of these simultaneous polymerization

reactions due to the slow energy deposition, which can be from 24 hours to several days. Other types of zeolite synthesis methods such as microwave synthesis are capable of depositing high energies in short time scales. However, the synthesis method is lacking the control of the excess heating of the full volume of the precursor suspension. During microwave heating, several hot spots form inside the precursor suspension, causing the boiling of the liquid. Growth by inhomogeneous heating leads to the formation of fused (i.e., interconnect) crystals instead of the discrete ones that dominate the end product in microwave-assisted synthesis method of zeolites.

Here, we introduce a novel femtosecond laser-assisted synthesis method for the synthesis of Silicalite-1 zeolites. Femtosecond laser pulses ensure the delivery of a precise amount of energy per area within a given time interval, and therefore the spatiotemporal control over the energy delivered to the precursor suspension could be done on the time scale of the polymerization reactions of the zeolite synthesis. Thanks to the femtosecond laser pulses, the appropriate environment for zeolite synthesis, such as local high temperature and local high pressure (shock waves), has been created. In the laser-assisted synthesis method, the time required for zeolite synthesis decreased drastically compared to the hydrothermal method, overall control and product quality increased compared to the microwave synthesis method of zeolites. Unlike other rapid synthesis methods such as microwave synthesis, the uncontrollable temperature rise over the full volume of precursor suspension was not observed, resulting in 'discrete' crystals in the final product. Energy intake of the transparent precursor suspension was achieved through multiphoton absorption of the femtosecond laser pulses inducing steep spatiotemporal thermal gradients. Since surface tension of fluid is a function of temperature, surface tension gradients form as well, causing Marangoni flow. The

‘stirring effect’ of these flows leads to the distribution of the formed clusters evenly to the system, which is not attained by static hydrothermal synthesis of zeolites. It is proposed that vigorous flow induced in the laser-assisted synthesis assembles nuclei/polymerized clusters much faster than the other synthesis methods, which may be the reason for the drastically reduced reaction times compared to hydrothermal synthesis (i.e., 30 - 48h for hydrothermal vs. 3h - 5h for laser-assisted syntheses). Growth kinetics of the Silicalite-1 zeolite was examined in detail. In addition, template-free nanosized microporous Zeolite Y, and mesoporogen-free hierarchical ZSM-5 zeolites with micro and meso-porosity were synthesized with reduced reaction times through laser-assisted synthesis method (i.e., 24 - 45h for hydrothermal vs. 1 - 5h for laser-assisted syntheses), which is important in terms of green synthesis approaches drawing attention in recent years.

Keywords: Zeolite, silicalite-1, nucleation, growth kinetic, femtosecond laser, green synthesis

ÖZ

SILICALITE-1 ZEOLİTİNİN FEMTOSANİYE LAZER DESTEKLİ SENTEZİ

Hagverdiyev, Mehdi

Yüksek Lisans, Malzeme Bilimi ve Nanoteknoloji Bölümü

Tez Yöneticisi: Asst. Prof. Dr. Serim Kayacan İlday

Yardımcı Danışman: Dr. Sezin Galioğlu Özaltuğ

Ocak 2022,

Zeolitler, periyodik moleküler gözeneklere ve yüksek yüzey alanlarına sahip mikro gözenekli (gözenek boyutları < 2 nm) inorganik alüminosilikat malzemelerdir ve katalizör, sorbent ve iyon değiştirici olarak çeşitli kimyasal işlemler için yaygın olarak kullanılır. 40 çeşit doğal zeolit dışında, 253 farklı sentetik zeolit kafes türü sentezlenmiş ve Uluslararası Zeolit Birliği (IZA) tarafından tanınmıştır. Zeolit sentezi, 50 °C - 270 °C gibi orta dereceli sıcaklıklar ve yüksek basınçlar gerektirir (120 bar'a kadar). Zeolit sentezindeki temel bir zorluk, zeolit kristallerinin çekirdeklenmesini ve büyümesini aydınlatmak ve kontrol etmektir. Bunun ana nedeni, zeolit sentezinin hızlı kinetiği ve yarı denge fazlar arasındaki hızlı konformasyonel geçişlerdir. Zeolit sentezi karmaşık bir sentezdir çünkü bir reaksiyon karışımında (yani öncü süspansiyon) 40'tan fazla farklı tipte silika polimerizasyon ve depolimerizasyon reaksiyonları aynı anda gerçekleşir. Silika polimerizasyon reaksiyonlarının reaksiyon süresi ölçekleri, pikosaniye ve femtosaniye aralığındadır. Termal dengeye yakın geleneksel hidrotermal sentez yönteminde, 24 saatten birkaç güne kadar olabilen yavaş enerji birikimi nedeniyle, bu eşzamanlı polimerizasyon reaksiyonlarının zaman skalasında bir kontrol

sağlayabilmek imkansızdır. Mikrodalga sentezi gibi diğer zeolit sentez yöntemleri, kısa zaman ölçeklerinde yüksek enerjileri biriktirme özelliğine sahiptir. Bununla birlikte, sentez yöntemi, öncü süspansiyonun aşırı ısınmasını kontrol etmede yetersizdir, çünkü mikrodalga ısıtma sırasında öncü süspansiyonun içinde sıvının kaynamasına neden olan çok fazla sayıda sıcak noktalar oluşur. Kontrol edilemeyen ısınma ile büyüme, son üründe baskın olan ayrı kristaller yerine kaynaşmış (yani birbirine bağlı) kristallerin oluşmasına yol açar.

Burada, Silicalite-1 zeolitinin sentezi için yeni bir femtosaniye lazer destekli sentez yöntemini tanıtıyoruz. Femtosaniye lazer darbeleri, belli bir zaman aralığı içinde alan başına kesin miktarda enerji verilmesini garanti eder ve bu sebeple, öncü süspansiyona gönderilen enerjinin kontrolü, zeolit sentezinin polimerizasyon reaksiyonlarının zaman ölçeğinde yapılabilmiştir. Femtosaniye lazer darbeleri sayesinde, zeolit sentezi için gerekli olan, yerel yüksek sıcaklık ve yerel yüksek basınç (şok dalgaları) gibi uygun ortam oluşturulmuştur. Mikrodalga sentezi gibi diğer hızlı sentez yöntemlerinin aksine, kontrol edilemeyen küresel sıcaklık artışı gözlemlenmemiştir, bu da, son üründe 'ayrık' kristallere yol açmıştır. Şeffaf öncü süspansiyonun enerji alımı, keskin uzaysal-zamansal termal gradyanları indükleyen femtosaniye lazer darbelerinin multifoton absorpsiyonu yoluyla sağlandı. Bir akışkanın yüzey gerilimi sıcaklığın bir fonksiyonu olduğundan, yüzey gerilimi gradyanları da oluşur ve bu da Marangoni akışına neden olur. Zeolitlerin statik hidrotermal sentezi ile elde edilmeyen indüklenmiş Marangoni akışı ile "karıştırma etkisi" elde edildi. Lazer destekli sentezde indüklenen kuvvetli Marangoni akışının, diğer sentez yöntemlerinden çok daha hızlı çekirdek/polimerize kümeler oluşturduğu ileri sürülmektedir; bu, hidrotermal senteze kıyasla büyük ölçüde azaltılmış reaksiyon sürelerinin nedeni olabilir (yani 30 - 48 saat hidrotermal sentez

sürelerine kıyasla, 3 - 5 saatlik lazer destekli sentezler). Tez kapsamında, Silicalite-1 zeolitinin büyüme kinetiği detaylı olarak incelenmiştir. Ek olarak, şablonsuz nano boyutlu mikro gözenekli Zeolit Y ve mikro ve mezo gözenekli mezoprojen içermeyen hiyerarşik ZSM-5 zeolitleri, lazer destekli sentez yöntemiyle az reaksiyon sürelerinde sentezlendi (yani 24 – 45 saatlik hidrotermal sentez sürelerine kıyasla, 1 - 5 saatlik lazer destekli sentezler), bu da, son yıllarda dikkat çeken yeşil sentez yaklaşımları açısından önem arz etmektedir.

Anahtar Kelimeler: Zeolit, silicalite-1, çekirdeklenme, büyüme kinetiği, femtosaniye lazer, yeşil sentez.

ACKNOWLEDGEMENTS

I would first like to thank my supervisor, Prof. Serim Kayacan İlday, who has been very kind, frank, and supportive of me as a supervisor. I have received a great deal of support from her throughout this project and she has been a perfect example for an ideal mentor.

I am grateful to my labmate and friend, co-advisor of this work, Dr. Sezin Galioğlu Özaltuğ for her endless supports both through the project and daily life. Her guidance and thoughts made the current progress possible.

I would also like to thank to Meryem Doğan, an undergraduate student of Bilkent University, junior member of our lab and great supporter of our research. Her interest and participation in this project enhanced our overall performance.

Special thanks go to lovely members of Simply Complex Lab, Dr. Esin Demir, Dr. Michael Barbier, and Seleme Nizam, they made the time spent in the lab and office more fun and exceptional. I was fortunate to work alongside them.

I want to thank all members of UFOLAB, especially Prof. Fatih Ömer İlday, Özgün Yavuz, Aladin Choura, Mesut Laçin, Dr. Ghaith Makey, Dr. Paul Repgen, and a former member, Dr. Parviz Elahi, for their technical support throughout my research.

Finally, I must express my very profound gratitude to my both families, the biological and the chosen one, my parents and my friends, for their endless encouragement and continuous support throughout the process of researching and writing this thesis. This accomplishment would not have been possible without them. Thank you.

TABLE OF CONTENTS

LIST OF TABLES

LIST OF FIGURES

LIST OF ABBREVIATIONS

ATR-FTIR	Attenuated Total Reflectance Fourier Transform Infrared Spectroscopy
BET	Brunauer - Emmett - Teller
EDX	Energy Dispersive X-ray Spectroscopy
HR-TEM	High-Resolution Transmission Electron Microscopy
IZA	International Zeolite Association
MFI	Mobil type-five
TEM	Transmission Electron Microscopy
TEOS	Tetraethyl orthosilicate
TPA	Tetra propyl ammonium hydroxide
SDA	Structure directing agent
SEM	Scanning Electron Microscopy
XRD	X-ray Diffraction Spectroscopy

CHAPTERS

CHAPTER 1

INTRODUCTION

Having a framework structure, zeolites are microporous (with pore sizes < 2 nm) crystalline alumina silicates. Their polyanionic networks are made up of SiO_4 and/or AlO_4 tetrahedra, interconnected through shared oxygen atoms. The empirical formula to denote zeolites is as follows.

$$M_x^{n+} \quad [(Al_2O_3)_x(SiO_2)_y] \quad \cdot \quad zH_2O,$$

where *M* is an exchangeable extra-framework cation with *n* valency, aluminum and silicon oxides constitute the framework, and water represents the adsorbed phase.[1,2] When tetrahedral components combine, this results in the generation of various secondary building units (SBUs), also called ring structures, for which some examples are given in Figure 1.

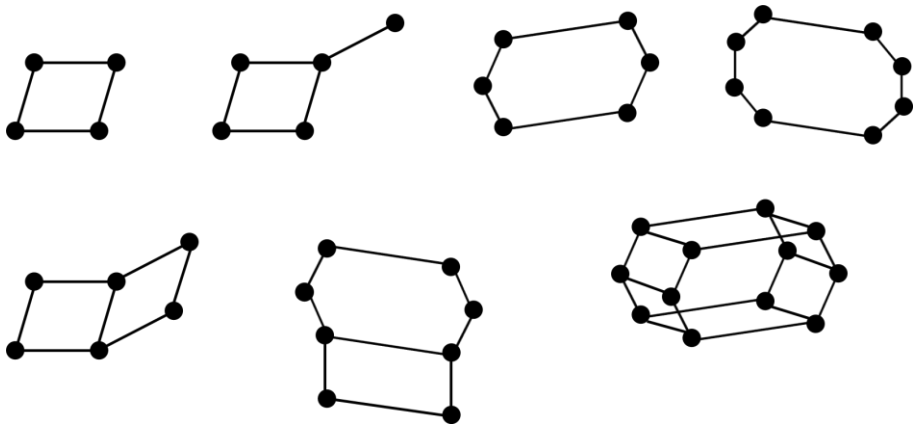

Figure 1. Examples to secondary building units (SBUs). The dots represent silicon or aluminum atoms.

Various framework types are formed depending on the number and type of these SBUs that self-assemble to form so-called cage structures. As described in Figure 2, the self-assembly of unit cells features regular channels or interconnected voids. These holes are in micropore range and capable of capturing molecules and ions, bringing selective catalysis capability to zeolites.[1–3]

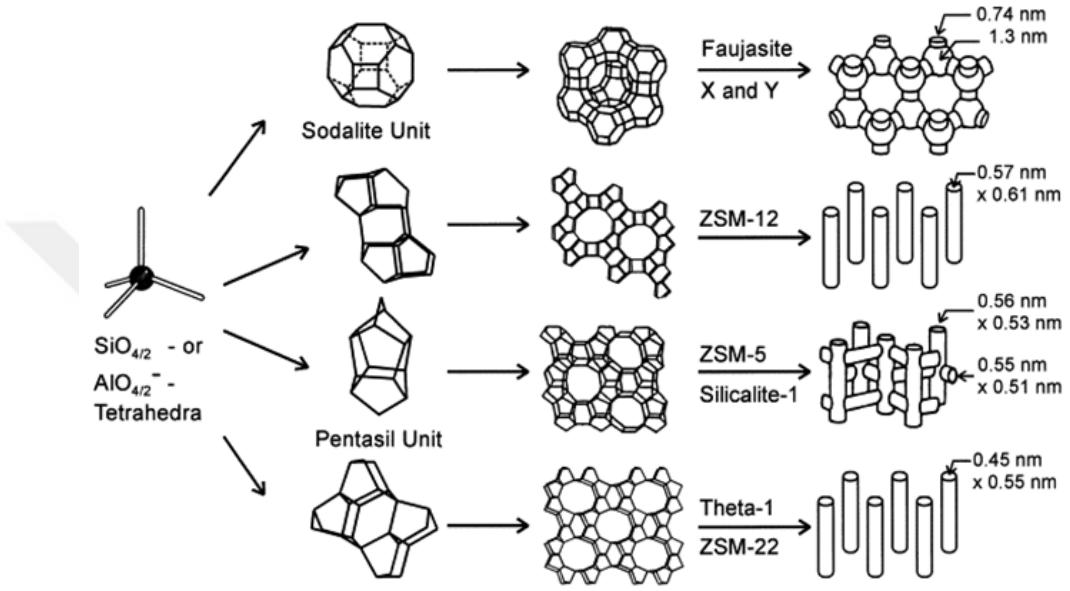

Figure 2. Examples of different cage structures forming unit cells of different zeolites. Adapted from reference [4].

Naturally formed zeolites can generally be found next to volcanic regions. They can also be synthesized in laboratories. A tremendous amount of effort has been put into synthesizing different zeolitic structures, and by now, 253 different zeolitic frameworks have been synthesized and recognized by the International Zeolite Association (IZA).[5] Synthesis processes for zeolites have been optimized for decades. It is well-known that each step of the synthesis procedure has a considerably significant impact on the characteristics and type of the final framework structure. In general, the entire process may not seem so complicated to manage, yet, the output functionalities and even the product itself can be affected readily by even minor variations in the

synthesis parameters. The first factor impacting the synthesis of zeolites is the content of the precursor suspension mixture. For instance, a higher ratio of SiO_2/Al_2O_3 enhances the thermal stability of the structure while the number of hydrophobic sites also increases.[1,2] The following major factors can be listed as the homogeneity of the gel, source of the materials, pH of the system both at the beginning and at the end of thermal treatment, crystallization temperature, and finally, the template molecules.

Numerous methods have been established for decades since the first achievements on laboratory synthesis of zeolites in Linde Company in 1950.[5] Still, among those, hydrothermal, microwave-assisted, ultrasonic-assisted, Ionothermal, and continuous flow synthesis are the most commonly used ones.[1,2] The reason to have so many synthesis methods for zeolites is coming from various disadvantages of synthesis procedures and product qualities. The benefits and drawbacks of these traditional synthesis methods have been discussed in detail in the next chapter. One of the most issued topics in the literature is nanosized (~100 nm) zeolitic particles with synthesis yield and crystallinity degrees comparable to those of micron-sized zeolitic particles.[6–9] Significantly increased external surface area and shortened diffusion lengths due to smaller particle sizes bring nanosized zeolite synthesis into focus. However, current challenges in front of the traditional methods are designing ways to produce smaller particle sizes that are more efficient in terms of high synthesis yield, high particle crystallinity, and controlling kinetics of zeolite crystallization reactions to understand the mechanism behind the nucleation stage.[8,9]

The laser-assisted synthesis method of zeolites, which is developed in the scope of this project, substantially decreased reaction time while producing zeolite crystals with similar properties compared to conventional methods. The thesis outline is as follows: Chapter 2 first presents the conventional zeolite synthesis methods, discusses

the challenges and characteristic drawbacks of these methods and suggests ultrafast laser-assisted synthesis as a state-of-art synthesis mechanism that could overcome those challenges. Sample preparation steps, the experimental setup, and the necessary calculations to complete the synthesis procedure are described in Chapter 3. Chapter 4 introduces the zeolites synthesized by laser-assisted method and investigates this pathway to gain insight into possible reaction kinetics. The quality of obtained crystalline zeolite powder is also analyzed with conventional characterization techniques and compared to those synthesized via the hydrothermal synthesis method. Chapter 5 summarizes highlights of the synthesis procedure and characterization of obtained zeolite products and discusses the potential scientific and future impacts of the work done in this thesis on industrial applications.

CHAPTER 2

BACKGROUND

The porous structure of zeolites allows them to be used in crucial sectors of the industry. Three-dimensional micropores make zeolites an ideal material for ion exchangers, heterogeneous catalysts, absorbers, mainly in oil refinement and water treatment facilities.[6,10–13] Global catalysis market is estimated to be around 35 billion USD as of 2021, while the value created by industrial catalytic processes is to be multi-trillion USD.[14,15] Zeolites are a crucial part of the heterogeneous catalysis industry mostly due to their molecular size micropores (< 2 nm). Natural zeolites are found mainly in lands rich in volcanic activities. First in the 19th century and starting from the previous century, extensive efforts have been spent on synthetic zeolites.[7] The general synthesis pathway of a zeolite is composed of the following stages: preparation of the chemicals, thermal treatment of the precursor solution, and calcination of the obtained product post-synthesis to get rid of the SDAs, if there is any. Currently, International Zeolite Association (IZA) has recognized 253 different zeolite frameworks that are synthesized in the labs. However, computational studies claim over five million possible zeolitic structures indicating current synthesis methods are insufficient to synthesize these new hypothetical zeolitic structures.[5,16] The main requirement for this is to control and understand the nucleation step of the crystal growth process. Continuous research efforts have been put into solving these problems to understand key dynamics of zeolite formation and engineer new hypothetical zeolitic structures.

According to the IUPAC classification, zeolite pore sizes are in the range of 0.3 to 2 nm. These pores allow zeolites to be the best candidates for various industrial

applications. A fundamental question is how do these pores form? To answer this question, we need to understand the self-assembly of basic units into “bridges,” “rings,” and “cages.” In most of the definitions, we see inorganic tetrahedrons merge and form zeolitic structures. Tetrahedrons are either silicon or aluminum-based molecules as shown in the TO_4 form.

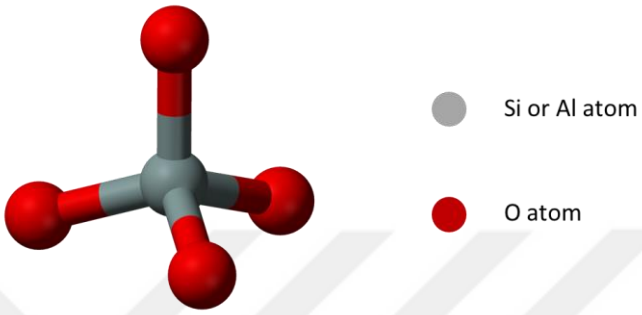

Figure 3. Schematic representation of a tetrahedron molecule; grey color indicates either a silicon or an aluminum atom, red color indicates the oxygen atoms.

Two of these tetrahedrons come together by sharing single oxygen, making a “bridge” structure. This is the most straightforward step in the silica oligomerization process. The silica oligomerization is considered as the basic set of reactions for all zeolitic materials.[17] Primary tetrahedron units start forming secondary units previously mentioned as “rings,” followed by forming “cages” by self-assembling rings. A schematic representation of this process for Mobil-type 5 (MFI) zeolites is provided in Figure 4. Zeolites are classified into different families according to the similarities in their cage structures and their self-assembly into the 3D bulk crystals.

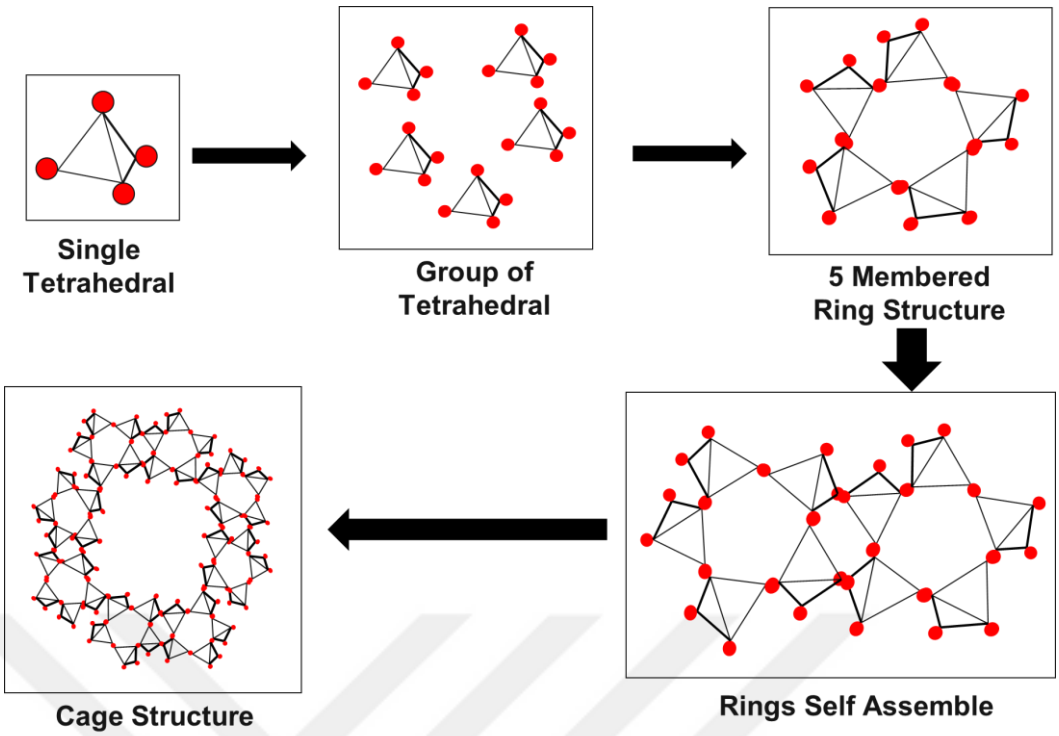

Figure 4. Schematic representation of MFI type zeolite self-assembly from primary tetrahedral units. From a group of tetrahedral units, 5-membered ring structures form. The self-assembly of these rings leads to the formation of zeolite cages. Red dots represent oxygen atoms.

Structure directing agents (SDA) have a considerable role in the formation of the final zeolitic framework. In the case of TPA-Silicalite-1 zeolite, TPA^+ ions act as SDA, and 10-membered rings form around this molecule. The structure is shown in Figure 5.

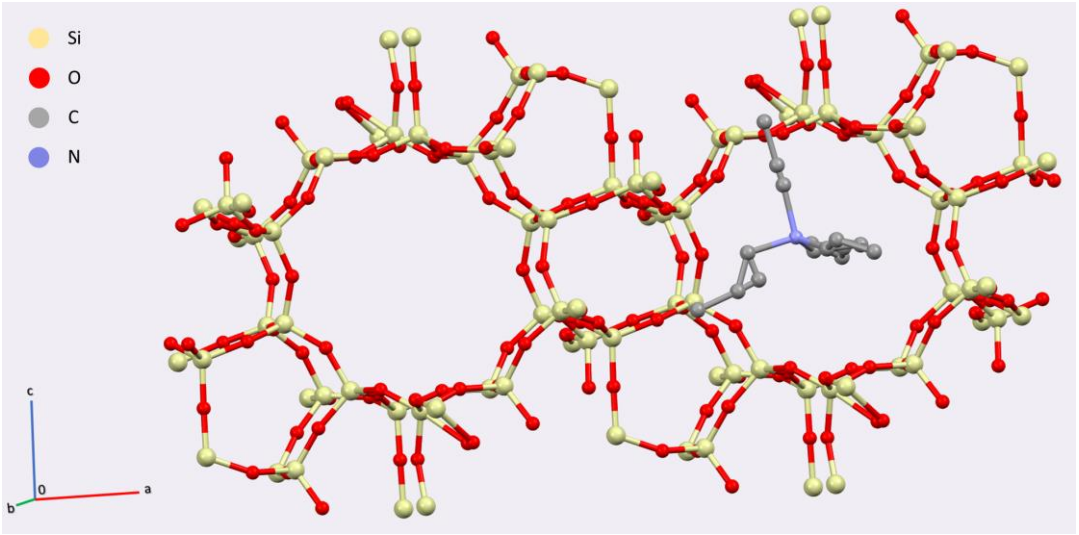

Figure 5. Schematic representation of TPA – Silicalite-1 framework. Yellow and red dots represent Silicon and Oxygen atoms, respectively. TPA is represented by Nitrogen (purple) and Carbon (grey) atoms and is surrounded by 10-membered rings of Silicalite-1 structure.

The silicate oligomerization process is composed of around 40 simultaneous reactions, each with different kinetics.[17] One parameter change may lead to considerable alterations of reaction rates and directions, followed by a concentration change of different oligomers, and finally, the synthesis process. Therefore, the source materials of the base chemicals, their ratio in the precursor suspension, pH of the solution, its mixing rate, mixing order, and the average medium temperature, each are key parameters affecting the synthesis.

To determine the direct or indirect impacts of a single parameter on the entire synthesis mechanism and the quality of the final product is crucial. Nowadays, nanosized zeolite synthesis draws attention because numerous advantages are introduced by smaller crystal sizes, such as increased surface area and shortened diffusion lengths.[9,18,19] The challenges of synthesizing zeolites at the nanoscale are as follows: *(i)* product quality in terms of crystallinity should be sustained while the size

of a single crystal gets smaller, *(ii)* yield of the synthesis needs to be comparable to those of micron-sized zeolites. A high degree of crystallinity ensures the sustenance of crucial characteristics of zeolitic materials such as thermal stability, chemical resistance, and mechanical stability. These factors make the already complicated synthesis procedure even more complex. Several zeolite synthesis mechanisms were developed to address these challenges, but different methods bring their problems in synthesis stages or to product quality.

2.1 Applications of Zeolites

In various fields of industry, mostly in oil refinement, wastewater treatment, and applications involving separation processes, zeolites are heavily employed due to their immense chemical and physical properties such as selectivity, porosity etc.[14,20–22] Global catalysis market is estimated to be around 35 billion USD as of 2021, while the value created by industrial catalytic processes is to be multi-trillion USD.[14,15] Zeolites are a crucial part of the heterogeneous catalysis industry mostly due to their molecular size micropores (< 2 nm), for this reason, they are called "molecular sieves". These pores bring zeolites their most important feature, the shape and size selectivity. The ability to interact with a specific molecule according to its size and shape makes them unique actors of oil refinement and useful for many industrial applications requiring heterogeneous catalysis. In addition to their porous nature, zeolites have high thermal resistance due to their siliceous nature up to 1000 K and higher temperatures.[14,20] Thermal resistivity is a major problem for most of the catalysts and zeolites are the best candidates for high-temperature processes. Higher Si/Al ratio of zeolite framework means higher thermal stability [1,2]As this ratio decreases, thermal resistance also

declines since siliceous matrix enhance thermal stability. However, Al atoms within the framework bring the additional features. To balance the negative charge introduced by Al atoms, positively charged Na^+ and K^+ ions act as extra framework cations which can be exchanged with negatively charged Ag, Pt ions.[23,24] Therefore, zeolites are widely used as ion-exchangers as well.[23,24]

Gas adsorption on a solid surface is a vital process for separation and catalysis purposes. Zeolites have active sites within their porous channels that can adsorb industrially and environmentally important gases such as hydrogen, methane, carbon dioxide, etc.[25,26] As particle sizes decrease, the available surface area for adsorption increases. For this reason, immense research efforts have been put into nanosized zeolite synthesis recently.[7–9,27] Another way to increase the available surface area and hence the adsorption capacity of zeolites is to introduce meso- (2 nm < pore < 50 nm) and macropores (50 nm < pore) to the structure. Zeolites with at least two types of pores (micro, meso, and macro) are called hierarchical zeolites. These types of zeolites have shown significant selectivity towards several industrially crucial gases. However, a general challenge is that the adsorbents with excellent selectivity (like zeolites) might often have poor adsorption efficiency when the size of the guest molecule is bigger than the sizes of the zeolite pores. One solution offered to this problem is forming hierarchical zeolites. The design of hierarchical zeolites and proper synthesis methods to obtain them is a challenging but economically worthy method considering the potential of application-specific design of pore sizes.

The increasing energy demand of the planet with arising human population and rapid industrialization of production facilities to compensate for high production demand already started to damage multiple vital sources of the earth. Global temperature is on an upward trend which is alarming us on current energy consumption.

On this basis, green synthesis methods are on serious concern also for zeolites. The use of organic SDAs makes synthesis easier. However, afterward separation of these agents from the mother zeolite framework requires calcination at high temperatures and they increase production costs. Moreover, calcination of organic templates causes a variety of greenhouse gas emissions directly to the atmosphere.[28,29] In summary, while designing new synthesis pathways and application-specific zeolites, as the research community we need to consider energy consumption and relevant pollution to minimize current and future potential hazards of these to our planet. [30]

2.2 Conventional Zeolite Synthesis Techniques

Thermal treatment of a precursor gel or suspension in a closed reactor is called conventional hydrothermal zeolite synthesis.[27] Primarily studied aspects of the hydrothermal method are crystallization time and temperature, source chemicals of T atoms, and type of SDAs.[28,31,32] The hydrothermal method dominates all other conventional synthesis mechanisms since it yields relatively high-quality products. In this method, precursor colloidal suspension or gel is subjected to convective thermal treatment. Heat is transferred to the colloidal suspension or gel through the air or other liquid medium. Mainly, ovens are used for this purpose. The process scheme for the hydrothermal synthesis of a TPA – Silicalite-1 zeolite is described in Figure 6.

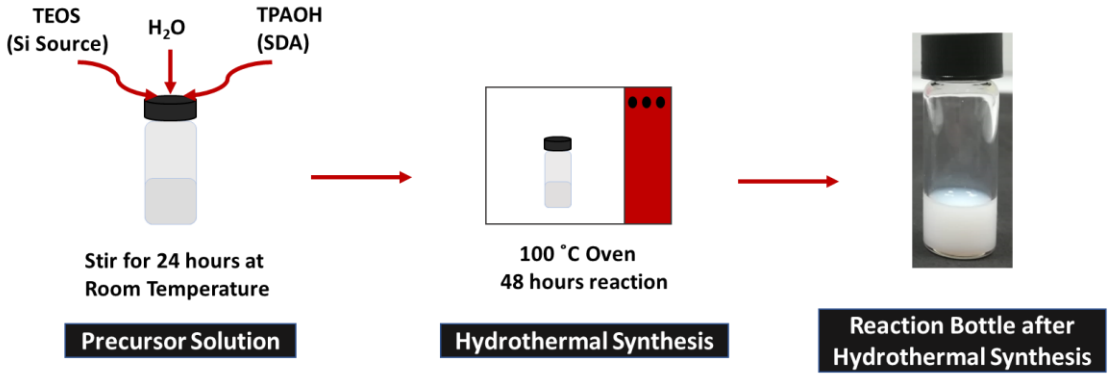

Figure 6. Synthesis steps of TPA – silicalite-1 zeolite with hydrothermal method; source chemicals were mixed at room temperature for 24 hours-aging; precursor solution was put into an oven at 100 °C for 48 hours; at the end of hydrothermal synthesis, transparent precursor suspension was turned to white opaque zeolite suspension.

The history of zeolite hydrothermal synthesis goes back to the studies of Richard Barrer and Robert Milton in the mid 20th century.[33] Typical hydrothermal synthesis can be briefly described through several basic steps:

i. The first step is to mix the source chemicals to form precursor suspension with a cation source in a basic medium for a given time is called the aging step.

ii. The aged suspension is then heated up at moderate temperatures between 50 °C - 270 °C and high pressures (up to 120 bar). When the suspension reaches moderate temperature, where the reactants are still in an amorphous phase, which is called the induction period. The induction period covers the nucleation stage where initial unit cells (i.e., rings, cages, secondary building units, etc.) of the zeolite crystals form, and then first zeolite blocks start to grow at the growth period, and their growth continues until there are no source materials left to be converted into the crystalline phase (i.e., saturation stage).

iii. Finally, the crystalline product obtained is being washed to decrease the pH of the solution near a neutral range and calcined at high temperatures to get rid of SDA.[33]

The hydrothermal Silicalite-1 zeolite synthesis parameters are broadly investigated in the past, specifically by Persson and his colleagues.[34] They examined the effect of each parameter on the post-synthesis product, such as the crystal sizes, product yield, and crystal growth rate. The researchers noted that the more prolonged synthesis and higher temperatures increased the particle size. The study also showed that fixing the molar ratio of the T atom to the SDA, different water content, and solution alkalinity directly affects the particle size, where higher alkalinity would yield smaller crystals. This finding is also implemented in this thesis, which is explained in detail in Chapter 4.

Hydrothermal synthesis is the preferred zeolite synthesis method among all conventional synthesis methods for providing a relatively higher yield, crystallinity, and a final product with discrete crystals. Long synthesis hours are required before crystallization, i.e., induction time is considerably high (12 - 24 hours).[29,33,35] Rapid synthesis methods, such as microwave heating, ultrasound-assisted and ionothermal, syntheses are developed to shorten the induction time. The theory of microwave heating relies on generated electromagnetic radiation in the microwave range transformed to the reactive medium by dipole and ionic conduction.[36] In zeolite synthesis, usually water absorbs microwaves, and dipole moment rotation causes the generation of heat.[37] Oscillations of ionic particles absorbing microwave radiation also generate heat and contribute to spreading of energy. Compared to the hydrothermal method, generated heat spread faster, hereby the reaction rate increases.[38,39]

The microwave heating method drastically reduces the typical induction period from days to minutes due to faster heat spread.[40,41] For TPA-Silicalite-1 zeolite which is also studied in this thesis, the induction period is reported to decrease from one day to 60 – 90 minutes.[42,43] The drawback of microwave synthesis is that during microwave

heating, several hot spots form inside the reaction medium, causing boiling of the liquid.[36,41,44] When this happens, solid clusters within boiled hot spot accumulate and fused crystals instead of discrete ones dominate the end product.[40,41,45,46] This results in a reduction of the available surface area of zeolite for adsorption purposes.[42,43] To overcome this drawback, staged microwave-assisted and hydrothermal combined microwave synthesis methods have been developed.[47,48] In the staged microwave-assisted synthesis method, the precursor solution is exposed to microwave heating, and the solution is allowed to cool down before the next stage. This brings additional challenges to the synthesis control.

Researchers tried to develop alternative zeolite synthesis methods that are faster compared to the hydrothermal and with easier control compared to the microwave methods, working not only for a specific family or group of zeolites but also for many others. Among these methods, ionothermal and ultrasound-assisted synthesis procedures have been developed.[49,50] Ionothermal synthesis uses ionic liquids such as hexanol, propanol, glycerol, etc. both as solvent and SDA.[49] The method was successful for Al based zeotype materials, however, most of the industrially important zeolites are silicon based and the solubility of silicon species in ionic liquids is much harder to control compared to Al based species.[49] The use of ultrasonic waves in zeolite synthesis brings several advantages as shortening induction period since they add a stirring effect due to traveling ultrasound waves within the reaction volume.[50] Ultrasound waves are absorbed by any type of material but in varying portions, which leads to non-uniform temperature distribution within precursor suspension. This phenomenon decreases the controllability of synthesis gel when ultrasound is used as the only source of energy in zeolite synthesis.[50] Developed synthesis methods should also produce comparable

product quality to the hydrothermal method in yield, crystallinity, and nanosized particle distribution.

2.3 Challenges of Nanosized Zeolite Synthesis: High Yield and Crystallinity

An emerging field in zeolite research is nanosized crystal (~100 nm) synthesis. The growing interest is due to the advantages of nanocrystal zeolites, such as increased external surface area, shorter diffusion length, and tunable bulk properties.[7–9,27] However, several crucial properties of zeolites, namely the selectivity and crystalline- and defect-free framework will deteriorate due to the size reduction of particles.[27] Synthesis of nanosized zeolite particles through conventional methods requires relatively mild synthesis conditions, namely long reaction times reaching several days (up to 30 days and more) and low reaction temperatures close to room temperature compared to their micron-sized counterparts.[6,9,51] Particle sizes are dependent on the competition between the nucleation and growth stages. The dominant nucleation during the synthesis, i.e., a greater number of nuclei produced, leads to smaller particle sizes. Therefore, low synthesis temperatures are preferred. This inevitably increases the synthesis time to several days. As synthesis time is kept long enough to allow further crystallization and higher yield, particle sizes will increase. Selectivity is the tendency of a certain particle to interact with a specific type of molecule, when diffusion length is shortened, reduction in selectivity is inevitable. Shorter diffusion lengths due to smaller particle sizes also decrease the selectivity. In short, synthesizing nanosized zeolites requires thorough optimization of the system specific to the desired application.

2.4 Ultrafast Lasers and Far From Thermodynamic Equilibrium

Lasers that can produce pulses at the time scale of 5 femtoseconds (1 fs = 10^{-15} s) to 100 picoseconds (1 ps = 10^{-12} s) are referred to as ultrafast lasers.[52,53] Through several decades plenty of applications have been developed involving ultrafast lasers, whereas the most widely usage of them is on femtosecond material removal (ablation).[52,54] Compared to longer pulse widths, pulses with such short duration (femtosecond) interact with the material in a time scale that is shorter than the heat diffusion time which is typically in the order of several picoseconds and nanoseconds, and hence can drive the system far from thermodynamic equilibrium by creating spatiotemporal temperature profile.[52–55] Laser light is first absorbed by electrons which is an instantaneous process (< 1 fs). Then absorbed energy is distributed to the atomic lattice through phonons, which takes approximately 5-10 picoseconds (5000 – 10000 femtoseconds).[56,57] For longer pulse widths, electrons, and atomic lattice stay on thermal equilibrium, whereas for femtosecond pulses this equilibrium cannot be achieved.[53,55,56] This phenomenon is widely exploited for femtosecond material ablation, where temperatures can rise to ~10000 K momentarily.[56,57] The less explored phenomenon which is explained by Ilday *et. al.*, is the huge gap between necessary ablation temperature and evaporation temperature of the material at thermal equilibrium.[54] For instance, a material evaporating at 1000°C may be brought to temperatures up to 10000°C through femtosecond pulses where almost no ablation occurs since critical ablation temperature is not reached. These extreme temperatures are achieved only instantly and decrease within several picoseconds.[56,57] During this process, chemical reactions may be triggered or accelerated. Zeolite synthesis reactions are complex polymerization reactions that occur in the precursor suspension simultaneously, within the time scales of pico- and femtoseconds.[17] Zeolite synthesis

requires moderate temperatures between 50°C – 270°C and high pressures (up to 120 bar).[58] During femtosecond laser-material interaction, another phenomenon that occurs in the system is momentarily created high pressure (shock waves ~100000 bar), which is coupled with instant temperature rises.[59] Hereby, a suitable environment for zeolite synthesis is formed by femtosecond laser pulses.

Formation of far-from equilibrium conditions in an optically transparent media hit by femtosecond laser pulses has been studied previously in a study by S. Ilday *et. al.*[60,61] The experimental setup composed of a colloidal solution of polystyrene particles sandwiched between two thin glass slides was hit by femtosecond laser pulses. Central limit theorem applied, i.e. normal fluctuations observed when the colloidal solution was not hit by laser pulses.[60] On the contrary, when the laser was turned on, flows induced by spatiotemporal thermal gradient formed via ultrafast laser pulses cause giant number fluctuations, showing that far-from equilibrium is established.[60] When the medium is optically transparent to irradiated laser light with wavelength of ~1040 nm, as is the case for the study by S. Ilday *et.al.* and for this thesis, energy intake is possible through multi-photon absorption of femtosecond laser pulses.[60] This process induces steep spatiotemporal thermal gradients. Since surface tension of fluid is a function of temperature, surface tension gradients form as well, causing Marangoni flow in addition to Stokes flow. The Marangoni flow takes place when a surface tension gradient is formed at the interface of two phases. One of the main advantages of the developed synthesis method for zeolites in this thesis is the immediate distribution of nucleated particles evenly to the reaction volume because of the induced Marangoni flow, leading to an increase in the number of nucleated clusters in the bulk volume. The uniform distribution of nucleated particles through whole reaction volume cannot be achieved by static hydrothermal synthesis of zeolites. Although the rotation of the autoclaves is

possible in conventional hydrothermal synthesis[58], the vigorous Marangoni flow induced in the laser-assisted synthesis increases number of nucleated particles in the bulk volume within much shorter time, which may be the reason for the short reaction times observed. Another advantage of laser-assisted synthesis is that although extreme temperatures are achieved instantly, the temperature of the bulk volume does not increase uncontrollably unlike microwave synthesis.[44,56,57] One can touch the synthesis bottle right after laser-assisted synthesis because instantly achieved extreme temperatures do not give rise to the global temperature of the reaction bottle similar to other examples of femtosecond laser-material interactions.[56,57] The absorbed energy is spent to formation of building units of zeolite structures. Moreover, femtosecond laser pulses assure the delivery of a precise amount of energy per area within a time interval, allowing accurate control over the reactive medium in the time scale of polymerization reactions in zeolite synthesis. None of the developed synthesis methods for zeolites can provide such controlled energy delivery over the system. The repeatability of the syntheses which is explained in the chapter 4.1.1 of the thesis proves controlled energy delivery over the system.

CHAPTER 3

METHODS

3.1 Chemicals Used

The source chemicals used in the this thesis are reagent grade 98% Tetraethyl orthosilicate (TEOS) from Sigma Aldrich, 500 ml with a formula weight of FW = 208.33 g/mol. Tetrapropyl ammonium hydroxide (TPAOH, Sigma Aldrich) 1M solution in water, 100 g with compound formula of [TPAOH · 45.19 H_2O] and FW = 1011.92 g/mol, Sodium hydroxide (NaOH, 99 %, Merck), SiO_2 (Ludox-HS 30, 30 wt. % SiO_2, pH=9.8, Aldrich), Al powder (325 mesh, 99.5 %, Alfa Aesar), Aluminum isopropoxide ($Al(iPro)_3$, >98 %, 220418, Aldrich), deionized water (DI water, resistivity = 18.2 MΩ). N9 and N13 vials and their compatible inserts were purchased from ISOLAB (Isolab Laborgerate GmbH).

3.2 Experimental Setup

The experiments were conducted within vial inserts which served as a closed system to precursor suspension integrated with an ultrafast laser (Spectra Physics, Spirit One, 1040 – 8 – SHG). The central wavelength and pulse repetition rates of the laser were set to 1040 nm and 200 kHz, respectively. The laser was directed to the reaction bottle through the optical path described in Figure 7. The bottle was pinned to a sample holder from its cap so that the bottle is hung in the air.

After leaving the laser, the beam hits a mirror, which directs it to two successive lenses. These lenses allow the beam to travel long enough without further diffraction. Then it is forwarded to a half-wave plate and a beam splitter, allowing beam attenuation for power adjustments. Finally, the beam passes through a 1″ lens with a 5 cm focal

length and shines on the reaction bottle at a distance where the beam is focused to the glass - solution interface (beam diameter ~ 9 µm).

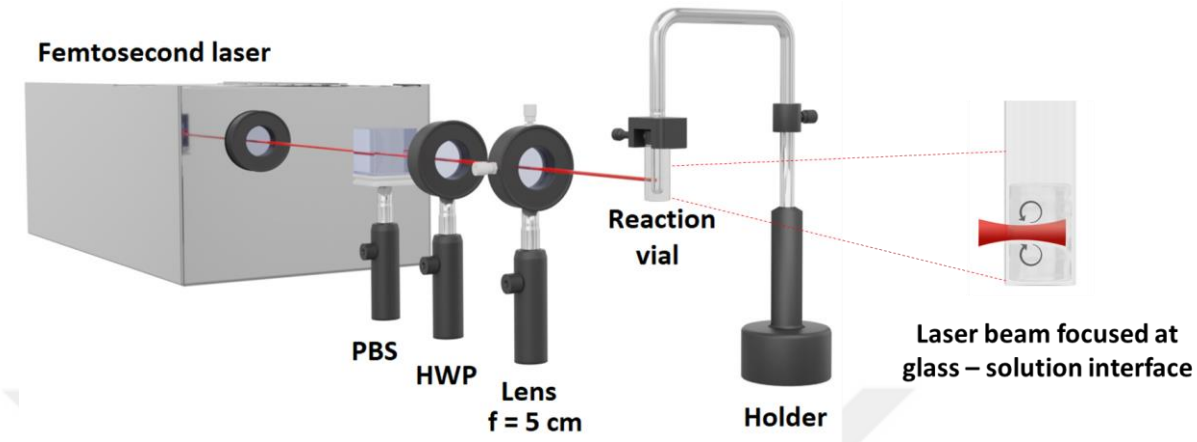

Figure 7. Schematic description of the experimental setup; the femtosecond laser beam is directed to the reaction bottle filled with the precursor suspension hung from the sample holder.

3.3 Synthesis Procedure

3.3.1 TPA – Silicalite-1

Synthesizing zeolites starting from the careful choice of the molecular formula to be employed and preparation of precursor suspension. Molar formulas for MFI type TPA-Silicalite-1 zeolites are found in the literature.[34,62] Three different molar formulas employed in this study for TPA – Silicalite-1 synthesis where the only difference is the water contents, which changes from 1450 for M1, to 480 and 450 for M2 and M3 molar formulas:

$$M1 = 25\ SiO_2 : 9\ TPAOH : 1450\ H_2O : 100\ EtOH^{34,62}$$

$$M2 = 25\ SiO_2 : 9\ TPAOH : 480\ H_2O : 100\ EtOH^{34}$$

$$M3 = 25\ SiO_2 : 9\ TPAOH : 450\ H_2O : 100\ EtOH^{34}$$

The molar formulas of M1, M2, and M3 were employed. Both hydrothermal and femtosecond laser treatments were applied to obtain TPA – Silicalite-1 crystals to compare.

We begin the procedure by mixing 0.500 g TPAOH 1M solution in water and 0.284 g TEOS, then stir them vigorously for 30 minutes at room temperature. Then, 1.025 g of DI water (1.025 g for M1 molar formula; 0.07 g for M2 molar formula and for M3 molar formula no water added, the water content comes from aqueous TPAOH solution) is added to the bottle. Then, precursor suspension was stirred for 24 hours at room temperature, this stage is called the "aging" step. The precursor suspension was used both for hydrothermal and laser reactions. For hydrothermal reaction, the transparent precursor suspension in a glass vial is placed in a preheated oven at 100 °C for 24 hours, no additional mixing applied (for M2 and M3 molar formulas reaction temp: 90 °C and reaction time: 30 hours).

For the laser-assisted reaction, 80 µl transparent precursor suspension in a glass insert is placed inside a glass vial (Isolab, 1.5 mL, N9). When the volume of precursor suspension was more than 80 µl (i.e., 400 or 600 µl), we used the N13 type of glass vial (Isolab, 4 ml) and a compatible glass insert was used. The laser is positioned to the one-third height of the insert from the bottom. The laser focal point was adjusted to be in the glass - precursor suspension interface (Figure 7-b). Reaction time was 5h. Average laser power on the sample and pulse repetition rate were adjusted to be 5.4W and 200 kHz, respectively. The spot size of the laser on the glass - precursor suspension interface was measured to be 9 µm by using a beam profiler (Thorlabs). The zeolites were centrifuged (14000 rpm) with DI water until pH value is reached to 7 and dried overnight at 45 °C. To obtain TPA-free Silicalite-1, calcination at 490 °C for 5h (Protherm, rate = 5 °C / min) was applied.

3.3.2 Template-free Zeolite Y

The nanosized FAU zeolite was synthesized from a clear precursor suspension with a molar composition: 9 Na_2O: 0.7 Al_2O_3: 10 SiO_2: 160 H_2O. The initial reactants were mixed to prepare two initial solutions denoted A and B. Solution A was prepared by dissolving 2 g of NaOH (Sigma-Aldrich) in 4 g double distilled water (dd H_2O) followed by addition of 0.189 g aluminum powder by parts (325 mesh, 99.5 %, Alfa Aesar). Solution B was prepared by mixing 10 g colloidal silica (Ludox-HS 30, 30 wt. % SiO_2, pH=9.8, Aldrich) with 1.6 g NaOH and 3.4 g dd H_2O; as a result, a turbid suspension was obtained. To transform the turbid into a water clear suspension, the container was placed in an oven at 100 °C for 6 minutes. Solution A was added dropwise under vigorously stirring to solution B; during the mixing, solution B was kept on ice. The resulting clear suspension was kept for 24 h at room temperature; this stage is ascribed as aging. The laser-assisted synthesis was conducted in insert compatible with N13 vial (Isolab), applying 5 W average power on glass insert wall with 200 kHz repetition rate. Hydrothermal crystallization was conducted at 50 °C for 45 h. The synthesized zeolites were centrifuged (14000 rpm) with the DI water until pH value is reached to 7 and dried overnight at 45 °C.

3.3.3 Mesoporogen-free Hierarchical ZSM-5

The molar formula of $Al(iPro)_3$: 50 TEOS: 9 TPAOH: 9 NaOH: 5709 H_2O was employed.[63] Two-step procedure was followed to obtain hierarchical zeolite without using any mesoporogen (i.e., template to obtain mesopores). In the first step, the initial precursor suspension was placed in an oil bath to stir at 100 °C for 44h. The amount of water in the initial precursor was limited to a certain amount to prevent ZSM-5 crystal growth (i.e., crystal size < 50 nm). In the second step, additional water is added to the

initial precursor suspension after 44h of aging at 100 °C. Finally, both hydrothermal and femtosecond laser treatments were employed to obtain hierarchical ZSM-5 crystals.

In bottle A: 0.83 g deionized water (DW) was added to 0.51 g TEOS. Then, 0.01 g $Al(iPro)_3$ was added slowly. It was stirred at room temperature (RT) for 1h. The color of the suspension was milky (almost opaque). Another bottle is prepared simultaneously (denoted as bottle B). 0.45 g TPAOH was added to bottle B. In a separate 5 mL beaker, 0.018 g NaOH powder was mixed with 0.96 DI water and stirred for 2 minutes until all NaOH is dissolved in the solution. Then, NaOH solution was added to bottle B. Bottle B was stirred at RT until 1h stirring time of bottle A elapsed. Afterward, bottle A is placed in an oil bath at 40 °C. Bottle B is added to bottle A dropwise, then stirred for 3h at 40 °C. Then, the temperature of the oil bath was increased to 100 °C to stir the initial precursor suspension for 44h. The initial precursor suspension was removed from the oil bath after 44h and additional DI water (2.88 g) was added to obtain the final precursor suspension and stirred at RT for 15 min.

The precursor suspension was used both for hydrothermal and laser reactions. For hydrothermal reaction, the milky precursor suspension was placed in Teflon line autoclave placed in stainless steel autoclave. The reaction was carried out at 150 °C for 24 h in without additional mixing. The product was centrifuged (14000 rpm) with DI water until pH value reached 7 and dried overnight at 45 °C. The collected zeolite powder was calcined at 490 °C for 5h (Protherm, rate = 5 °C / min).

For laser reaction, 200 µl milky precursor suspension was placed in a glass insert (Supelco, Merck, 0.75 mL) that was placed inside a glass vial (Isolab, 4 mL, N13). The laser is positioned to the one-third height of the insert from the bottom. The laser focal point was adjusted to be in the glass - precursor suspension interface. Reaction time was 5h. Average laser power on the glass insert and pulse repetition rate were adjusted

to be 5W and 200 kHz, respectively. The spot size of the laser was measured to be 9 μm by using a beam profiler (Thorlabs). Fluence was calculated to be 39.31 J/cm^2. The product was centrifuged (14000 rpm) with DI water until pH value reached 7 and dried overnight at 45 °C. The collected zeolite powder was calcined at 490 °C for 5h (Protherm, rate = 5 °C / min).

3.3.4 Mass Composition Calculations for TPA – Silicalite-1 Zeolite Synthesis Mixture

For a certain molar formula, the amount of source chemicals to prepare precursor solution should be calculated in terms of weight. In all molar formulas used in the study for synthesis of TPA – Silicalite-1, TEOS, and TPAOH were silicon source and structure directing agent (SDA) to form micropores in the structure, respectively. The amount of water affects the alkalinity of the suspension, which determines the growth rate and average crystal size. For the M1 molar formula with the composition of 25 SiO_2: 9 TPAOH: 1450 H_2O: 100 EtOH, corresponding TEOS, TPAOH, and DI water masses are calculated. Since TPAOH is in the form of a 1M aqueous solution, water coming along with TPAOH should be subtracted from the total water needed.

Table 1. Molar composition of reagents necessary to form TPA – Silicalite-1 zeolite synthesis mixture (M1 molar formula).

	25 SiO_2	9 TPAOH	1450 H_2O
25 TEOS	25 mol -25 mol		
9 (TPAOH · 44.92 H_2O)	0	9 TPAOH -9 TPAOH	1450 H_2O -404.28
1045.72 H_2O		0	1045.72 -1045.72
			0

Densities of TPAOH 1M and TEOS solutions are 1.012 g/ml and 0.94 g/ml. Multiplying densities with corresponding molar ratios of compounds for the M1 molar formula gives mass ratios. Keeping mass ratios as same, one may obtain precursor suspension for TPA – Silicalite-1 zeolite complying with M1 molar formula.

Table 2. Mass composition of reagents necessary to form TPA-Silicalite-1 zeolite synthesis precursor suspension (M1 molar formula).

Compound formula	**Moles**	**FW (g/mol)**	**Mass (g)[a]**	**Solution density (g/ml)**	**Volume [b] (ml)**	**Volume (%)**
TEOS	25	208.33	5208.25	0.94	5540.7	16.61
(TPAOH · 44.92 H_2O)	9	1011.92	9107.28	1.012 [c]	8999.29	26.98
H_2O	1045.72	18	18822.96	1	18822.96	56.41

[a] Mass = Number of moles x FW (formula weight)

[b] Volume = Mass / density

[c] Solution density of 1M TPAOH

Summary of important measures and molarities of compounds within M1 precursor suspension solution is provided in Table 3. All molarity values for molar formulas that are used in this thesis for TPA – Silicalite-1 synthesis are given in Table 4. Mass composition calculations for M2 and M3 molar formulas can be found in Appendix A.

Table 3. Molarities of compounds in precursor solution for M1 molar formula.

Compound formula	Number of moles	MW (g/mol)	Mass (g) [a]	Molarity (mol/l solution) [b]
SiO_2	25	208.33	5208.25	0.75
TPAOH	9	203.36	1830.24	0.27
H_2O	1045.72 + 404.28 = 1450	18	26100	43.46

[a] Mass = Number of moles x MW (molecular weight)

[b] Molarity = mole / liter of solution. The total volume of the solution is 33362.95 ml (Table 2).

Table 4. Molarities of compounds for different molar formulas (M1, M2, and M3)

Molar Formula	Molarities of compounds (mol/l)		
	SiO_2	**TPAOH**	**H_2O**
M1	0.75	0.27	43.46
M2	1.57	0.57	30.2
M3	1.71	0.61	28.03

3.4 Calculation of the Incident Energy Deposited by Femtosecond Laser Pulses

As a simple approach for the interaction volume, one can simply draw a cylinder with a diameter of spot size and with the height of beam waist (Figure 8). It is assumed that all the interactions (i.e., zeolite polymerization reactions and crystal growth) occur in this interaction volume. Energy incident per mol of SiO_2 in the zeolite precursor suspension is calculated. The precursor suspension has SiO_2, tetrapropyl ammonium hydroxide (TPAOH, structure directing agent -TPA^+ cation that forms micropores in the structure), and water (Table 2).

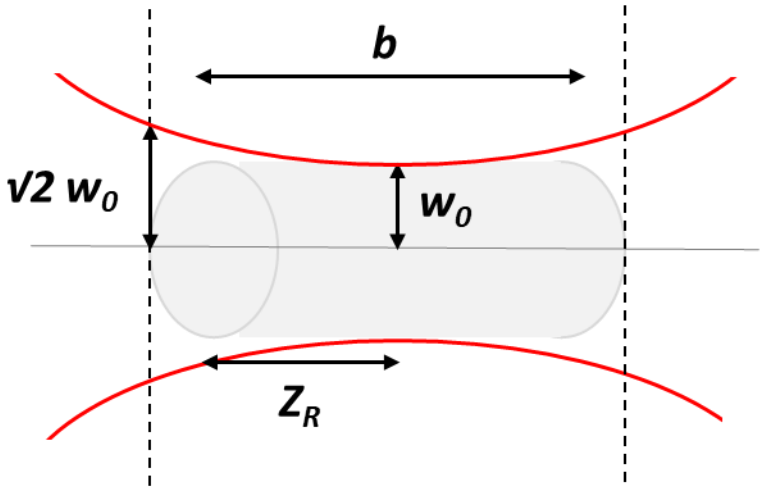

Figure 8. Schematic representation of interaction volume of the laser beam with precursor suspension at its most focused state.

In the calculations to determine the interaction volume the of laser beam with the precursor suspension, irradiance distribution of the laser beam is assumed to be Gaussian.[64] The spot size of the laser beam was measured to be 9 µm by using a beam profiler (Thorlabs, BP 209-IR2).

$$Z_R = Rayleigh\ length$$

$$b = beam\ waist = 2\,Z_R$$

$$Z_R = \frac{\pi\omega_0^2}{\lambda}$$

$$Z_R = \frac{(3.14)(4.5\ x\ 10^{-6}\ m)^2}{(1040\ x\ 10^{-9}\ m)}$$

$$Z_R = 61.1\ \mu m$$

Interaction volume (V_i)

$$V_i = \pi\omega_0^2 b$$

$$V_i = (3.14)(4.5\ \mu m)^2(122.2)\ \mu m$$

$$V_i = 7.77 \cdot 10^{-6}\, mm^3$$

In almost all of the reactions (except scale-up trials) 80 µl of precursor suspension used. So, in this calculation, total volume is taken as 80 µl. For the batch with the M1 molar formula, the molarity (mol/liter) of SiO_2 in the precursor suspension was calculated to be 0.75 mol/l (Table 2). If it is assumed that SiO_2 is distributed along with the V_i evenly, then the mol of SiO_2 in the V_i is

$$n_{SiO_2} = (7.77 \cdot 10^{-6}\ \mu l\ suspension)\frac{0.75\ mol\ SiO_2}{10^{-6}\ liter\ suspension}$$

$$n_{SiO_2} = 5.83 \cdot 10^{-6}\ \mu mol\ SiO_2$$

3.4.1 Power Absorption in Zeolite Synthesis

For a better approach to power absorbed by the precursor suspension during zeolite reactions, we measured the losses due to light passing through interfaces of different phases. The reaction system used is described below: Transparent precursor suspension is filled to glass insert, with a wall thickness of 0.92 mm (Figure 9). Then the glass insert is placed in a glass vial (Isolab code: N9) which has a wall thickness of 1.16 mm.

Figure 9. Reaction system used in zeolite synthesis: precursor solution is filled to glass insert, which stays in a glass vial.

In this case, incoming laser light passes through several air-glass interfaces before reaching out to the power meter. Schematic description of the traveling laser beam through reaction bottle until reaching out to power meter is described in Figure 10.

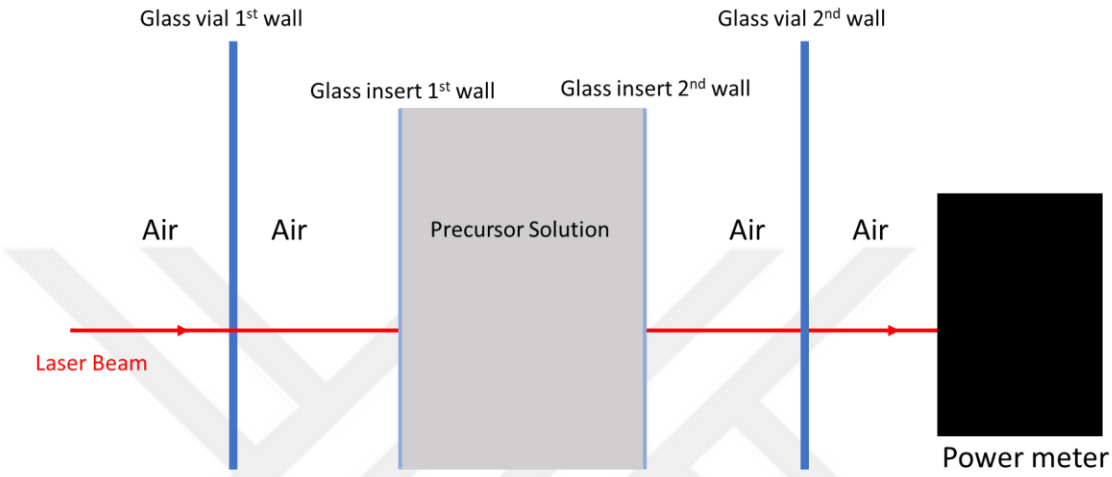

Figure 10. Schematic description of traveling laser beam through zeolite reaction bottle.

For such a system, power losses due to interfaces which beam passes through are calculated. To consider losses due to each interface, three different measurements were carried out (Appendix C). For all measurements, average laser power has been set to 5.3 W. This power value was measured at a point just before the laser beam hits the first wall of the glass vial (or glass insert for second and third measurements) (Figure 10). Then second power measurement was made just after the beam leaving second wall of the glass vial (or glass insert for second and third measurements). For a system as described in Figure 10, unknowns are listed in Figure 11.

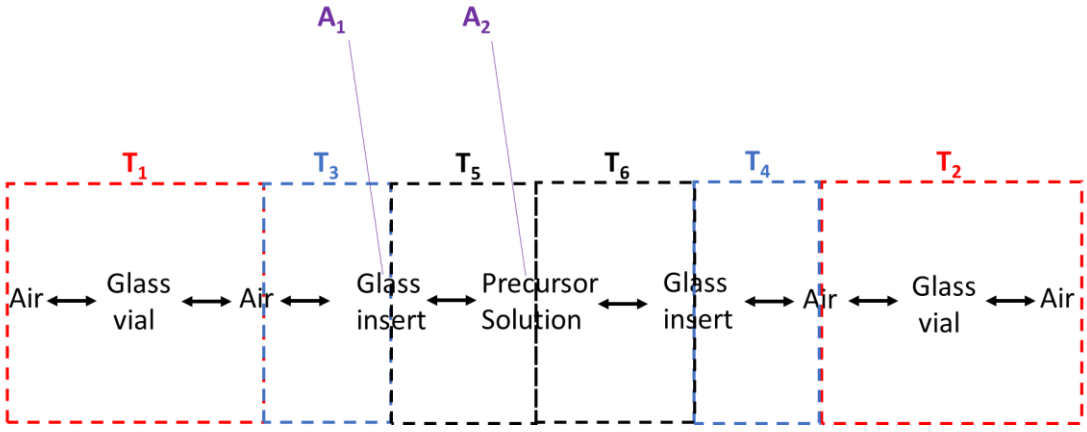

Figure 11. The travel path of the laser beam and sources of power loss. T_1 – (or T_2, they are identical) is the transmittance of light when passing from Air – Glass vial – Air interfaces; T_3 – (or T_4, they are identical) is the transmittance of light when passing from Air – Glass insert interface; T_5 – (or T_6, they are identical) is the transmittance of light when passing from Glass insert – Precursor Solution interface; A_1 – absorbed portion of laser light by 1st wall of glass insert; A_2 – absorbed portion of laser light by precursor suspension

Incident power used in most of the zeolite reactions were set to be 5.4W on a glass vial, and 5W on a glass insert. For the details of average laser power absorption by precursor suspension, see Appendix C. It is found that only 22.5 % of the average power incident on glass insert is absorbed by precursor solution. So, power absorbed by the precursor solution when 5 W power is incident on the glass insert is;

$$5\ W\ \cdot 0.225 = 1.12\ W$$

Then, pulse energy (E_P) is calculated to be:

$$E_P = \frac{\text{Average laser power}}{\text{Pulse repetition rate}}$$

$$E_P = \frac{1.12\ \text{W}}{200\ \text{kHz}}$$

$$E_P = 5.6 \cdot 10^{-6}\text{J} = 5.6\ \mu\text{J}$$

If it is considered that energy per pulse in that interaction volume (V_i) interacts with the laser, then one can simply divide pulse energy to the volume of the precursor suspension. It is known that, $5.83 \cdot 10^{-6}$ μmol ($5.83\ pmol$) SiO_2 is present in V_i (see above). Then E_i can be calculated as follows,

$$E_i = \frac{Pulse\ energy}{n_{SiO_2}}$$

$$E_i = \frac{5.6\ \mu J}{5.83\ pmol\ SiO_2}$$

$$\boldsymbol{E_i = 0.96 \frac{MJ}{mol\ SiO_2} = 960 \frac{kJ}{mol\ SiO_2}}$$

It is found that, when the M1 molar formula used for the laser-assisted synthesis of TPA – Silicalite-1 zeolite, 960 kJ of laser energy is absorbed per mol of SiO2 within the reaction suspension.

3.5 Characterization Techniques

3.5.1 X-ray Diffractometer

Synthesized zeolite powder samples have been analyzed through Malvern Panalytical X'Pert Pro Multi-purpose Diffractometer. X-ray source of the device is Cu Kα radiation (Kα = 1.54187 Å) operating at 45 kV and 40 mA. Powder zeolite samples have been scanned between the 2θ range of 5° - 50°. For crystallinity calculation from XRD patterns, 2 mg of powder was measured before each measurement.

3.5.2 Scanning Electron Microscopy

Scanning Electron Microscopy micrographs have been obtained by FEI Quanta 200F operating at a high voltage value of 30 kV. Micrographs have been used to observe the morphology of the TPA – Silicalite-1 zeolites at varying crystallization times. 10 nm Au/Pd conductive layers were coated on zeolite samples via Gatan Model 682 Precision Etching Coating system. Crystal sizes have been determined by taking an average of at least 100 – 300 zeolite particles per sample through Image J software.

3.5.3 Scanning Electron Microscopy Energy-dispersive X-ray Spectroscopy

Energy-dispersive X-ray spectroscopy is conducted through Genesis Apex 4 EDAX tool coupled with Quanta FEI 200 Scanning Electron Microscope. Measurements were done at 10 kV voltage with a spot size of 4. Analyzed samples were not coated with conductive material.

3.5.4 Transmission Electron Microscopy

High resolution TEM images were recorded through TECNAI G^2 20 S TWIN Transmission Electron Microscope by FEI company at high tension of 200 kV. The zeolite powder samples have been dispersed in ethanol and dropped on copper TEM grids.

3.5.5 Thermogravimetric Analysis

Thermal stability, zeolitic water, and SDA contents of zeolites have been determined by SDT650 TGA-DSC device on air medium between 25° - 900° C

temperature range by the heating rate of 5° C/min. Differential Thermal analysis of the samples acquired taking the differential of TGA graphs through Origin Software.

3.5.6 BET Physisorption Chemisorption

Quantachrome Autosorb IQ2 MP Gas Sorption system was used for BET surface area determination. External and pore surface areas for TPA – Silicalite-1 synthesized via laser-assisted method have been measured through Brunauer-Emmett-Teller method with N_2 adsorption-desorption isotherm at 77.3 K. The sample was outgassed at 300° C for 16 hours before the measurement. BET method employed for the total surface area where t-plot (DeBoer) method used for external surface area and micropore volume. The pore size distribution was calculated according to the BJH method.

3.5.7 Attenuated Total Reflection – Fourier Transform Infrared Spectroscopy

Before the growth period starts, no powder particle can be collected during femtosecond laser-assisted synthesis of zeolites. To analyze the period before growth, laser-treated reaction solutions were analyzed through ATR – FTIR. Attenuated Total Reflection technique enables the determination of IR spectrum for solid samples dispersed in a liquid medium. Vertex 70V model device by Bruker was used. The liquid sample is dropped (~10 µl) on a diamond tip, the IR light is reflected at the liquid–diamond interfaces, and an evanescent field is formed. Through the evanescent field, light can interact with samples at the interface, and absorption measurement can be made.

3.5.8 Analyses of Particle Size Distribution

Particle size distribution was observed to be narrower for laser-assisted synthesis in SEM images compared to hydrothermal synthesis for all batches with M1, M2, and M3 molar formulas.

$$M1 = 25\ SiO_2 : 9\ TPAOH : 1450\ H_2O : 100\ EtOH$$

$$M2 = 25\ SiO_2 : 9\ TPAOH : 480\ H_2O : 100\ EtOH$$

$$M3 = 25\ SiO_2 : 9\ TPAOH : 450\ H_2O : 100\ EtOH$$

To prove this observation, particle size distribution analysis for a big sample size (i.e., 298 independent crystals) was performed.

Particle size distribution analyses were performed by using ImageJ and Origin software. Particle sizes were obtained by using ImageJ software from a minimum of 4 different SEM images of the same sample taken from different spots. The number of the crystals analyzed was fixed to be 298 for all zeolite samples (i.e., for the syntheses with M1, M2, and M3 molar formulas). Distribution analyses were performed by using the Analysis – Statistics option of the Origin software. To display a fitted curve on histogram Plot Details Dialog - Data - Distribution Curve - Normal option was applied. Mean, standard deviation (SD) values were obtained from fitting analyses.

CHAPTER 4

RESULTS and DISCUSSION

4.1 Characterization of Femtosecond Laser-assisted Synthesis of TPA-Silicalite-1

4.1.1 X-ray Diffraction Characterization

The main characterization of synthesized samples by the laser-assisted method has been carried out by X-ray diffraction pattern analysis. After hydrothermal and laser-assisted syntheses, samples were washed with deionized water and centrifuged 4 times to lower the pH of the solution to a near neutral range (~7). Later, samples were let dry and 2 mg of powder weighted for XRD analysis. The same amount of zeolite powders was weighted for further analysis of crystallinity and proper comparison between hydrothermal and laser-assisted methods. Figure 12 illustrates X-ray diffraction patterns for TPA – Silicalite-1 samples synthesized by hydrothermal (blue) and laser-assisted methods (red), and reference pattern for Silicalite-1 obtained from the IZA web page (black). The structure directing agent used in Silicalite-1 synthesis is TPAOH, which separates TPA^+ and OH^- ions within the aqueous medium. Oligomerization of Silica molecules around TPA^+ ion gives Silicalite-1 zeolite its final structure, and TPA^+ ions are present within the framework until removal through calcination. The removal of SDA from the zeolite framework is possible through calcination, where the sample is heated up to high temperatures (~ 400 – 550 °C) to ignite (calcine) SDA (TPA^+ in this case), but the zeolite framework remains as it is. This process affects X-ray diffraction patterns as well, where in the case of a sample that is not calcined, signal intensity is lowered for some planes because of organic SDA filling the pores. Peak

intensities representing (011), (020), and (051) planes (Figure 10) are lower for not calcined samples (hydrothermal and laser) compared to the calculated powder pattern obtained from IZA.

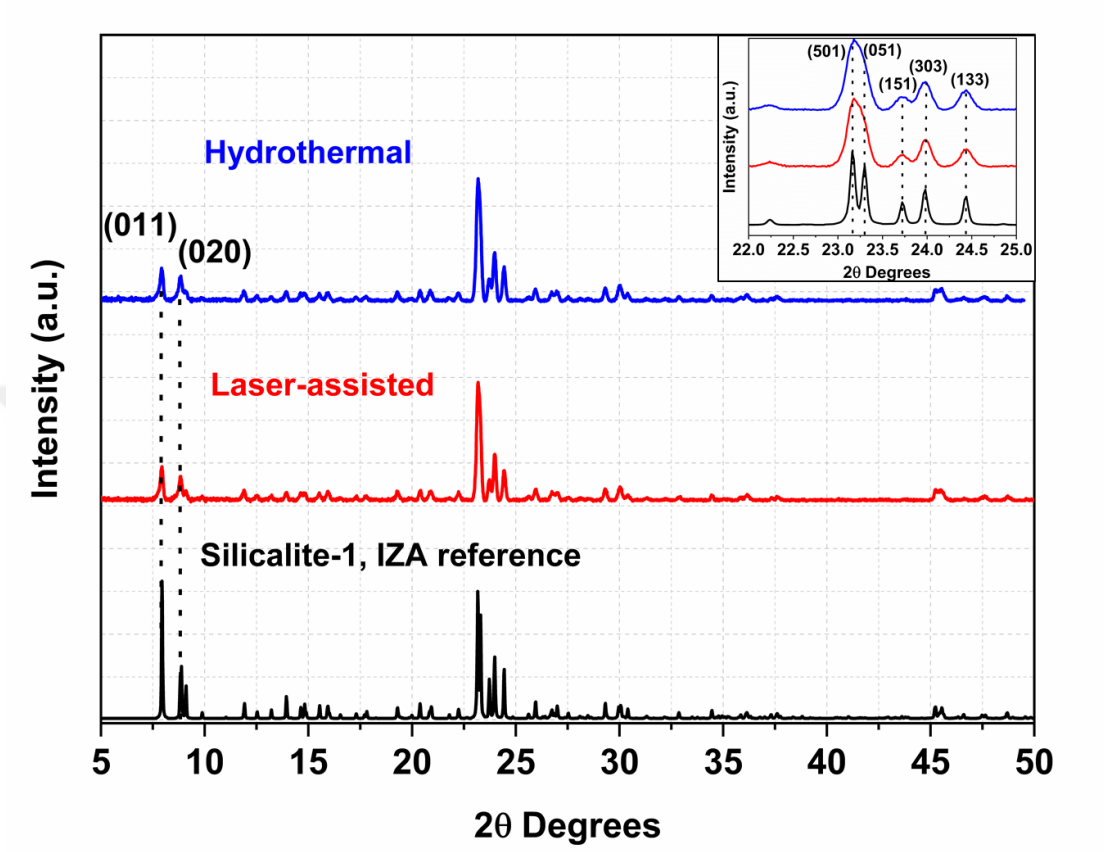

Figure 12. Baseline subtracted X-ray diffraction patterns of the TPA – Silicalite-1 samples synthesized by hydrothermal (yellow), laser-assisted (blue) methods, and IZA reference for Silicalite-1 (red).

An X-ray diffraction pattern is commonly used to determine the crystallinity of a synthesized material relative to a reference material. For zeolites, characteristic peaks on the powder pattern are considered on crystallinity calculation.[65,66] Characteristic peaks for Silicalite-1 zeolite are those representing 5- and 10-membered ring structures of the framework. Here, peaks corresponding to (501), (051), (151), (303), and (133) planes on the powder pattern are characteristic to Silicalite-1 zeolite.[67] On the powder XRD pattern, these five peaks are located in the 22°-25° 2θ range.

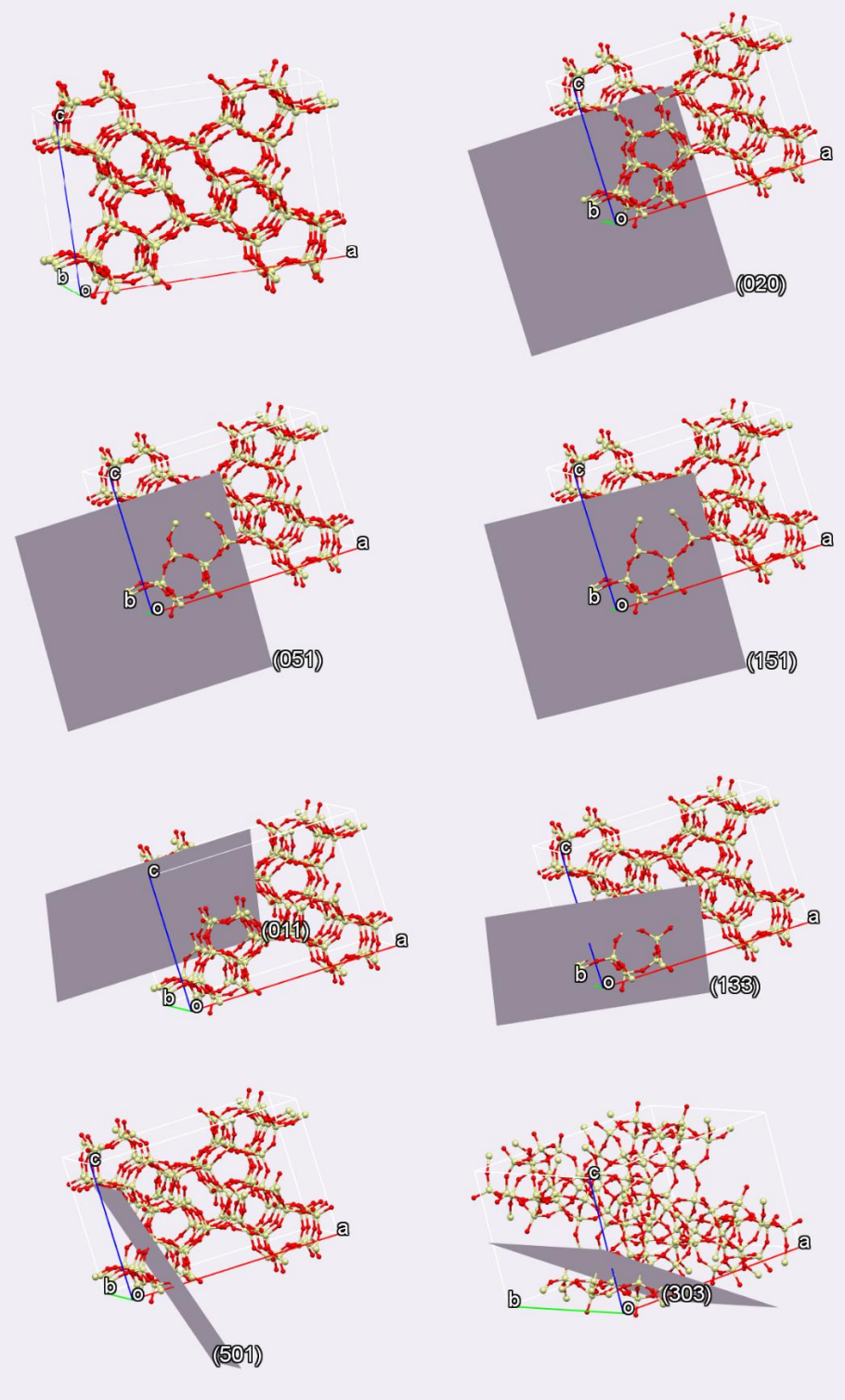

Figure 13. 3D drawings of Silicalite-1 unit cells and characteristic planes representing peaks in the XRD powder pattern.

Four independent experiments show repeatability of the laser-assisted synthesis method. It is observed that if the reaction bottle cap is sealed properly to prevent any

leakage due to increasing pressure inside the reaction vial throughout the reaction, synthesis is repeatable. By applying the same reaction conditions, one can obtain highly crystalline zeolites each time (Figure 14). The reference X-ray diffraction pattern of Silicalite-1 is obtained from the IZA web page.

Table 5 shows detailed crystallinity calculations of these four independent trials by femtosecond laser-assisted method. Crystallinities of the samples were found to be 72, 86, 75, and 80 % for Trials 1, 2, 3, and 4, respectively. To determine crystallinity of a zeolite from XRD pattern, a reference point is needed.[5,65] The zeolite synthesized via the laser-assisted method that has maximum achievable crystallinity was chosen as a reference to calculate the crystallinities of the zeolites synthesized via the laser-assisted synthesis method. For the details of crystallinity calculations see section 4.2.1 of this thesis.

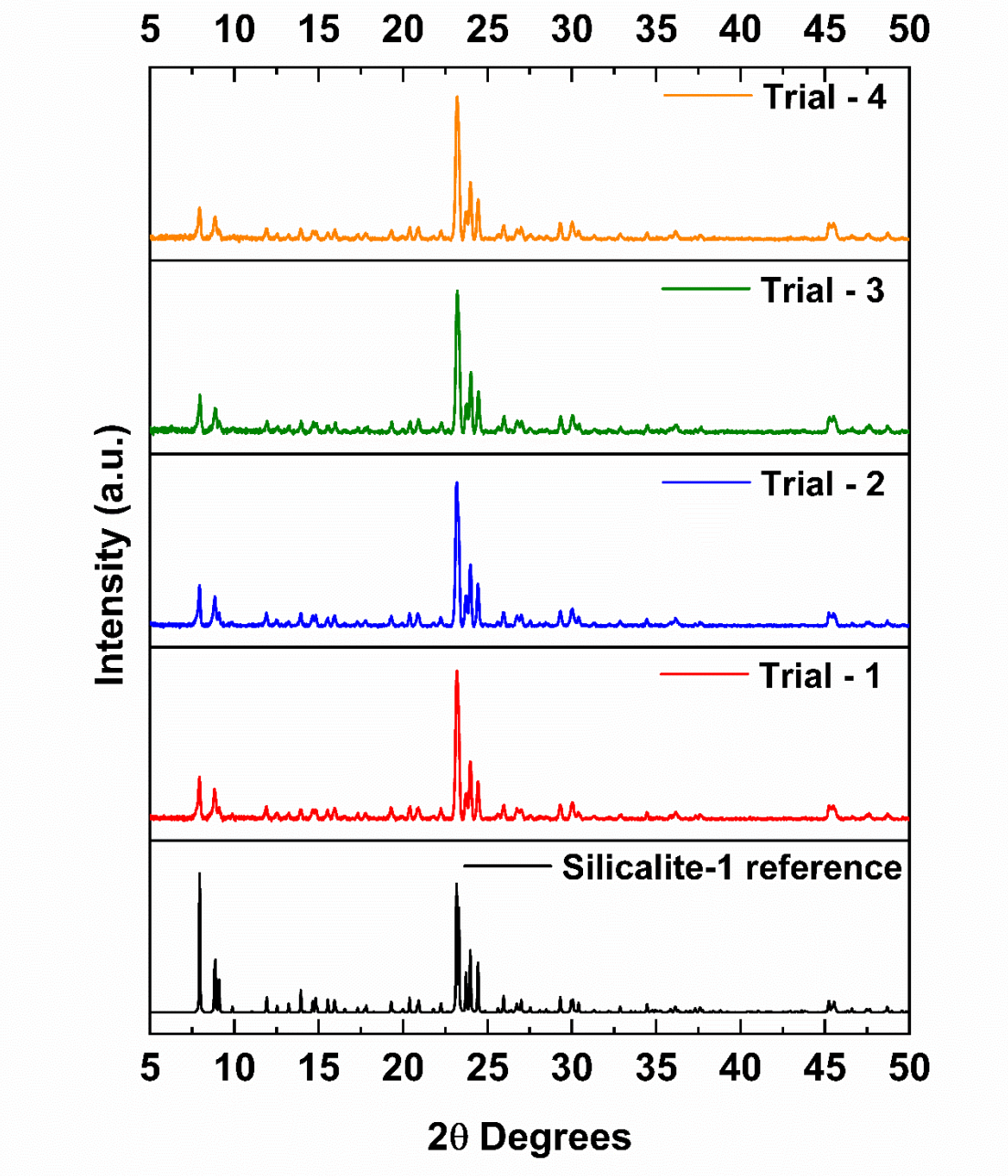

Figure 14. XRD patterns of TPA – Silicalite-1 zeolites synthesized with commercial laser. Reference X-ray diffraction pattern of Silicalite-1 is obtained from the IZA web page. Reaction time for all samples was set to 3 hours, M1: 25 SiO_2: 9 TPAOH: 1450 H_2O: 100 EtOH molar formula was used. Laser parameters were set to 1.12 W average power on the sample, 200 kHz repetition rate.

Table 5. Crystallinity calculation of TPA – Silicalite-1 synthesized with femtosecond laser. Trial 1 (Exp. code: C11), Trial 2 (Exp. code: C12), Trial 3 (Exp. code: C14) and Trial 4 (Exp. code: C24) indicate four independent experiments. Hydrothermal synthesis was carried out with M1 molar formula at 100° C for 48 h. AVG and PA are the abbreviations of average and peak area, respectively.

Peak No	**Bragg Angle**	**Peak Area**					
		Trial 1	**Trial 2**	**Trial 3**	**Trial 4**	**AVG**	**Reference Sample**
1	**23.18**	1235.4	1409.1	1301.6	1240.5	1296.7	1338.9
2	**23.31**	369.3	456.7	306.9	480.2	403.5	796.8
3	**23.73**	175.1	246.7	216.1	199.9	209.5	292.4
4	**23.98**	401.4	503.7	422.2	462.1	447.4	568.8
5	**24.44**	266.7	342.2	298.0	324.0	307.7	406.3
$\sum_{n=1}^{5} PA_{n,sample}$		2447.9	2958.3	2544.7	2706.6	2664.8	3403.2
Crystallinity (%) $\alpha = \frac{\sum_{n=1}^{5} PA_{n,sample}}{\sum_{n=1}^{5} PA_{n,REF}}$		**72**	**86**	**75**	**80**	**78**	**100**

***** Total peak area (3403.2) of the sample synthesized via laser-assisted method was taken as reference in crystallinity calculations.

4.1.2 Scanning Electron Microscopy and Particle Size Distribution Analyses

The same molar formula (i.e., M1) was studied for both hydrothermal and laser-assisted syntheses. Preparation steps (preparation of precursor suspension, aging) for both methods were kept the same and both reactions started once 24 hours aging period ended. Figure 15 shows SEM images and particle size distribution analyses of TPA – Silicalite-1 crystals synthesized via hydrothermal and laser-assisted methods.

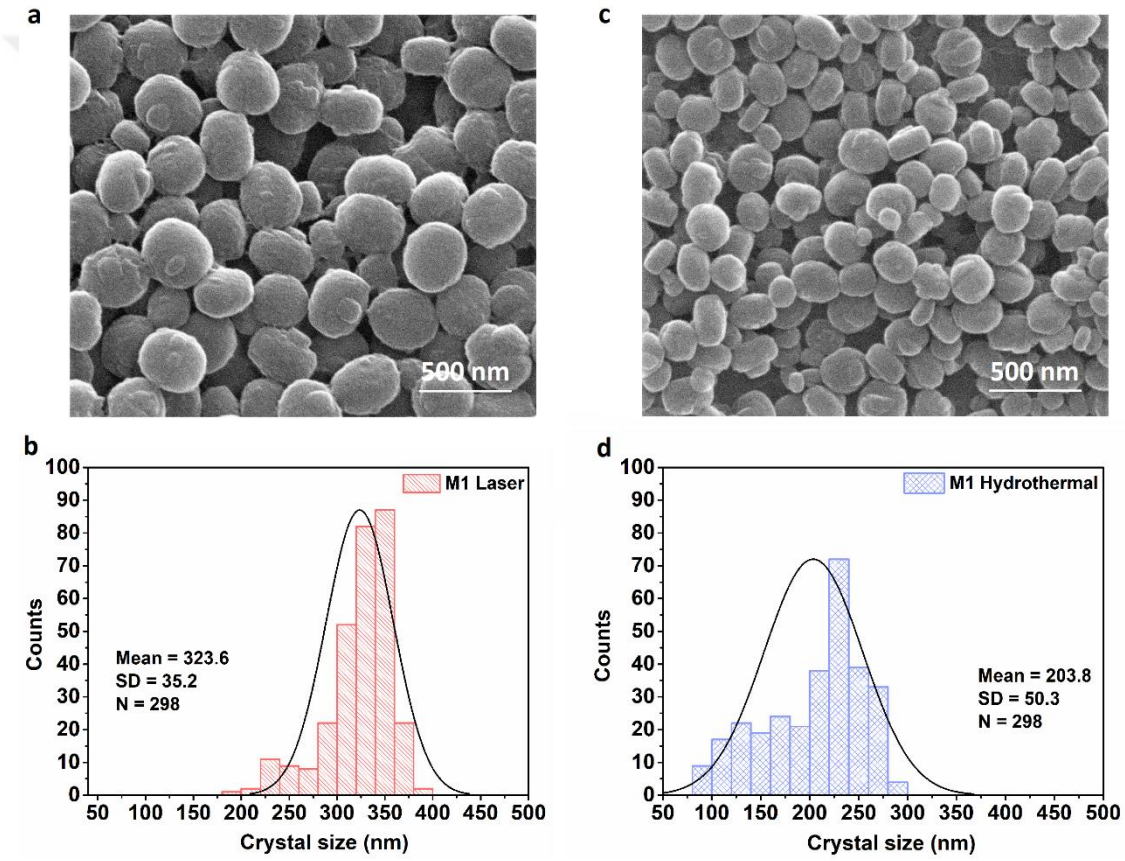

Figure 15. SEM image (a) and particle size distribution (b) of the TPA – Silicalite-1 crystals synthesized via the laser-assisted method (3h reaction, 1.12 W average laser power on the glass-precursor interface, 200 kHz repetition rate, M1 molar formula); SEM image (c) and particle size distribution (d) of the TPA – Silicalite-1 crystals synthesized via the hydrothermal method (48h reaction at 100 °C oven, M1 molar formula).

From the SEM images, one can easily deduce that the average crystal size for the hydrothermal method is smaller compared to that of laser-assisted method. Besides, at first glance, the laser-assisted method seems to produce much more uniform crystals in terms of particle size. To prove these observations, image analyses were applied to SEM images of crystals synthesized via both hydrothermal and laser-assisted methods by using ImageJ software. The length scale obtained from SEM images optimized to be used within software, then lengths of each single particle measured and recorded. Analyses were done for a large field of view (the sample size N = 298 individual crystals). The result showed that particle size distribution was narrower for laser-assisted synthesis compared to hydrothermal synthesis (Figure 15 b and d). The average crystal size and standard deviation (SD) of the crystals synthesized via laser-assisted method were found to be 323.6 nm and 35.2 nm, respectively. For the sample synthesized via the hydrothermal method, average crystal size and SD were found to be 203.8 nm and 50.3 nm, respectively. For the batch with the M1 molar formula, the laser-assisted method results in 119.8 nm bigger crystals on average. Standard deviations in particle size were found to be 10.9 % and 24.7 % for laser-assisted and hydrothermal methods, respectively. The noticeably different SD of the samples shows the observation of narrower particle size distribution for the laser-assisted method.

Comparison of full width at half maximum (FWHM) and intensity values of characteristic XRD peaks of TPA – Silicalite-1 crystals can be found in Table 6. For the same characteristic peaks, intensity values seem to be similar for both methods. Besides, FWHM values indicate that XRD peaks are narrower for the laser-assisted method, further strengthening the phenomenon observed above for particle size analyses. The values in the Table 6 suggest that the sample synthesized via laser-assisted method is comparable with the sample synthesized with the hydrothermal

method. Both particle size distribution analyses and XRD patterns indicate that the laser-assisted method produces relatively bigger particles with much uniform size distribution compared to the conventional hydrothermal method.

Table 6. Comparison of intensity and FWHM of the Bragg peaks of the samples synthesized via hydrothermal (Exp code: A1-C14) and femtosecond laser-assisted (Exp. code: C12) methods for the batch with M1 molar formula. To compare intensities of the samples, 2 mg powder was measured from each experiment and XRD analyses were performed with the same conditions (a.u. indicates arbitrary units).

	Hydrothermal Synthesis		**Laser-Assisted Synthesis**	
Bragg Peaks (2θ°)	**Intensity (a.u.)**	**FWHM**	**Intensity (a.u.)**	**FWHM**
23.18	6646	0.194	6526	0.178
23.31	2730	0.143	2734	0.127
23.73	1247	0.164	1092	0.151
23.98	2744	0.161	2622	0.144
24.44	1848	0.16	1655	0.151

4.1.3 Transmission Electron Microscopy

For TEM analysis, fully crystalline (crystallinity relative to hydrothermal sample > 1.0) TPA – Silicalite-1 zeolite synthesized via laser-assisted method was dispersed in ethanol and sonicated for 5 minutes, then a drop of the obtained solution was placed on copper TEM grid with a carbon cover. The fully crystalline sample is expected to have a smooth surface.[68] Observations from the analysis suggest that synthesized zeolite crystals have smooth surfaces (Figure 16-a). Selected area diffraction pattern and lattice fringes are clearly shown on HR-TEM images imply high crystallinity which is complementary to XRD analyses and previous works reported in the literature (Figure 16 – b, c, d).[18,68–70]

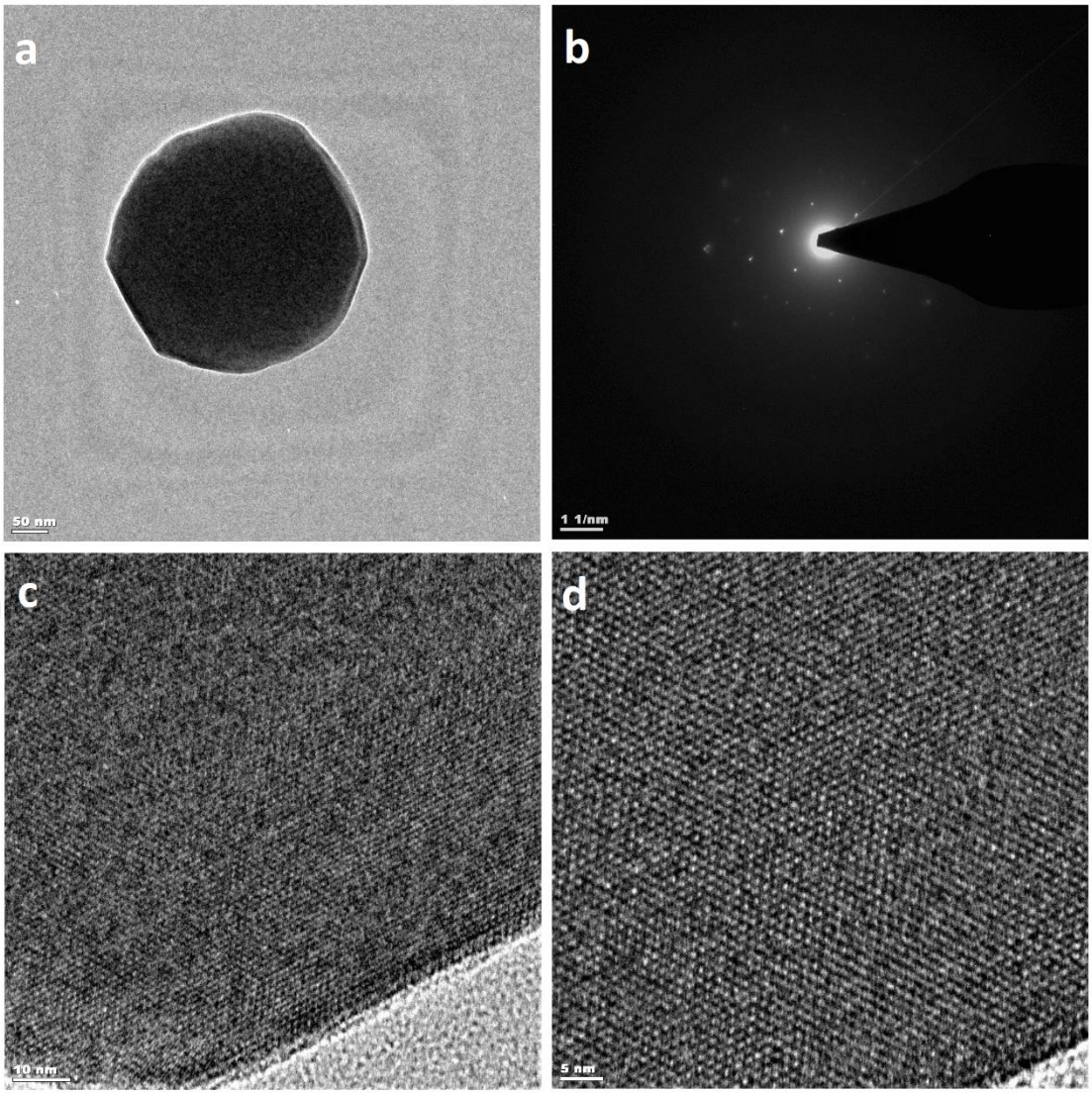

Figure 16. TEM images of (a) TPA – Silicalite-1 (b) corresponding selected area electron diffraction pattern; (c), (d) High-resolution TEM images of same TPA – Silicalite-1 crystal with different magnifications.

4.1.4 Brunauer Emmett Teller Surface Area and Pore Analyses

External and pore surface areas for TPA – Silicalite-1 synthesized via laser-assisted method have been measured through Brunauer-Emmett-Teller method with N_2 adsorption-d isotherm at 77.3 K. The sample was outgassed at 300°C for 16 hours before the measurement. BET method employed for the total surface area where t-plot (DeBoer) method used for external surface area and micropore volume. The pore size distribution was calculated according to the Barrett – Joyner – Halenda (BJH) method. The BET adsorption-desorption isotherm for TPA – Silicalite-1 synthesized by the laser-assisted method is provided below:

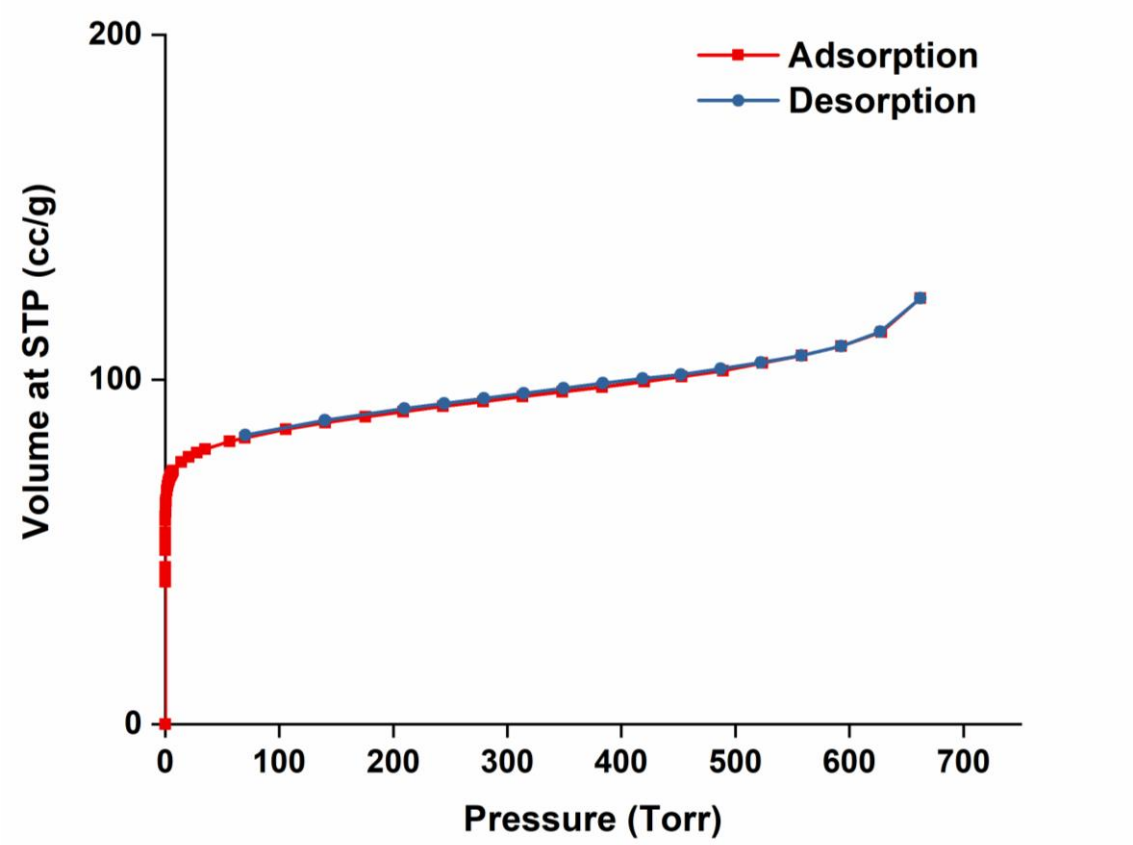

Figure 17. BET adsorption-desorption isotherm of TPA – Silicalite-1 synthesized via the laser-assisted method. The isotherm complies with type 1 of BET isotherms as shown in Figure 18, which refers to the presence of microporous structures. [71–73]

The sample analyzed has a crystallinity of 90 % among samples synthesized via the laser-assisted method. From six different isotherm types defined by Brunauer *et al.*, 1st refer to microporous structures and usually zeolites have type 1 isotherm.[71–73] The isotherm described in the figure above comply with the type 1 of IUPAC adsorption isotherms, indicating microporous structure (Figure 18).[71,72] The types 2, 3 and 5 of isotherms represent macro-porous (pore size > 50 nm) or nonporous materials, where types 4 and 6 represent meso-porous and nonporous materials, respectively.[74]

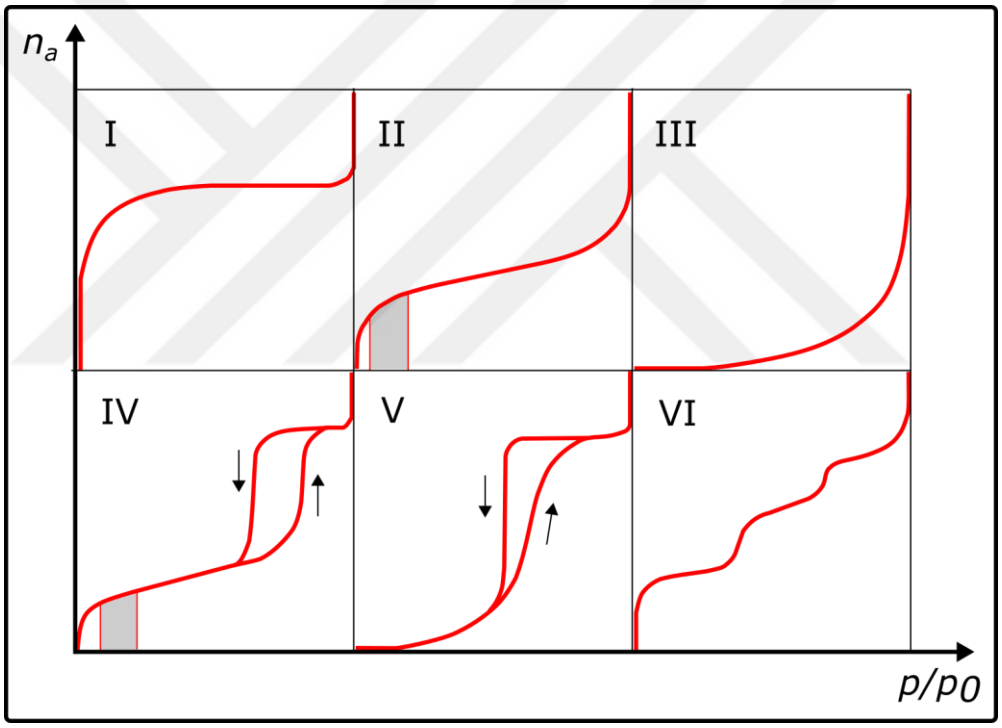

Figure 18. IUPAC classification of adsorption isotherms; n_a refers to adsorbed volume, p/p_0 refers to relative pressure. Adapted from ref [74].

The pore size distribution plot of the sample can be found in Figure 19. A slight accumulation next to the main peak of micropores indicates the interporosity of aggregated crystals.[69,73] Total surface area found from the analysis is 335.5 m^2/g with a micropore area of 266.8 m^2/g. The average pore size determined from BET analysis

through the BJH method is 17.03 Å (1.7 nm). Typical total adsorption areas for Silicalite-1 zeolites range between 300-450 m^2/g.[69,73,75–77] These results show that TPA – Silicalite-1 synthesized via laser-assisted method has similar adsorption behavior compared to zeolite synthesized via conventional hydrothermal method. Only, the laser-assisted method is faster and produce zeolite particles with more uniform average particle size distribution compared to the hydrothermal synthesis method.

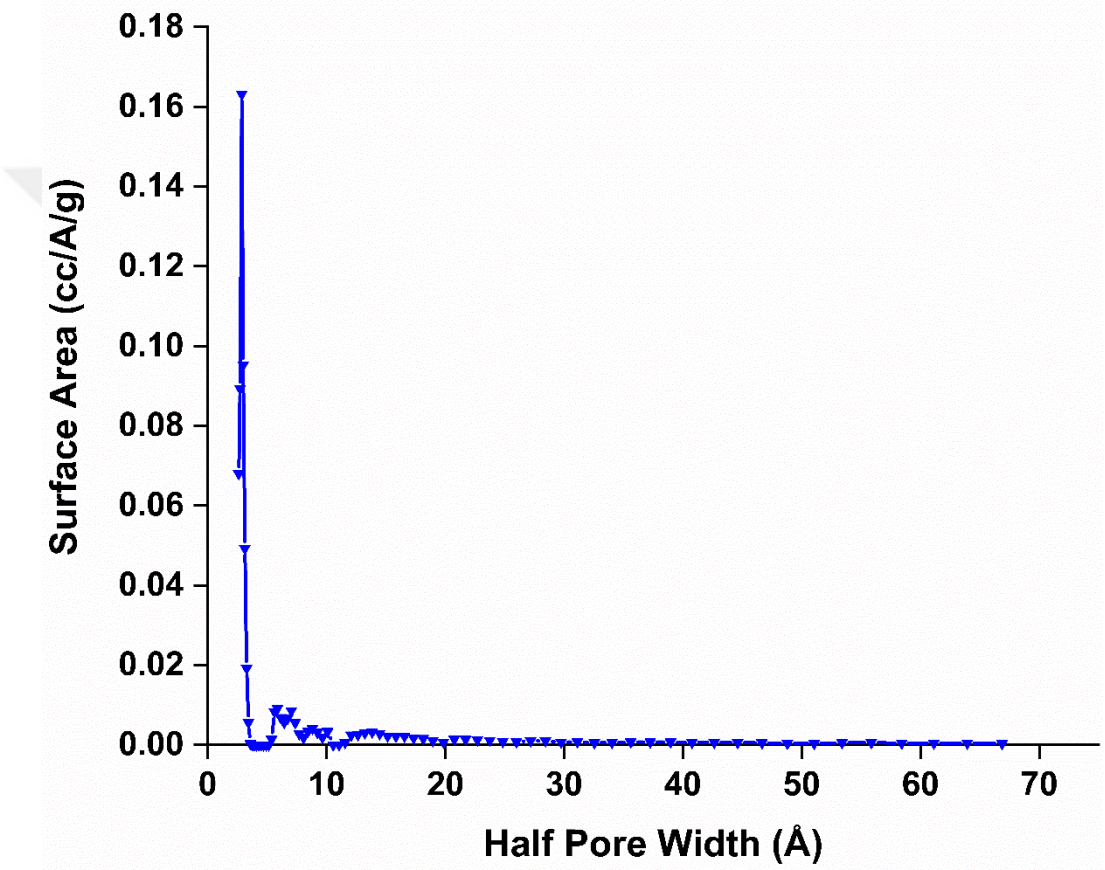

Figure 19. Pore size distribution of laser-assisted TPA – Silicalite-1 sample from BET isotherm.

4.1.5 Thermogravimetric Analyses

This analysis is common for zeolite characterization to determine the temperature for removal of structure directing agent (SDA), which is TPA in this study, and the amount of adsorbed water by zeolite. As explained previously, SDA in the pores

of TPA-silicalite-1 is an organic cation and it can be ignited at around 330 °C.[78] In addition to that, zeolite can capture water molecules in its pores and release it upon heating. Therefore, to calculate the yield of the synthesis, TGA analyses are need to be done to determine the weights of SDA and adsorbed water in the pores (the details can be found in chapter 4.4.2).

The TGA analyses were performed under air flow in the range of 25 to 900 °C, with a 5 °C/minute heat flowrate. The Differential Thermal Analysis (DTA) curve is obtained from data gathered through thermogravimetric analysis via differentiation. Origin software tools were used for this purpose. The DTA curve show temperature values for water and SDA removals from the structure. Three samples have been examined: the sample synthesized via laser-assisted synthesis method (Figure 20), the sample synthesized via the hydrothermal synthesis method before (Figure 21) and after calcination at 445°C for 3 hours (Figure 22).

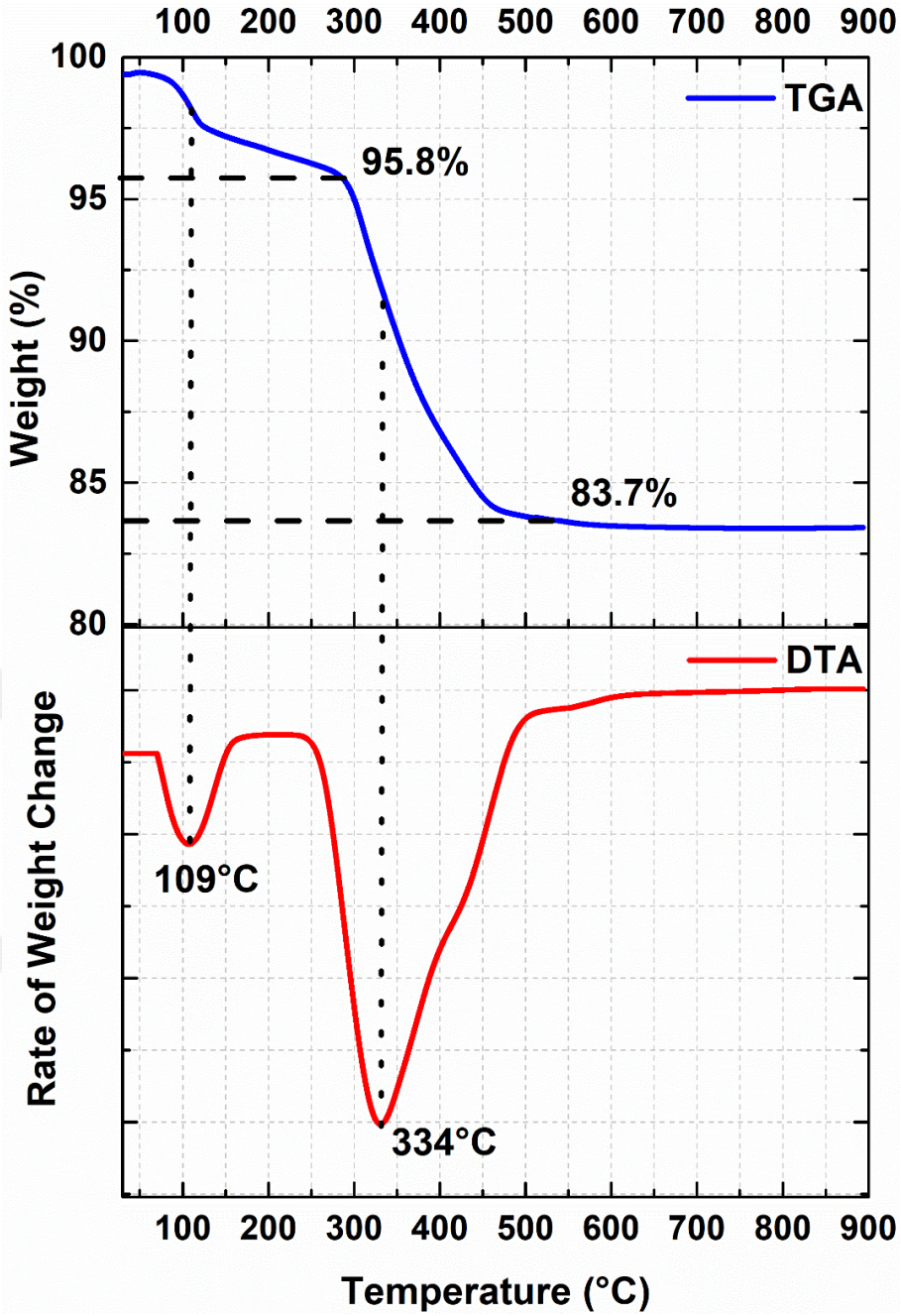

Figure 20. TGA-DTA graph of TPA – Silicalite-1 zeolite synthesized via the laser-assisted method for the batch with M1 molar formula (without calcination).

Figure 20 shows TGA and DTA curves in the range of 25 – 900 °C with a 5°C heating rate for the sample synthesized via the laser-assisted method (exp. code: C12). The first ramp in the TGA curve and corresponding DTA peak show removal of water,

while the second ramp and its related peak correspond to TPA content within the structure. From the analysis, water and TPA contents were found to be 4.2 % and 12.1 %, respectively.

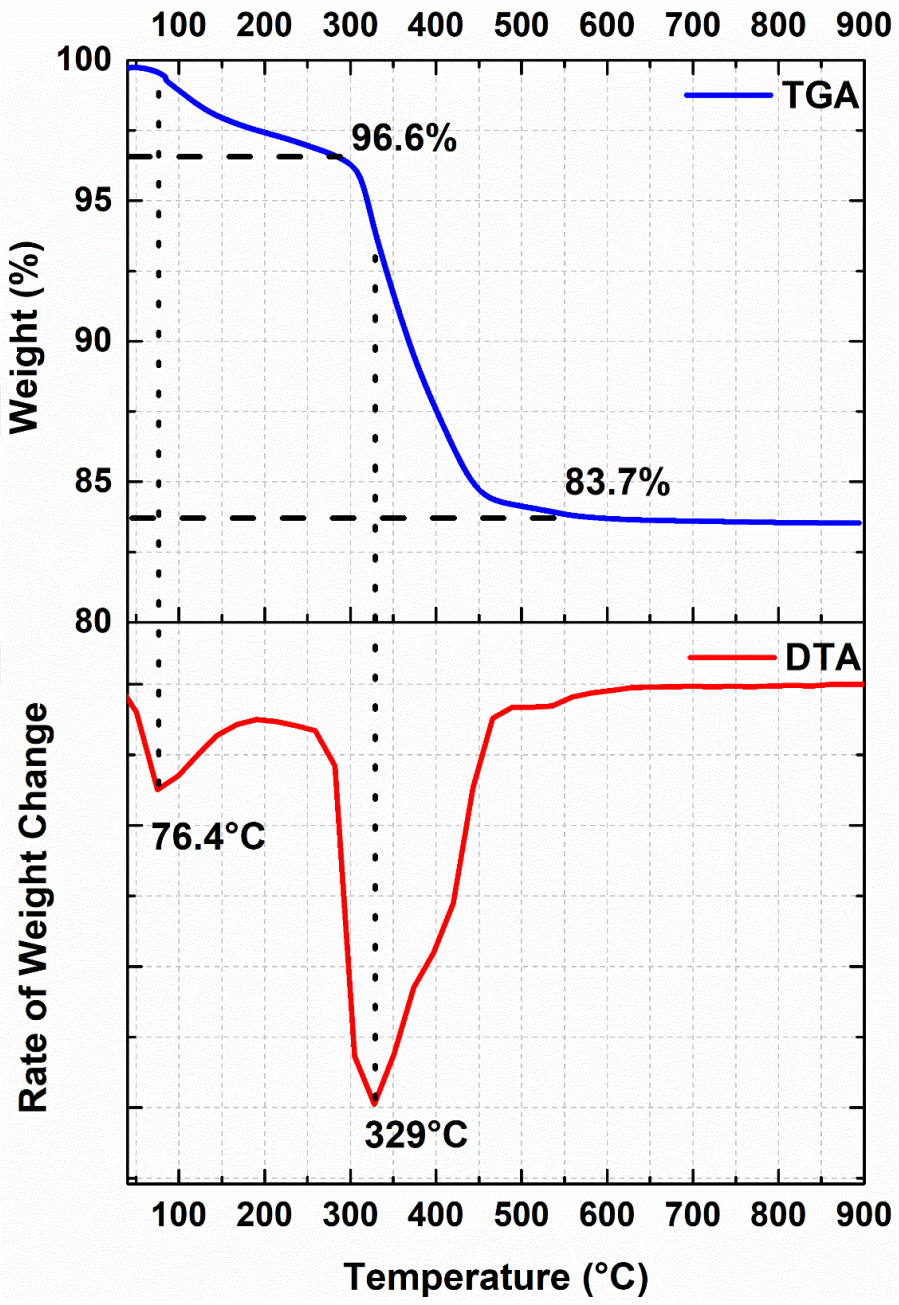

Figure 21. TGA-DTA graph of TPA – Silicalite-1 zeolite synthesized via the hydrothermal method for the batch with M1 molar formula (without calcination).

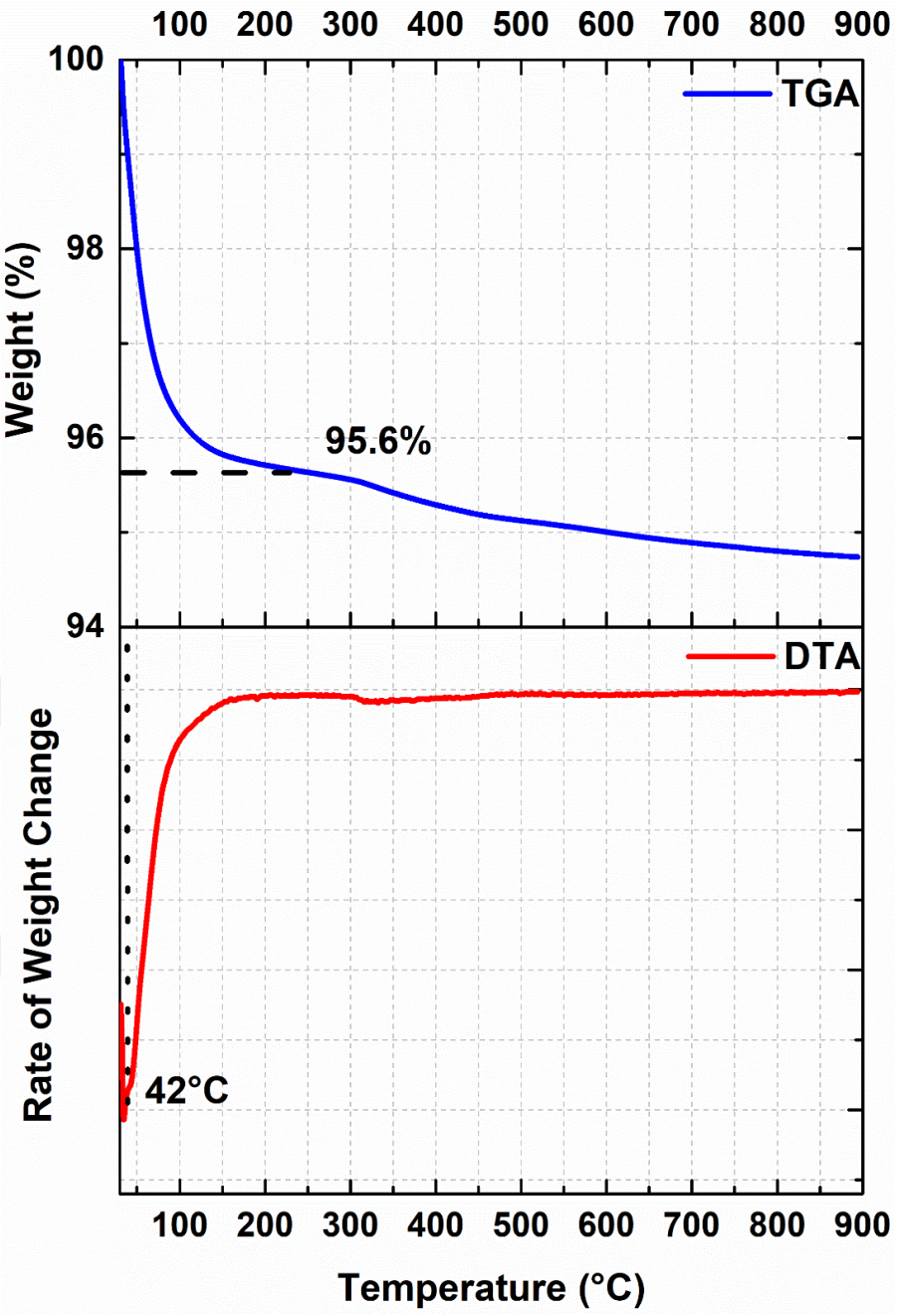

Figure 22. TGA-DTA graph of Silicalite-1 zeolite synthesized via the hydrothermal method for the batch with M1 molar formula (after calcination).

Figure 21 depicts TGA and DTA curves in the range of 25° – 900° C with a 5° C/min heating rate for the sample synthesized via the hydrothermal method (exp. code: A1-C14). From the analysis, corresponding water and TPA contents were found to be 3.4 % and 12.9 %. Figure 22 shows TGA and DTA curves for the same sample in

Figure 21 after calcination at 445 °C. During calcination, TPA is removed from the structure, and hence, only a single ramp and peak are observed. The water content of the calcined sample was found to be 4.4 % of the total weight.

Comparing two samples synthesized by hydrothermal and laser-assisted method, corresponding water desorption and TPA contents within the pores are very similar. The weight losses in TPA – Silicalite-1 structures in other studies indicate similar behavior as well.[73,79]

4.1.6 Energy Dispersive X-ray Spectroscopy

Elemental analysis of zeolite crystals synthesized via laser-assisted method has been carried out through EDX. Obtained TPA – Silicalite-1 zeolites were calcined to get rid of TPA content. Silicalite-1 zeolite has a chemical formula of SiO_2. The powder was sprinkled on carbon tape covering the aluminum grid, no conductive coating was used. Analyses were performed on 10 kV with a spot size of 4 at a magnification of 5000. Silicon and Oxygen weight percentages were measured and divided to corresponding atomic mass (AMU Si = 28.09, AMU O = 16.0) to find molar percentages. Three independent measurements were performed. Results of these three measurements and their average are given in Table 7. The average Si/O ratio found is different from the theoretical value of ½ by 7.5%

Table 7. Elemental analysis of Silicalite-1 synthesized via the laser-assisted method.

Measurement No	**Weight Percentage**		**Molar Percentage**		**Result**
	Si	**O**	**Si**	**O**	
1	41.62	46.21	1.48	2.89	**$SiO_{1.95}$**
2	48.74	51.26	1.73	3.21	**$SiO_{1.86}$**
3	50.31	49.69	1.79	3.11	**$SiO_{1.74}$**
Average					**$SiO_{1.85}$**

4.2 Crystallinity and Yield of TPA – Silicalite-1 Synthesized via Femtosecond Laser-assisted Method

4.2.1 Crystallinity of TPA – Silicalite-1

To calculate the crystallinity of a zeolite synthesized by laser-assisted method, XRD patterns are used. Each sample weighed in equal amount (2 mg) by using assay balance and powder patterns obtained keeping measurement parameters the same each time. Once powder pattern is obtained, the baseline is subtracted and areas under each characteristic peak are determined through the Origin software. Characteristic peaks are fitted using the Gaussian fitting function and the results of fitting for a sample synthesized by the laser-assisted method is provided in Figure 23.

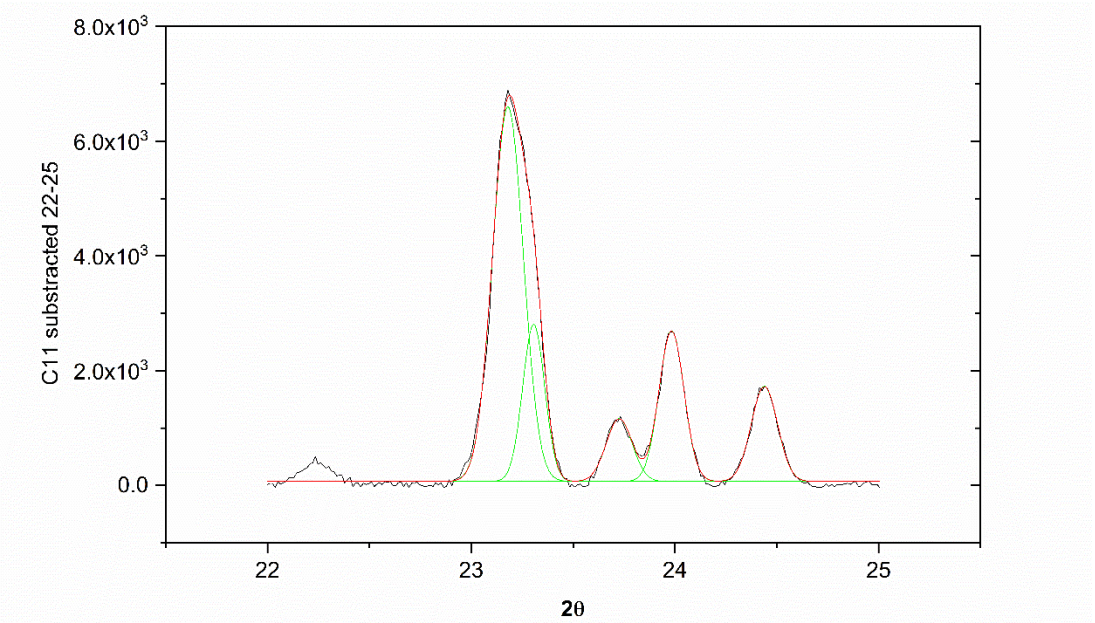

Fitting Results

Peak Index	Peak Type	Area Intg	FWHM	Max Height	Center Grvty	Area IntgP
1	Gaussian	1235.41762	0.17784	6526.14165	23.17974	50.46833
2	Gaussian	401.4232	0.14381	2622.35213	23.98299	16.39863
3	Gaussian	266.70879	0.15139	1655.01603	24.43867	10.89538
4	Gaussian	369.26642	0.12685	2734.6559	23.3063	15.08499
5	Gaussian	175.09064	0.15061	1092.10763	23.72605	7.15267

Figure 23. Peak analysis results for a sample synthesized via the laser-assisted method.

Since there are five characteristic peaks for TPA – Silicalite-1 zeolite located in the 22-25° 2θ region of the diffraction pattern, areas of five peaks are summed for each

sample. Crystallinities of zeolites synthesized via laser-assisted method are determined taking the sample synthesized via laser-assisted method that have maximum achievable crystallinity as a reference. Then α, the crystallinity, calculated according to the equation below:

$$\alpha\ (\%) = \frac{\sum PA_{sample}}{\sum PA_{reference}} \cdot 100 \qquad (1)$$

where *PA* indicates peak area in the XRD pattern referring to the characteristic planes of the structure.

For the samples synthesized via the laser-assisted method, crystallinities were determined through this procedure, considering the sample synthesized via the laser-assisted method that have maximum achievable crystallinity as a reference.[2,35,65] Change of crystallinity with synthesis time for zeolites synthesized via laser-assisted method has been studied for the batch with M1 molar formula (M1: 25 SiO_2: 9 TPAOH: 1450 H_2O: 100 EtOH). Per each independent trial sample synthesized via laser-assisted synthesis method, 80 µl of precursor suspension prepared with M1 molar formula exposed to the laser. If the sample synthesized via laser-assisted method that have maximum achievable crystallinity, is taken as 100% crystalline, crystallinities of TPA – Silicalite-1 zeolites synthesized via laser-assisted method are listed in Table 8. The values for crystallinities are average of at least three experiments. Since the yield of syntheses with 70 and 90 minutes of reaction time is low, several experiments were conducted (~7) per each data point. After 240 minutes of laser treatment, crystallinity reach a saturation value of 100%.

Table 8. Change of crystallinity (%) with synthesis time for TPA – Silicalite-1 zeolite synthesized via the laser-assisted method

Synthesis Time (minute)	**α – Crystallinity % (± error)**
70	48.1
90	55.0
120	62.3 (± 2.5)
150	69.6 (± 3.6)
180	77.9 (± 6.4)
200	87.8 (± 1.2)
220	96.6 (± 3.1)
240	99.0
260	98.8
280	99.2
300	100

Powder sample can be collected for laser-assisted synthesis method after 70 minutes of synthesis time when 80 µl of precursor suspension is irradiated by laser. When synthesis time is 200 minutes or higher, crystallinities of samples synthesized via laser-assisted method are higher compared to the sample synthesized via hydrothermal method. The degree of crystallinity seems to reach a saturation value for 240 minutes and higher synthesis times.

4.2.2 Yield of TPA – Silicalite-1 Synthesized via Femtosecond Laser-assisted Method

The weight percent yield of the synthesis is determined from the initial amount of silica within batch suspension and the final weight of the powder obtained post synthesis. Taking 80 µl of a batch with M1 molar formula as a basis, the amount of silica present in the solution is:

$$M_{SiO_2} \cdot V_{sol} = 0.75\ M \cdot 80\ \mu l = 60\ \mu mol$$

$$MW_{SiO_2} \cdot 60\ \mu mol = 3.6\ mg$$

where M_{SiO_2} is molarity of silicon dioxide in batch solution (Table 4 in section 3.3), V_{sol} is the total volume of the solution and MW_{SiO_2} is molecular weight of the silicon dioxide (MW_{SiO_2} = 60.08 g/mol). The weight percent yield of the synthesis was calculated from the weights of SiO_2 in suspension forming the batch and the products. The equation below will be used to calculate weight percent yield. Knowing these, the yield of synthesis is determined as:

$$Yield\ (wt.\%) = \frac{Weight\ of\ Product\ (mg)}{\text{Weight of } SiO_2 \text{ in Batch } (mg)}\ x\ 100$$

To calculate the weight of the product, TGA analysis was carried out and the amount of zeolitic water adsorbed was determined as shown in chapter 4.1.5. In Figure 9, TGA – DTA analysis of the laser-assisted sample is provided where two peaks in the DTA graph at 109° and 334° C correspond to vaporization of water and TPA present within the pores. The amount of water and TPA present within the powder obtained after centrifugation was found to be 4.2% and 12.1% of total mass, respectively. Then, the weight of the SiO_2 that is obtained as the product is determined from:

$$Weight\ of\ Product\ (mg) = 3 \cdot (0.837) = 2.51$$

The yield of the synthesis on SiO_2 basis for the laser-assisted method is:

$$Yield\ (wt.\%)\ = \frac{2.51\ mg}{3.6\ mg}\ x\ 100 = 69.7\ \%$$

Using the same approach, the weight percent yield of hydrothermal synthesis can be found. From TGA – DTA analysis carried out for hydrothermal synthesis, after removal of water and TPA within the pores, corresponding weight changes were found to be 3.4% and 12.9%, respectively. In total, 16.3% should be subtracted from the measured weight to find the yield of hydrothermal synthesis. The measured weight of hydrothermal synthesis was found 59.5 mg, taking 1600 µl of a batch as a basis. Then the weight of zeolite after subtracting water and TPA content is:

$$59.5\ mg\ \cdot 83.7\% = 49.8\ mg$$

The molarity of SiO_2 in M1 molar solution is 0.75 M (Table 10 in section 3.3 Sample preparation). The total weight of SiO_2 in 1600 µl of batch suspension is:

$$1600\ \mu l \cdot 0.75\ M = 1200\ \mu mol$$

$$MW_{SiO2} \cdot 1200\ \mu mol = 72\ mg$$

where MW_{SiO2} is molecular weight of the silicon dioxide (MW_{SiO2} = 60.08 g/mol). The weight percent yield of the hydrothermal synthesis is:

$$Yield\ (wt.\%)\ = \frac{Weight\ of\ Product\ (\mathrm{mg})}{\text{Weight of } SiO_2 \text{ in Batch } (mg)}\ x\ 100$$

$$Yield\ (wt.\%)\ = \frac{49.8\ mg}{72\ mg}\ x\ 100 = 69.2\ \%$$

Table 9. Comparison of weight percent yields of samples synthesized via hydrothermal (48 h reaction) and laser-assisted (3 h reaction) syntheses for the batch with M1 molar formula.

Molar Formula	**Hydrothermal Synthesis**	**Laser-Assisted Synthesis**
M1	**Yield (wt. %)**	**Yield (wt. %)**
	69.2	69.7

4.3 Decreasing Particle Size of TPA – Silicalite-1 Synthesized via Femtosecond Laser-assisted Method

This thesis was carried out mainly with the suspension prepared according to the M1 molar formula (i.e., M1: 25 SiO_2: 9 TPAOH: 1450 H_2O: 100 EtOH). It is known that different molar formulas, the molar ratio of source materials, lead to various zeolitic frameworks.[5,34,80,81] Moreover, reduction of water content for the same molar composition alters the alkalinity of precursor suspension, which results in decreased particle size. Persson et. al.[34] studied the effects of changing ratio of all contents (SiO_2, TPAOH, H_2O, EtOH) used in the synthesis of TPA – Silicalite-1 zeolite. Effects of decreasing water content of a molar composition are explained below:

(i) increase in the alkalinity of suspension;

(ii) as alkalinity increase, the linear growth rate of zeolite crystals decreases[34];

(iii) since the linear growth rate is lowered by higher alkalinity, resulting in particle size reduction as well;

(iv) it is also shown that in zeolite nucleation studies, change of alkalinity due to water content affects nucleation, higher alkalinity means higher nucleation rates.[17]

(v) decrease in water content means more silicate and SDA within the same volume of precursor suspension.

(vi) as water content increases, acidic sites shared between zeolite crystals and water transform into localized clusters, leading to an increase in crystal size as well.[34]

In the current study, proposed laser-assisted syntheses were also carried for M2 (M2: 25 SiO_2: 9 TPAOH: 480 H_2O: 100 EtOH) and M3 (M3: 25 SiO_2: 9 TPAOH: 450 H_2O: 100 EtOH) molar formulas. 100 nm and 90 nm-sized crystals are expected from hydrothermal syntheses of the precursor suspensions of M2 and M3 molar formulas, respectively.[34] Both hydrothermal and laser-assisted syntheses were carried out in our laboratory. The study aimed to examine if the crystal size will be smaller with increased alkalinity (i.e. lower water content in precursor suspension) while keeping Si/TPAOH ratio the same for the femtosecond laser-assisted synthesis method, as is the case for the hydrothermal synthesis method.

Preparation of precursor suspensions and further reaction steps applied for the samples with M1 molar formula, performed for these sets of reactions in the same way. 80 µl of precursor suspensions of M2 and M3 molar formulas exposed to laser for 3 hours where average power on glass-precursor interface and repetition rates of laser were set to 1.12 W and 200 kHz. Figures 23 and 24 show SEM images and particle size distribution profiles for the samples synthesized with hydrothermal and laser-assisted methods with M2 and M3 molar formulas.

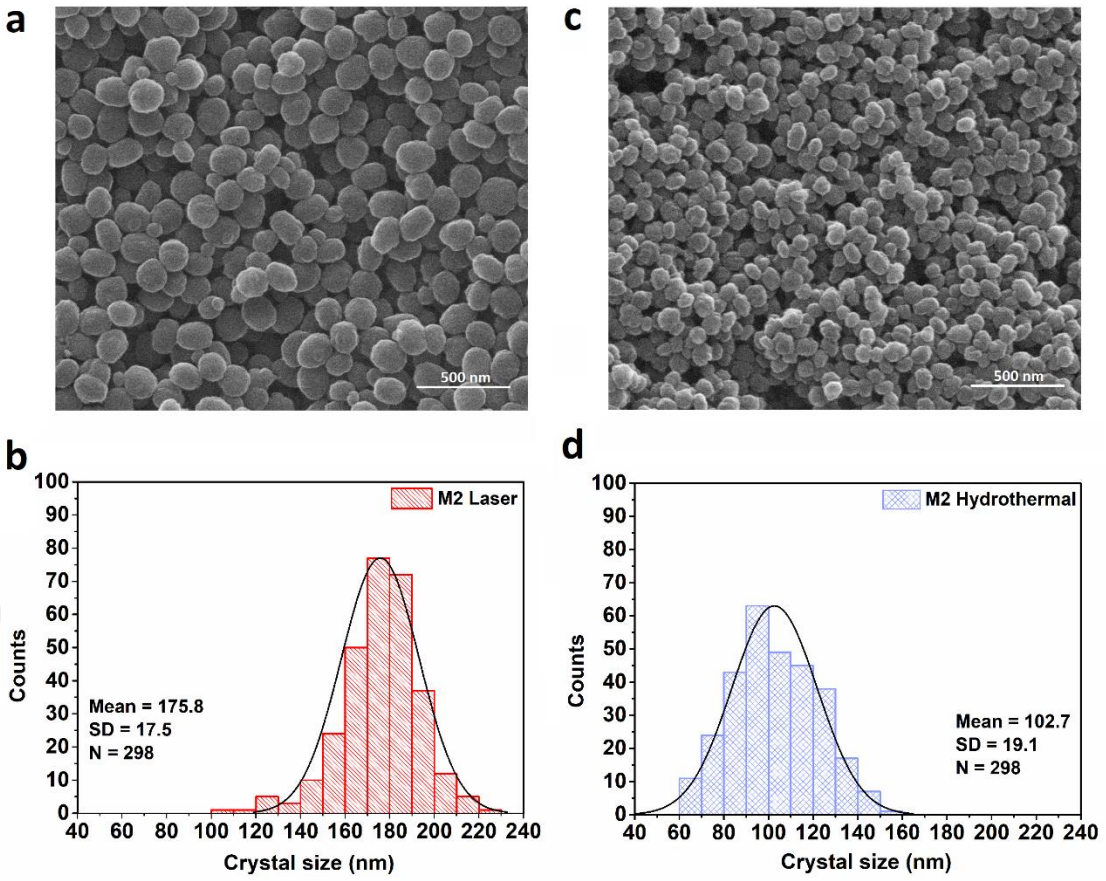

Figure 24. SEM image (a) and particle size distribution (b) of the TPA – Silicalite-1 crystals synthesized via the laser-assisted method (Exp code: C51, 3h reaction, 1.12 W average laser power on the glass-precursor interface, 200 kHz repetition rate, M2 molar formula); SEM image (c) and particle size distribution (d) of the TPA – Silicalite-1 crystals synthesized via the hydrothermal method (Exp code: A4 – C51, 30h reaction at 90 °C oven, M2 molar formula).

The average size of the TPA – Silicalite-1 crystals determined from SEM images by using Image J software are 102.7 nm and 175.8 nm for hydrothermal and laser-assisted syntheses with M2 molar formula. Standard deviations were found to be 17.5 nm (10.0 %) and 19.1 (18.6 %) nm for laser-assisted and hydrothermal methods, respectively. Similar to synthesis with the molar formula of M1, laser-assisted synthesis gives rise to larger zeolite crystals compared to hydrothermal synthesis (119.8 nm larger).

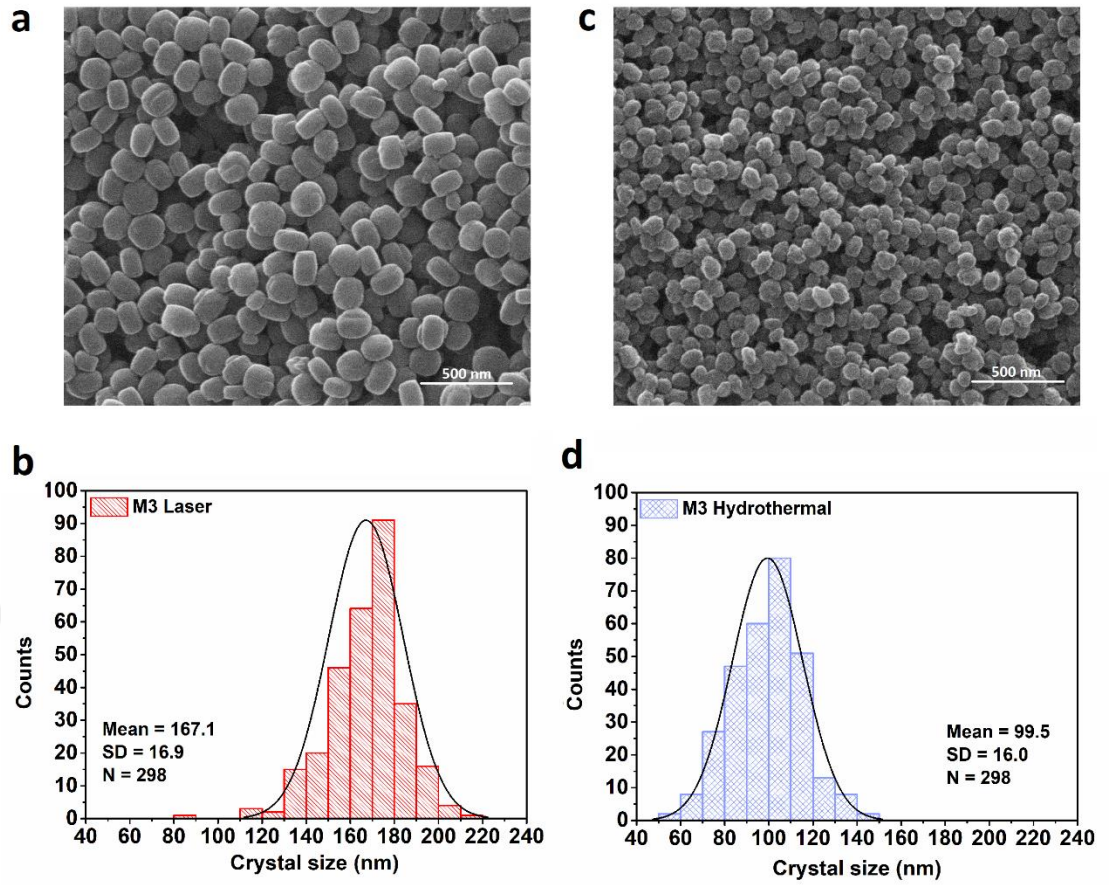

Figure 25. SEM image (a) and particle size distribution (b) of the TPA – Silicalite-1 crystals synthesized via the laser-assisted method (Exp code: C52, 3h reaction, 1.12 W average laser power on the glass-precursor interface, 200 kHz repetition rate, M3 molar formula); SEM image (c) and particle size distribution (d) of the TPA – Silicalite-1 crystals synthesized via the hydrothermal method (Exp code: A5 – C52, 30h reaction at 90 °C oven, M3 molar formula).

A similar phenomenon on size distribution occurs when TPA – Silicalite-1 crystals are synthesized using precursor suspension with M3 molar formula. In the case of the laser-assisted synthesis method, the average size of the TPA – Silicalite-1 crystals determined from SEM images by using Image J software is 167.1. The average size of crystals is bigger compared to the sample synthesized by the hydrothermal method which is 99.5. Standard deviations were found to be 16.9 nm (10.1 %) and 16.0 nm (16.1 %) nm for laser-assisted and hydrothermal methods, respectively. Once again, the

noticeably different SD of the samples proves the observation of narrower particle size distribution for the laser-assisted method.

Figure 26 depicts XRD patterns of TPA – Silicalite-1 samples synthesized by laser-assisted and hydrothermal methods, both with batches of M2 and M3 molar formulas and Silicalite-1 reference XRD pattern obtained from the IZA webpage. Table 10 summarizes intensity and FWHM values of characteristic XRD peaks for TPA – Silicalite-1 crystals synthesized by laser-assisted and hydrothermal methods, both for M2 and M3 molar formulas. For the same characteristic peaks, intensity values seem to be lower for samples of the laser-assisted method. Lower intensity values for zeolite crystals via laser-assisted synthesis methods indicate 3 hours of reaction times are not sufficient for 80 µl of precursor suspension with M2 and M3 molar formulas. Besides, FWHM values indicate that XRD peaks are narrower for the laser-assisted method, proving the phenomenon observed for particle size analyses from SEM images for M2 and M3 molar formulas.

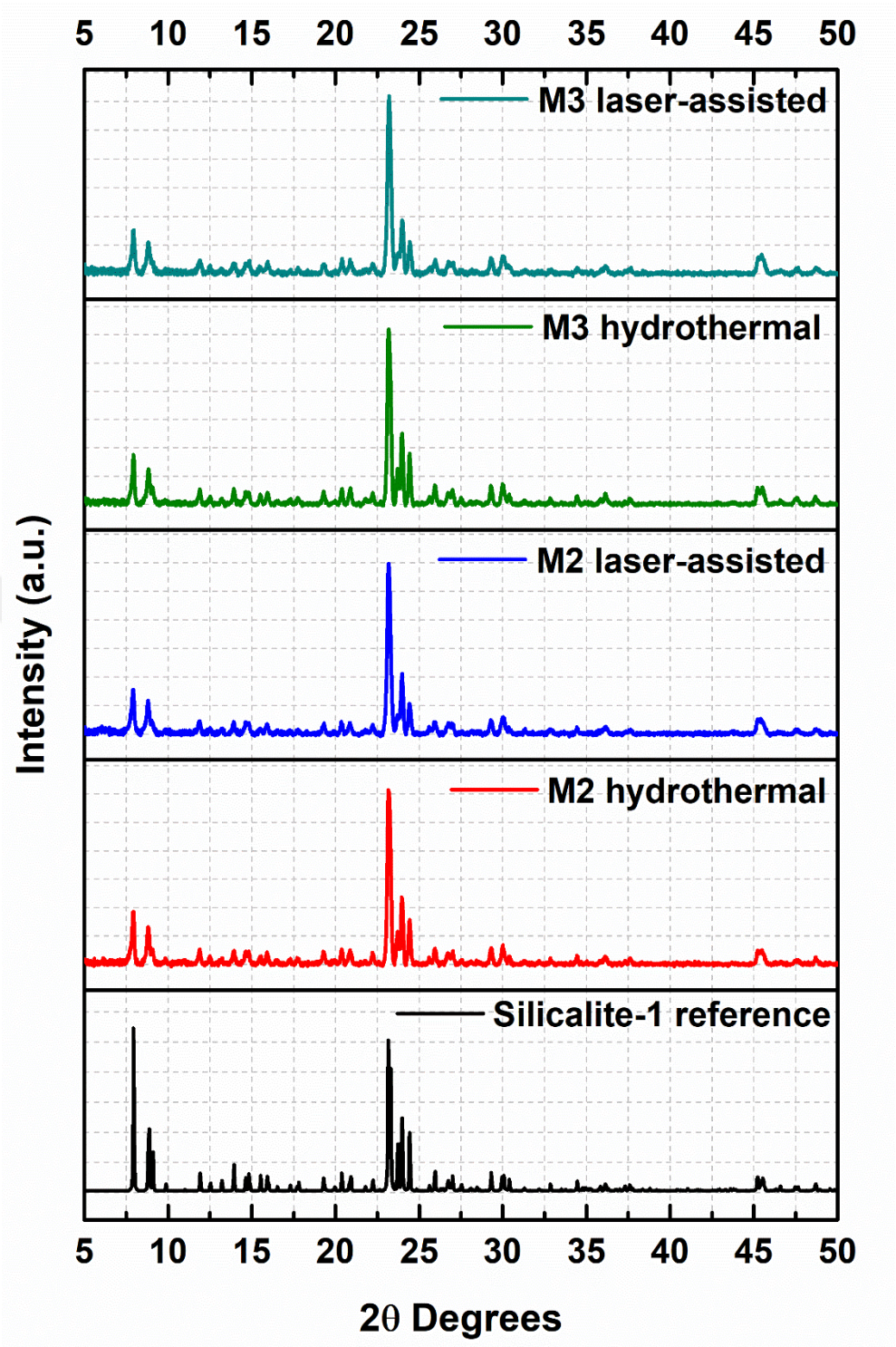

Figure 26. XRD patterns **(a)** hydrothermal synthesis (Exp code: A4 – C51, 30h reaction at 90 °C oven, without calcination) vs. **(b)** laser-assisted synthesis (Exp code: C51, 3 h reaction, M2 molar formula suspension, 1.12 W average laser power on the sample, 200 kHz repetition rate).

Table 10. Comparison of intensity and FWHM of the Bragg peaks of the samples synthesized via hydrothermal and femtosecond laser-assisted methods for the batches with M2 and M3 molar formulas. To compare intensities of the samples, 2 mg powder was measured from each experiment and XRD analyses were performed with the same conditions (int. and a.u. indicate intensity and arbitrary units).

	Hydrothermal Synthesis of M2		**Laser-assisted Synthesis of M2**		**Hydrothermal Synthesis of M3**		**Laser-assisted Synthesis of M3**	
Bragg Peaks (2θ°)	**Int. (a.u.)**	**FWHM**	**Int. (a.u.)**	**FWHM**	**Int. (a.u.)**	**FWHM**	**Int. (a.u.)**	**FWHM**
23.18	410	0.208	311	0.186	447	0.242	356	0.218
23.31	6142	0.246	5689	0.230	6489	0.257	5572	0.240
23.73	1155	0.234	638	0.176	1328	0.262	674	0.166
23.98	2366	0.161	2017	0.153	2620	0.168	1699	0.154
24.44	1571	0.190	1020	0.166	1905	0.189	1009	0.161

The weight percent yields for hydrothermal and laser-assisted syntheses of M2 and M3 molar formulas have been calculated. Product weights have been measured after centrifugation and drying, water and TPA contents found from TGA – DTA and subtracted from weighed amounts for yield calculation. TGA – DTA plots for TPA – Silicalite-1 zeolites synthesized via the laser-assisted method for M2 and M3 molar formulas are provided in Appendix D. Crystallinity values determined from XRD plots according to the procedure explained in section 4.2.1. The resulting weight percent yield values, crystallinities, and average crystal sizes for hydrothermal and laser-assisted syntheses of M1, M2, and M3 molar formulas are given in Table 11.

Hydrothermal syntheses have been carried out following suggested synthesis procedures (Hedlund *et al.*, 1999 and Persson *et al.*, 1994).[34,62] First, reaction times for the laser-assisted samples in Table 11 were set to 3 hours. Lower wt. % yield values suggest that longer reaction times are needed for samples prepared with M2 and M3 molar formulas. As explained previously, this phenomenon is due to lower water

content and hence, lower linear growth rates which are explained in detail in section 4.2.1 of the thesis.[34,82,83] Crystallinity (%) and wt. % yield values calculated and provided in Table 11.

Table 11. TPA – Silicalite-1 hydrothermal and laser-assisted synthesis comparison. The average particle sizes of the crystals were determined from SEM images by using Image J software. SD indicates standard deviation. The sample size (N) for particle size distribution analyses was set to 298.

Synthesis Method	Exp. Code	Molar Formula	Average Crystal Size ± SD (nm)	Avg. Laser Power (W)	Reaction Time (h)	Repetition Rate (kHz)	Crystallinity (%)	Yield (wt %)
Hydrothermal	A1-C14	M1	203.8 ± 50.3	-	48	-	**100**	69.2
Hydrothermal	A4-C51	M2	102.7 ± 19.1	-	30	-	**100**	59.9
Hydrothermal	A5-C52	M3	99.5 ± 16.0	-	30	-	**100**	56.6
Laser-assisted	C12	M1	323.6 ± 35.2	1.12 W	3	200	**91 ***	69.7
Laser-assisted	C51	M2	175.8 ± 17.5	1.12 W	3	200	**89 ***	55.6
Laser-assisted	C52	M3	167.1 ± 16.9	1.12 W	3	200	**81 ***	41.7

***** Samples synthesized via hydrothermal method are taken as reference for crystallinity calculations, i.e. A1-C14 is reference for M1, A4-C51 is reference for M2 and A5-C52 is reference for M3 molar formulas.

4.4 Scale-up of TPA – Silicalite-1 Zeolite Synthesis via Femtosecond Laser-assisted Method

The compatibility of the laser-assisted method for scale-up synthesis has been tested. The volume of precursor suspension used for TPA – Silicalite-1 synthesis via the laser-assisted method with the batch of M1 molar formula first increased from 80 µl to 400 µl (reaction time was to be 5 hours) and 600 µl (reaction time was set to be 6.5h). Types of glass vial and insert were Isolab N9 (1.5 ml, vial diameter = 11 mm, and compatible glass insert with diameter = 6 mm) and N13 (4 ml, vial diameter = 15 mm, and compatible glass insert, diameter = 8 mm), respectively. When volumes of precursor suspension used increased, necessary reaction times to obtain zeolite crystals with similar properties increased as well, however, there is no linear correlation between the volume of precursor solution and reaction time (Figure 28).

It is observed that when the volume of suspension (for M1 molar formula) increased to 400 µl, the first color change was observed after ~160 minutes, where the first color change was observed after ~70 minutes when 80 µl of precursor suspension was used previously, i.e. induction period increased from 70 to 160 minutes. The average crystal sizes, crystallinities, and wt. % yield values were calculated, results are summarized in Table 12. Yield (wt. %) values were found after subtracting TPA content found from TGA analysis.

Table 12. Changes of average crystal size, crystallinity, and yield values with different volumes of precursor suspensions treated with the laser for varying times. SD indicates standard deviation. The sample size (N) for particle size distribution analyses was set to 109.

Sample Name	Reaction Time (h)	Volume of Precursor Suspension (µl)	Vial Type	Average Crystal Size ± SD (nm)	Crystallinity (%)	Yield (wt. %)
M1-80 µl	3	80	N9	333.8 ± 35.2	72	69.7
M1-80 µl	5	80	N9	445.8 ± 34.4	100	76.7
M1-400 µl	5	400	N13	299.3 ± 37.1	81	56.7
M1-600 µl	6.5	600	N13	291.1 ± 34.9	98	48.4
M2-80 µl	3	80	N9	175.8 ± 17.5	72	55.6
M2-300 µl	6	300	N13	123.1 ± 21.4	100	52.1

* The slight difference in average particle size values for M1-hydrothermal and M1-80 µl in Table 11 and Table 12 is due to analyzed sample sizes, i.e. N = 109 for Table 12 where N = 298 for Table 11.

**M1 and M2 in the sample names indicate the type of molar formula used for the precursor suspensions.

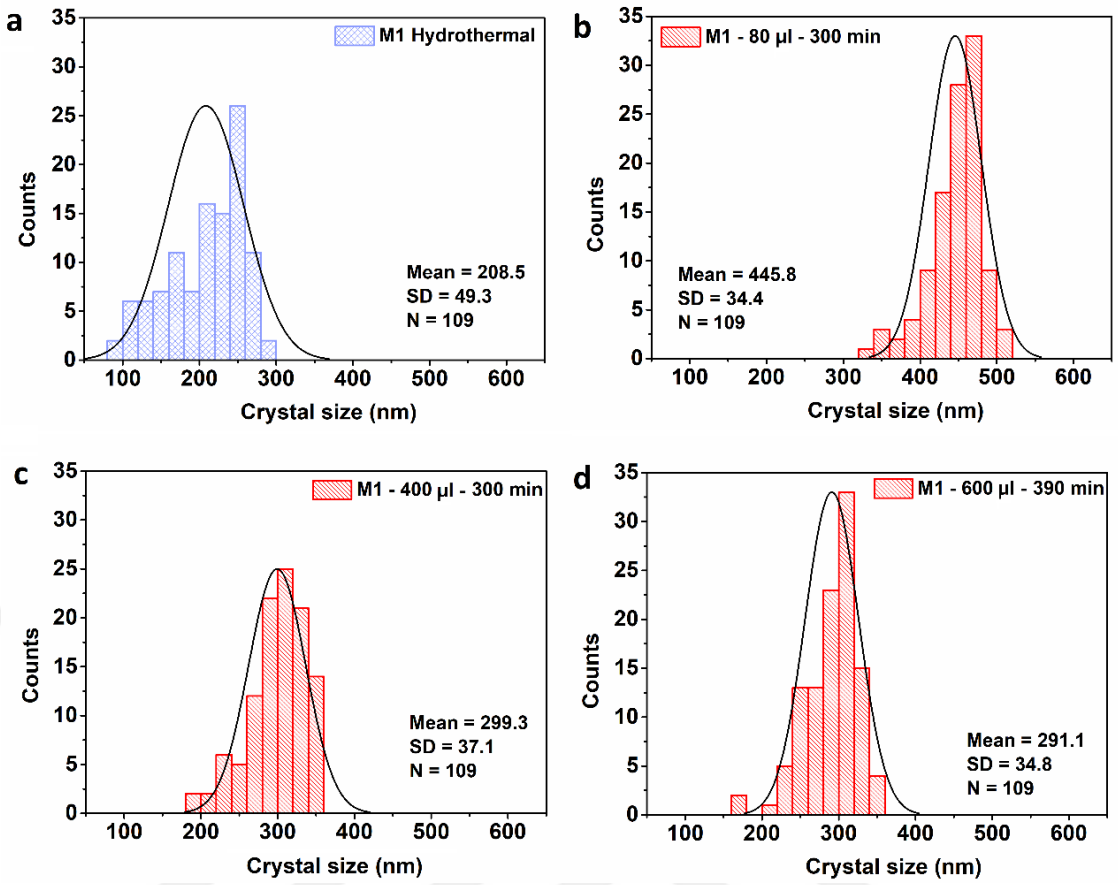

Figure 27. Particle size distribution analyses of TPA – Silicalite-1 synthesized via (a) hydrothermal and (b, c, d) laser-assisted methods. M1 indicates the suspension with M1 molar formula is used. 80, 400, 600 µl show volumes of the precursor suspensions. 300 min and 390 min indicate reaction times for laser-assisted syntheses. SD and N indicate standard deviation and sample size, respectively.

Although the volume of suspension increases 5 (for 400 µl) and 7.5 (for 600 µl) times compared to 80 µl precursor suspension, the necessary reaction time to obtain zeolite crystals with similar crystallinity and yield values do not have to increase in the same correlation (i.e., linearly) (Figure 28). This finding clearly shows that the laser-assisted synthesis method is compatible with scale-up. Besides, with proper equipment installed to the setup to get multiple laser beams (for example through the spatial light modulator, SLM), several spots in the precursor suspension can be irradiated with a laser at the same time. This can significantly lower the reaction time from several hours to several minutes.

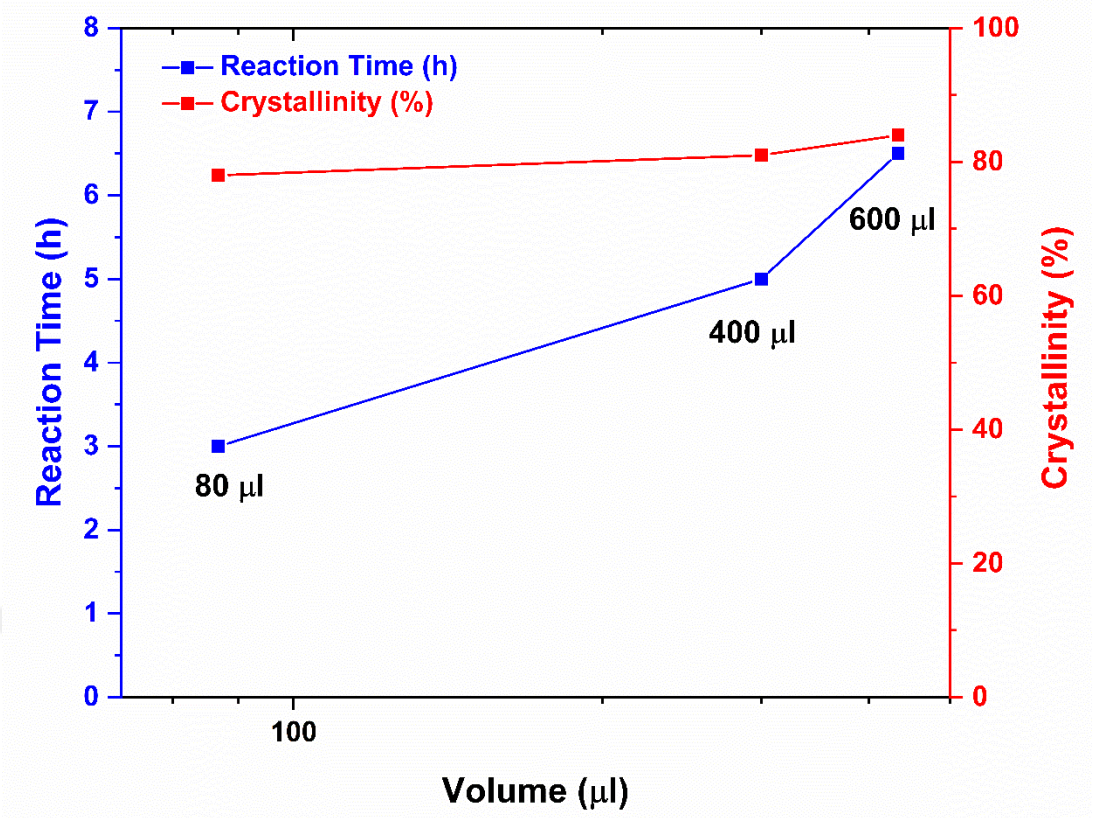

Figure 28. As the volume of precursor suspension used in laser-assisted synthesis increases, the necessary reaction time to obtain zeolite crystals with similar properties does not increase with a linear correlation. X (Volume) axis is presented in logarithmic scale.

4.5 Crystallization Kinetics of TPA – Silicalite-1 Synthesized via Femtosecond Laser-assisted Method

Nucleation and growth mechanisms of Silicalite-1 have been studied for decades to gain insight into general zeolite crystallization.[19,84–87] Several hypotheses have been postulated on the either classical or non-classical pathway is dominant on Silicalite-1 crystallization. While the classical pathway suggests aggregation of silica molecules leads into final zeolite crystals (Figure 29), the nonclassical route is about the direct attachment of nanoparticles (Figure 30).[84,85,88,89] In homogenous precursor suspensions where organic SDA is used, as is the case for precursor suspensions of M1, M2, and M3, silica oligomerization around hydrophobic SDA lead into primary units.[88]

In the previous sections of the thesis, the importance of the amount of water content in the precursor suspension is emphasized in a way that leads to an increase or decrease in the linear growth rate since it directly affects the nucleation stage as illustrated in Figure 29. Overlapping of hydrophobic silica oligomers and hydrophobic SDA molecules lead into nanosized primary units of zeolites. In the next stage, both classical and non-classical growth mechanisms are present. Several in-situ Atomic Force Microscopy, Small Angle X-ray Spectroscopy (SAXS) studies also revealed that 2D layer nucleation and spread of the layer through crystal surface are also present in zeolite growth (Figure 30).[84,85] Although current techniques allow us to study and understand growth kinetics, due to the time scale of processes taking place during the nucleation stage (e.g., silicate oligomerization reaction steps are in the femtosecond and picosecond range), in-situ analyses are not capable of detecting fast steps of nucleation.[17,84,85] The hydrothermal reactions were carried out between 24h and up to several days usually. Although the reaction time scale of silica polymerization-depolymerization reactions is in the range of femtosecond and picosecond ranges, the induction time, defined as the amount of time elapsed between the achievement of a supersaturated solution and the observation of crystals, of the zeolite reactions in hydrothermal synthesis is in the range of >15 hours or days. It makes it complex to analyze more than 40 polymerization-depolymerization reactions taking place simultaneously during this long period. In the current study, induction time is decreased to 70 min for 80 µl precursor suspension for the laser-assisted synthesis method.

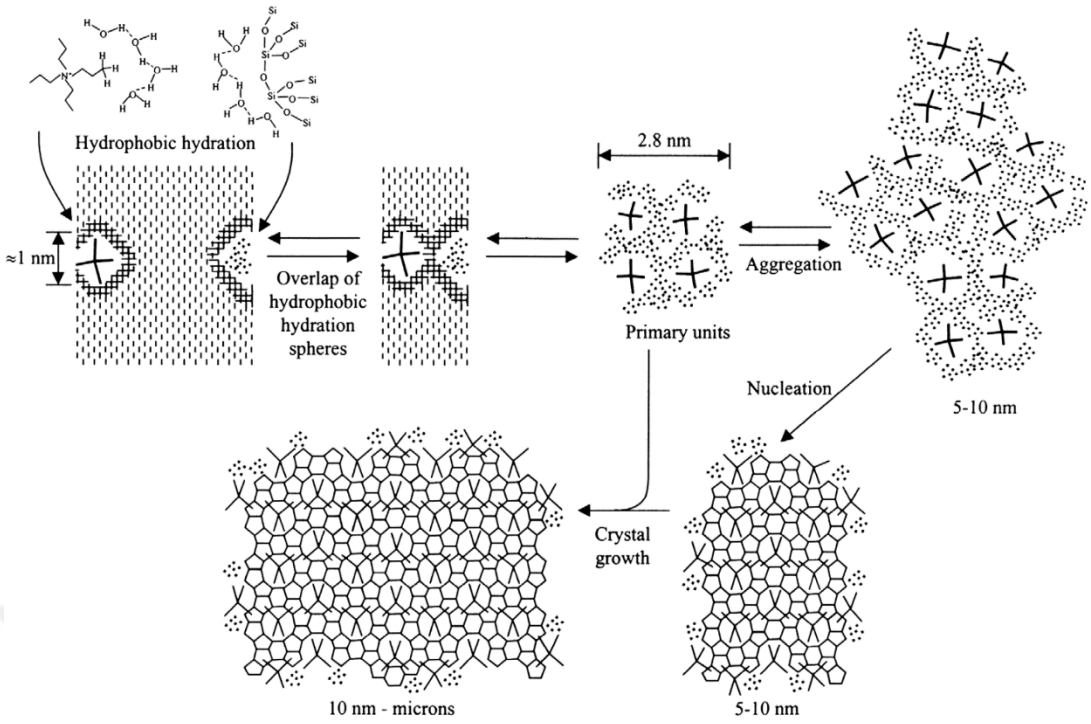

Figure 29. Schematic representation of crystallization mechanism for TPA – Silicalite-1 zeolite. Adapted from ref [88].

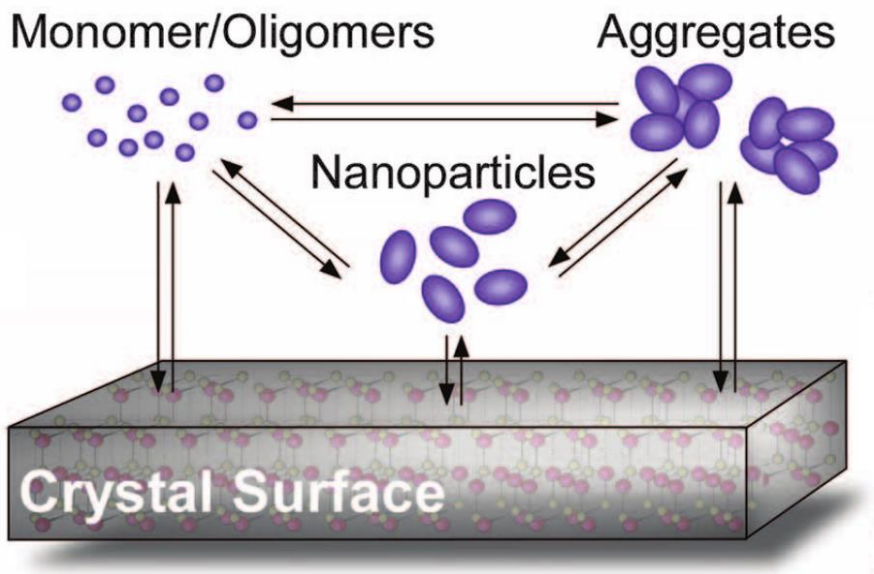

Figure 30. Precursor attachment to Silicalite-1 crystals, pathways of Silicalite-1 crystallization. Adapted from ref [84].

4.5.1 Scanning Electron Microscopy (SEM) and XRD Crystallinity

Crystallization and growth of the TPA – Silicalite-1 synthesized via laser-assisted method first observed through a color change of the transparent precursor suspension into opaque white solution. For 80 µl of precursor suspension, after ~70 minutes of laser exposure, the first color change can be observed, as exposure time gets longer, opacity increases (Figure 31).

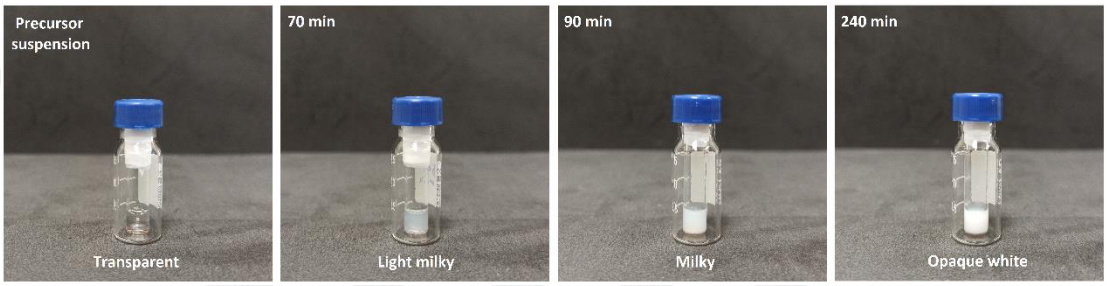

Figure 31. Photos of reaction bottles before (clear precursor suspension) and after 70, 90, and 240 minutes of laser-assisted syntheses.

For the laser-assisted synthesis method, crystallization kinetic studies of TPA – Silicalite-1 zeolite were carried out for 80 µl of precursor suspension with M1 molar formula. SEM images and XRD patterns of zeolite samples were collected for different reaction times (Figure 32 and Table 13). For lower reaction times (70, 90, 120, and 150 minutes), smaller nanosized particles along with zeolite crystals were observed from SEM images (Figure 32-a, b, c, d). After 180 minutes of laser exposure, fully crystalline zeolite crystals with an average particle size of 323.6 ± 35.2 nm (mean ± SD) nm were observed. For longer reaction times, crystal sizes increase and reach a saturation value of ~ 430 nm on average.

XRD crystallinity analyses were applied to samples synthesized with 70 min or longer reaction times since powder zeolite samples can be obtained after ~70 minutes of laser exposure. As the color of the initial transparent suspension turns to milky white,

the powder sample can be collected through the centrifugation. The dried powder samples were analyzed in terms of crystallinity through their X-ray diffraction patterns as explained in section 4.1.2 of the thesis. For the measurements to be comparable, ~ 2 mg of each sample was weighed before XRD analyses. For the samples synthesized with 70-min and 90-min reaction times, several syntheses were performed to collect enough amount of powder material (2 mg). The analyses details are summarized in Table 13.

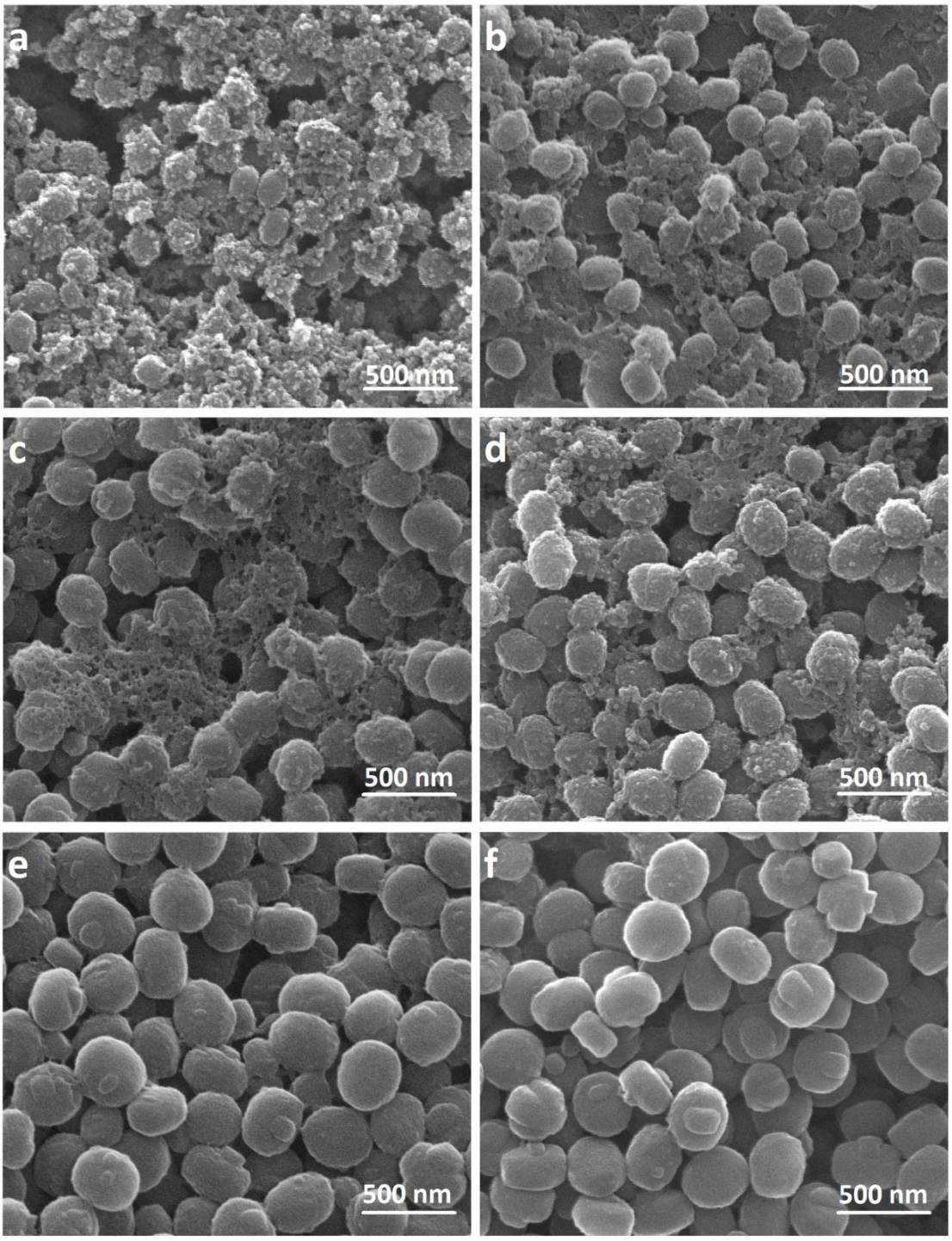

Figure 32. SEM images of laser-assisted syntheses with different reaction times. **a)** 70 min., **b)** 90 min., **c)** 120 min., **d)** 150 min., **e)** 180 min., **f)** 200 min. Before SEM analyses, samples were washed and centrifuged with deionized water for 4 times to lower the pH of the suspension to ~ 7 and dried at 45 °C oven

Table 13. Crystallinities and yield (wt. %) values of TPA – Silicalite-1 zeolite synthesized via the laser-assisted method for different reaction times. 80 µl precursor suspension of the batch with M1 molar formula used. The sample synthesized via the hydrothermal method was used as reference for crystallinity calculations. SD indicates standard deviation. The sample size (N) for particle size distribution analyses was set to 109.

Batch Molar Formula	**Crystallization Time (min)**	**Color of the Suspension**	**Yield * (wt. %)**	**Crystallinity (%)**
M1	70	Light Milky	9.3	48
	90	Milky	11.6	55
	120	Opaque white	46.5	62
	150	Opaque white	60.4	69
	180	Opaque white	69.7	78
	200	Opaque white	69.7	88
	220	Opaque white	74.4	96
	240	Opaque white	72.0	99
	260	Opaque white	74.4	98
	280	Opaque white	72.0	99
	300	Opaque white	76.7	100

* To calculate the yield of the syntheses, zeolitic water, and TPA contents determined from TGA subtracted from weighed amount.

To examine the growth stage of TPA – Silicalite-1 crystallization, crystallinity (%) vs. time graph is used. For the syntheses through conventional methods, the shape of this curve is similar to the one obtained for the laser-assisted synthesis of TPA – Silicalite-1 (Figure 33).

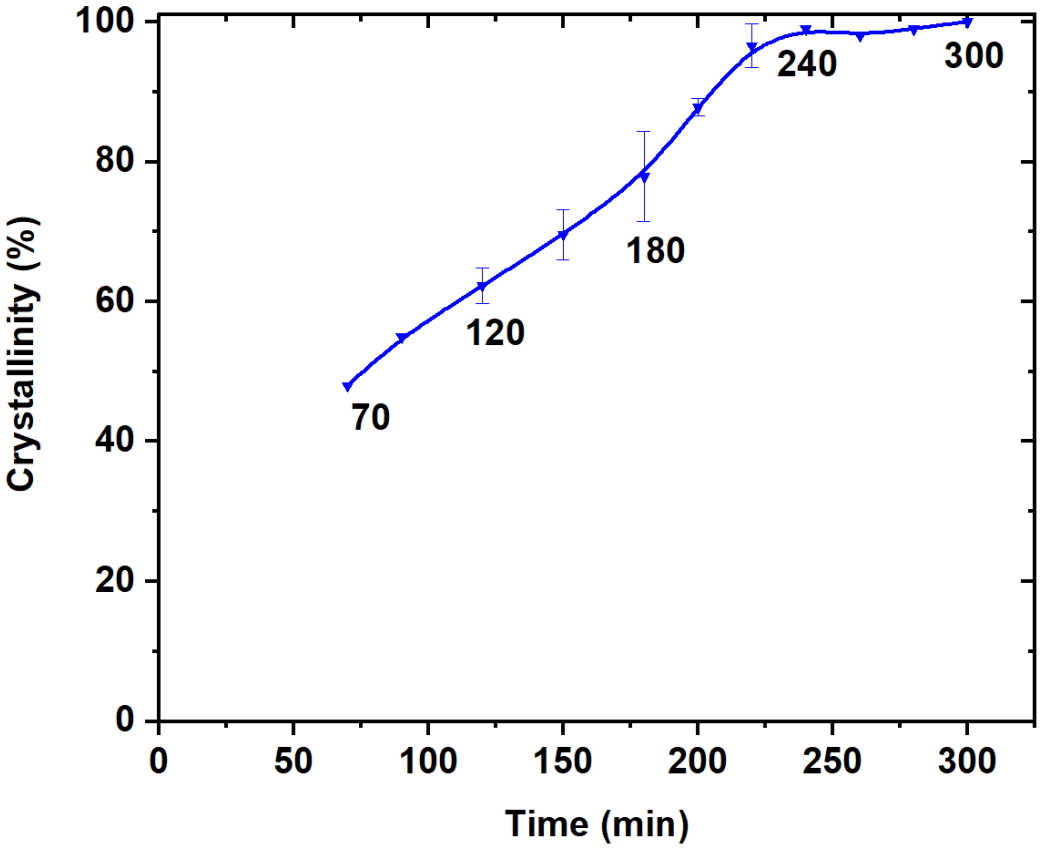

Figure 33. Crystallinity (%) vs reaction time graph for TPA – Silicalite-1 synthesized via the laser-assisted method. Crystallinities calculated from XRD powder pattern analyses relative to the sample synthesized via hydrothermal method.

Great efforts have been put to investigate and accelerate the crystallization process of zeolites.[90,91] In a study where UV light was used to accelerate crystallization processes of zeolites - such as Na-A, Na-X, and Silicalite-1, it is found that free hydroxyl radicals act as catalysts.[91] Similar phenomenon can be expected in laser-assisted synthesis method as well, where absorbed laser pulses by basic precursor

suspension would lead to an increase in the number of free hydroxyl radicals. In the hydrothermal crystallization of zeolites from basic media, hydroxide ions (OH^-) catalyse the depolymerization of the aluminosilicate gel by breaking the Si/Al-O-Si/Al bonds and catalyse the polymerization of the aluminosilicate anions around the hydrated cation species by remaking the Si/Al-O-Si/Al bonds.

4.5.1.1 Saturation of Crystal Growth

Crystallinity analyses through XRD patterns indicate that crystal growth reaches a saturation value after 240 min. reaction time, when 80 µl of precursor suspension of M1 molar formula used in TPA – Silicalite-1 synthesis for laser-assisted method. The yield (wt. %) values also support the results of crystallinity analyses on saturation of growth. Particle size distribution analyses were performed for the samples synthesized with 240 minutes and longer reaction times. The average crystal sizes were found to be 427.1 ± 34.1, 432.7 ± 39.1, 404.8 ± 36.5, 445.8 ± 34.4 (mean ± SD, N=109) for 240 min., 260 min., 280 min., and 300 min. reaction times. Similar average particle size (~ 430 nm) values showed that crystal growth reached saturation.

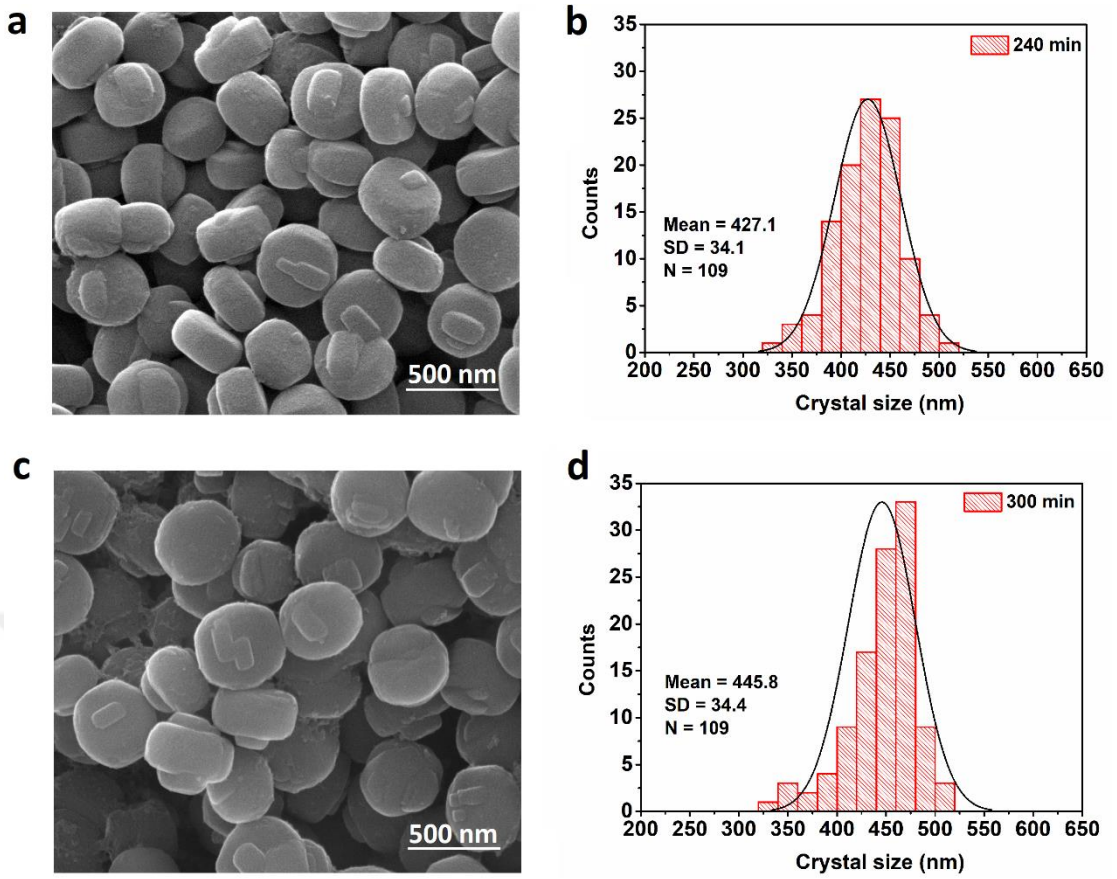

Figure 34. SEM image (a) and particle size distribution analysis (b) of TPA – Silcalite-1 synthesized via the laser-assisted method with 240 minutes reaction time; SEM image (c) and particle size distribution analysis (d) of TPA – Silcalite-1 synthesized via the laser-assisted method with 300 minutes reaction time.

4.5.2 Attenuated Total Reflectance – Fourier-transform Infrared Spectroscopy Analysis

As discussed in chapter 4.5.1, the crystallinity of the sample synthesized via laser-assisted method could be calculated from XRD patterns after reaction times of 70 minutes since it can be collected by centrifugation after this reaction time as the color of the suspension changes from transparent to milky white (Figure 31). To examine the nucleation period before the reaction time of 70 min. (i.e., where first zeolite crystal growth starts), Attenuated Total Reflectance – Fourier-transform Infrared Spectroscopy analysis was conducted.

The characteristic vibration of Silicalite-1 occurs at 540 – 550 cm^{-1} on the IR band, corresponding to double five-membered ring.[69,92–94] In the full IR spectrum of Silicalite-1, the peak around 470 cm^{-1} is associated to typical Si – O – Si bending, and the intensity ratio of 550 cm^{-1} peak to 470 cm^{-1} is used to determine the crystallinity of the powder sample.[69,93,94] Attenuated Total Reflection technique enables the determination of IR spectrum for solid samples dispersed in a liquid medium. The liquid sample is dropped on a diamond tip, the IR light is reflected at the liquid–diamond interfaces, and an evanescent field is formed. Through the evanescent field, light can interact with samples at the interface, and absorption measurement can be made. It has been recently reviewed that, ATR – FTIR is a promising tool to study especially heterogeneous catalysts in water.[95] Travelling pathway of IR light in water medium is minimized and measurement takes place at the liquid solution – solid tip interface.

The IR spectra of TPA – Silicalite-1 samples synthesized via laser-assisted method have been measured through ATR – FTIR. Figure 34 (a) illustrates IR spectra of amorphous SiO_2 (Stober Silica), Silicalite-1 dispersed in water, and powder Silicalite-1 between 400-1350 cm^{-1}. The absorption bands at ~1200 and 550 cm^{-1} are not observed for amorphous SiO_2 (Stober Silica) since they are associated with Silicalite-1 zeolite. Same absorption bands with the addition at ~900 cm^{-1} are observed for fully crystalline TPA-Silicalite-1 sample synthesized via the laser-assisted method (Figure 35b). The additional absorption band is associated with TPA.[94,96]

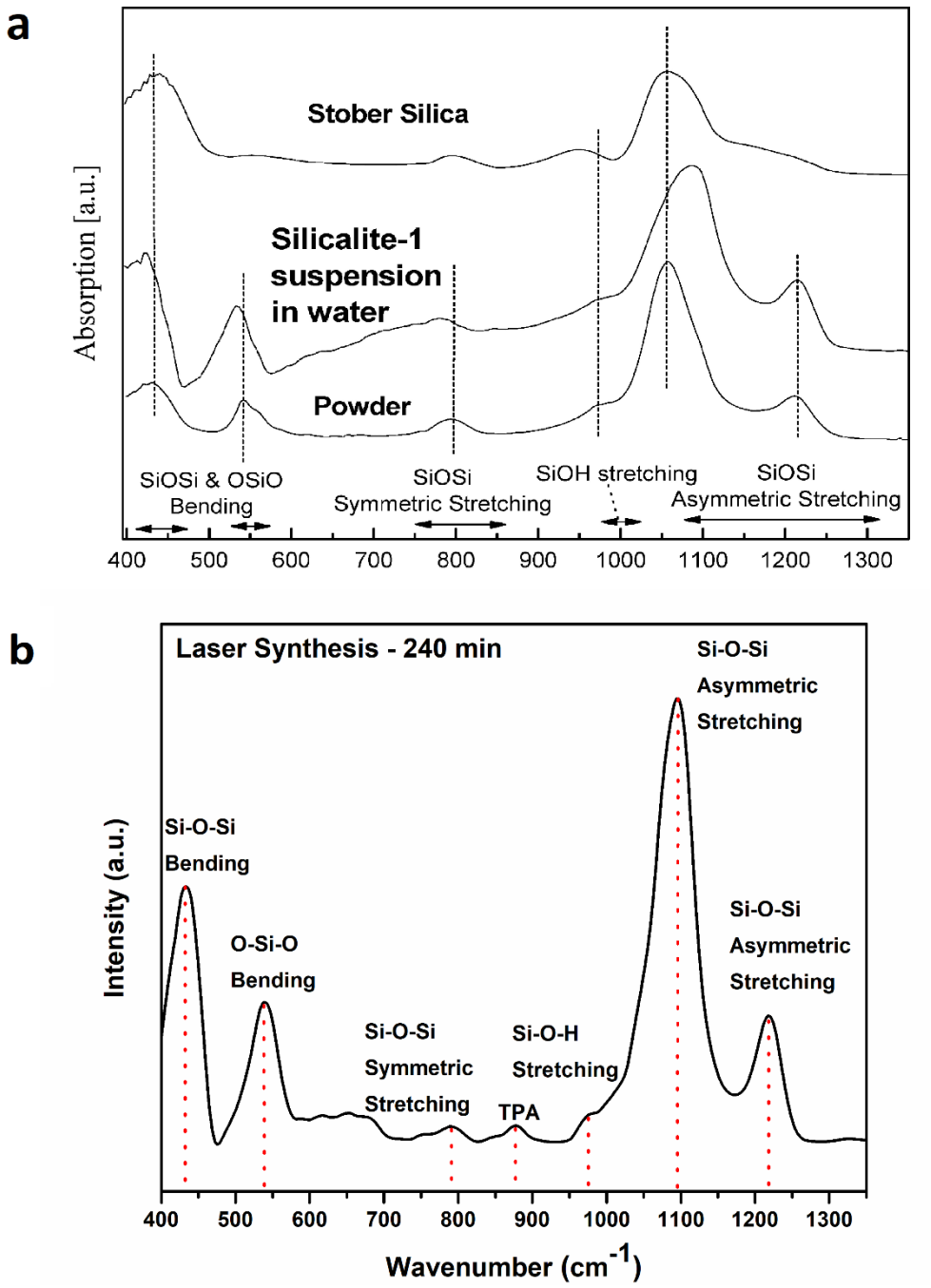

Figure 35. (a) The IR spectra of Stober Silica (amorphous), Silicalite-1 dispersed in water and in powder forms, adapted from ref [97]; (b) IR spectrum of TPA - Silicalite-1 synthesized via the laser-assisted method with 240 minutes reaction time in the current thesis.

Most striking differences in absorption bands of amorphous silica and Silicalite-1 are observed at ~1200 and 550 cm^{-1}. In the IR spectra of TPA – Silicalite-1 samples

synthesized via the laser-assisted method with different reaction times, no distinct absorption peaks are observed at ~1200 and 550 cm^{-1} for the samples with reaction times less than 70 minutes, and distinct peaks appear for the sample with 70 min. or longer laser treatments (Figure 35). As shown in chapter 4.5.1 in Figures 31 and 32, the color change of transparent precursor suspension into light milky white, and subsequent powder material collection through centrifugation was attributed to the first zeolite crystal growth. A similar phenomenon was observed in ATR-FTIR analyses of the samples as the appearance of absorption bands associated with Silicalite-1 zeolite starts after 70 minutes of laser treatment (for 80 µl of precursor suspension with M1 molar formula). In the IR spectra of the samples synthesized with less than 70 minutes of laser treatment, absorption bands associated with Silicalite-1 zeolite at ~ 550 cm^{-1} and ~ 1200 cm^{-1} regions are missing (Figure 35). Besides, a wide shoulder appears between 500 – 800 cm^{-1} regions and disappears when zeolite crystal growth starts after reaction times of 70 min. and more.

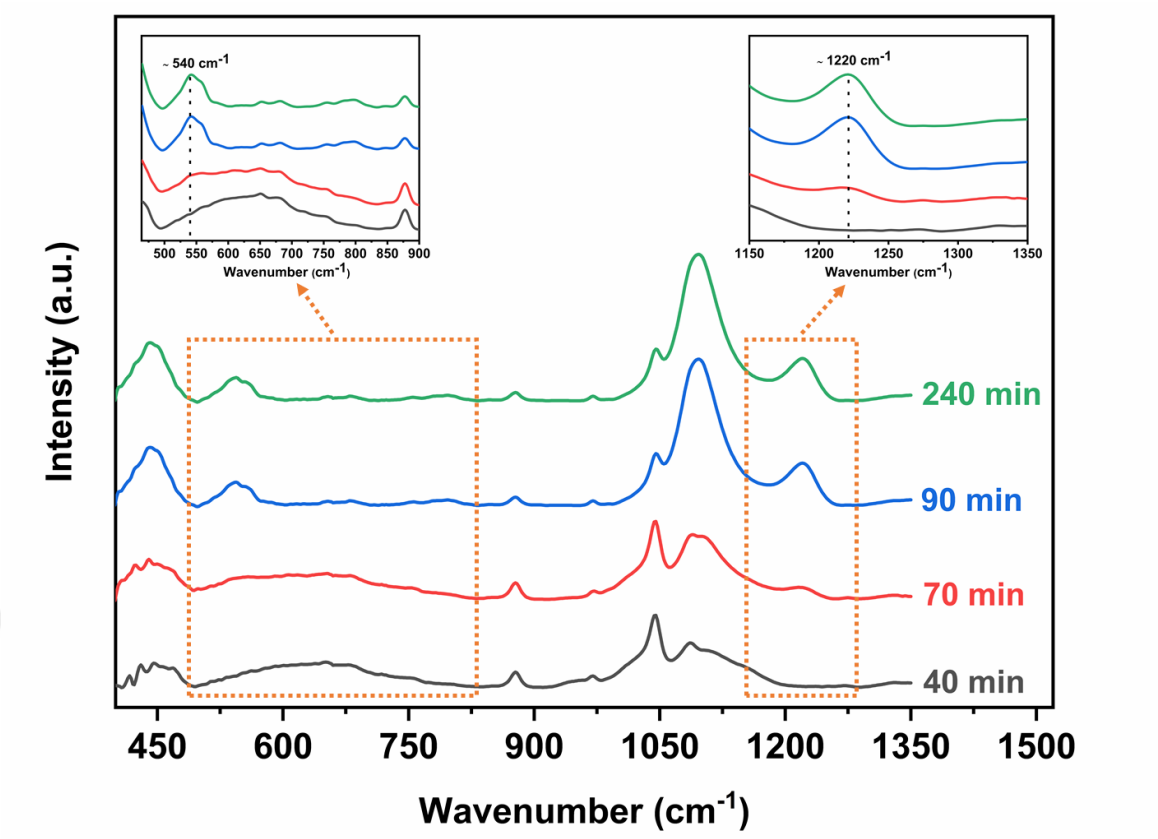

Figure 36. IR spectra of TPA – Silicalite-1 samples synthesized via the laser-assisted method with reaction times of 40, 70, 90, 240 minutes. Since zeolite growth did not start for the sample with 40 minutes of laser treatment, characteristic absorption bands at 550 and 1220 cm-1 are absent.

Computational studies by Lesthaeghe *et al.* suggest that in the very beginning of mixing of TEOS – TPAOH couple (which are source chemicals used in TPA – Silicalite-1 synthesis), single five-membered rings form and they have absorption band at ~ 650 cm^{-1}.[94] As nucleation proceeds and more condensed Silica oligomers form, new absorption bands should appear according to a computational study by Lesthaeghe *et al.* (Figure 37).[94] Until growth starts, condensed Silica and MFI precursor units are dominant within the suspension. It explains the shoulder observed in the IR bands of samples synthesized via the laser-assisted method with less than 70 minutes. The diminished shoulder in between 500 – 800 cm^{-1} regions indicates that, as reaction

proceeds, the condensed units formed in the transition are converted into zeolite crystals in time (Figure 36).

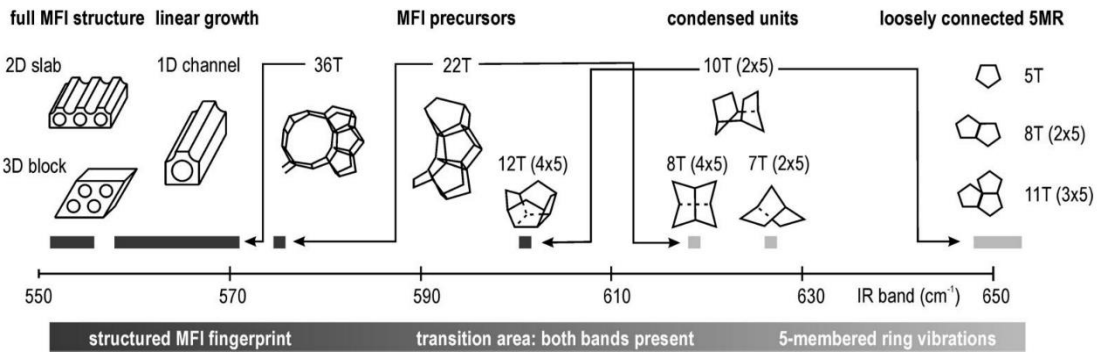

Figure 37. Different building units that are present in nano growth of Silicalite-1 and their corresponding shift in IR band. Adapted from ref [94].

Peak deconvolution was applied to the FTIR spectra of the samples synthesized with less than 70 minutes of laser treatment to investigate the region between 500 – 840 cm^{-1} in the IR band further (i.e., the wide shoulder). Figure 38 shows the applied deconvolutions for IR bands of the samples synthesized with 0, 20, 40, 60, and 70 minutes of laser treatment. It was observed that as laser reaction proceeds and more condensed units were formed, the deconvoluted peak appearing firstly at absorption band of ~ 570 cm^{-1} (20 min. sample), shifts to lower wavenumbers and finally appears as a peak at ~ 550 cm^{-1} after 70 minutes of laser treatment (Figure 38 and Table 14). This result is in agreement with the computational study by Lesthaeghe *et al.*

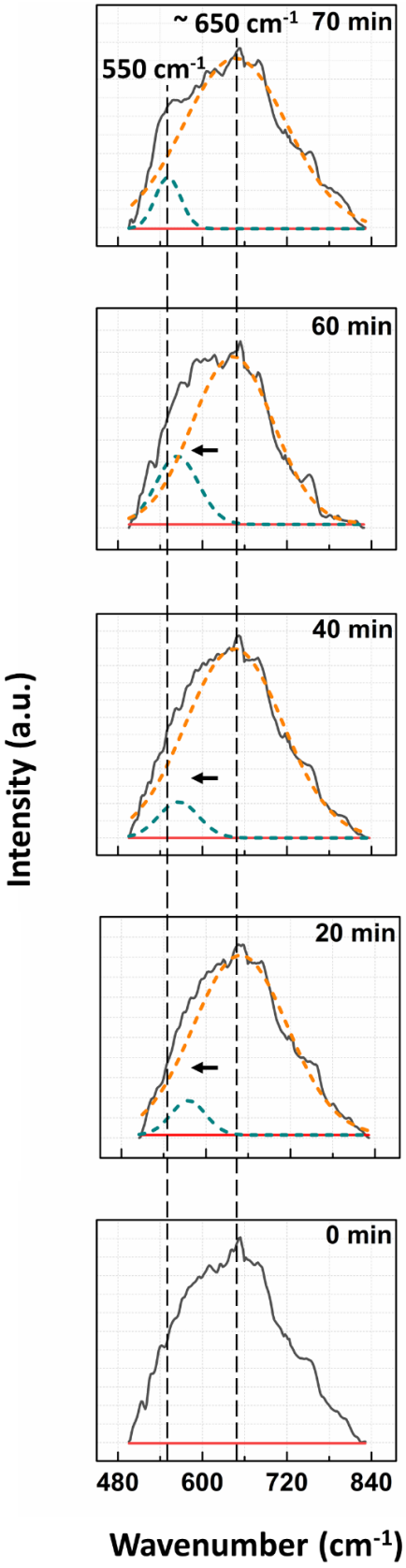

Figure 38. IR spectra of reaction mixtures with different laser treatment times between 480 – 840 cm^{-1} region. The shoulder appearing in full IR spectra of the samples analyzed and deconvoluted.

The shift observed in the deconvoluted characteristic IR band of the samples synthesized with less than 70 minutes of laser treatment time could be used as an alternative method for crystallinity calculation. The shift of characteristic absorption band for each sample may be assigned to degree of crystallinity by taking characteristic absorption band of 240 min sample (538.64 cm^{-1}) as the end of crystallization (since XRD pattern analyses suggest so) and 570 cm^{-1} as the start of the crystallization (since a study by Lesthaeghe *et al.* suggests so). For example, if the Δ_{shift} = 570 – 566.20 = 3.80, Δ_{shift} / (570 – 538.64) = 3.80 / 31.36 = 0.15. The samples with no and 20 minutes of laser treatment have crystallinity of zero, and this period can be assigned to the nucleation period of the crystallization and it proceeds between 20 and 70 minutes. The crystallinities according to FTIR spectra and XRD patterns are given in the table below.

Table 14. FTIR and XRD crystallinities for the samples analyzed through ATR-FTIR. FTIR crystallinities were calculated and adjusted to XRD crystallinities.

Reaction Time (min)	**Absorption Band (cm^{-1})**	**FTIR Crystallinity (%)**	**XRD Crystallinity (%)**
0	-	0	-
20	574.99	0	-
40	566.20	12	-
60	564.36	18	-
70	551.23	60	48
90	544.05	82	55
120	543.32	85	62
240	538.64	100	100

4.5.3 Transmission Electron Microscopy

To gain insight into the growth kinetics of TPA – Silicalite-1 synthesized via the laser-assisted method, samples with different laser treatment durations were analyzed through TEM. As explained in previous sections, the sample with 70 minutes of reaction time (when 80 µl precursor suspension of M1 molar formula was used) was investigated since the first color change is observed at that reaction time (Figure 31). A distinct difference in morphologies of crystals synthesized with reaction times of 300 minutes (fully crystalline) and 70 minutes can be seen from Figure 39-a and Figure 39-b, -c, -d, respectively. The surface of the 300-min-sample is smooth and sharp while surfaces of crystals synthesized with 70 minutes of reaction time are rough. As known from the literature, a smooth crystal surface is attributed to fully crystalline samples.[18,68]

From SEM images of samples with different reaction times, it was observed that nanosized particles around crystals disappeared gradually as laser treatment time increases, and they are consumed completely after a reaction time of 180 minutes (Figure 32). Nanosized particles around crystals observed in SEM images of 70-min-sample (Figure 32-a) were investigated through TEM analysis to reveal the growth process. Figure 39 (c) shows their appearance. Contrast differences in bright field (BF) and dark field (DF) TEM images are due to variations in intensities of diffraction planes, i.e. crystalline parts appear as bright in DF and vice versa.[98] The DF TEM image of the 70-min-sample indicates nanosized particles seen around crystals are also crystalline (Figure 39 f). The analysis suggests that the nonclassical pathway of growth mechanism (Figure 30) is dominant, i.e. aggregate attachment on the crystal surface leads to bigger fully crystalline zeolites.

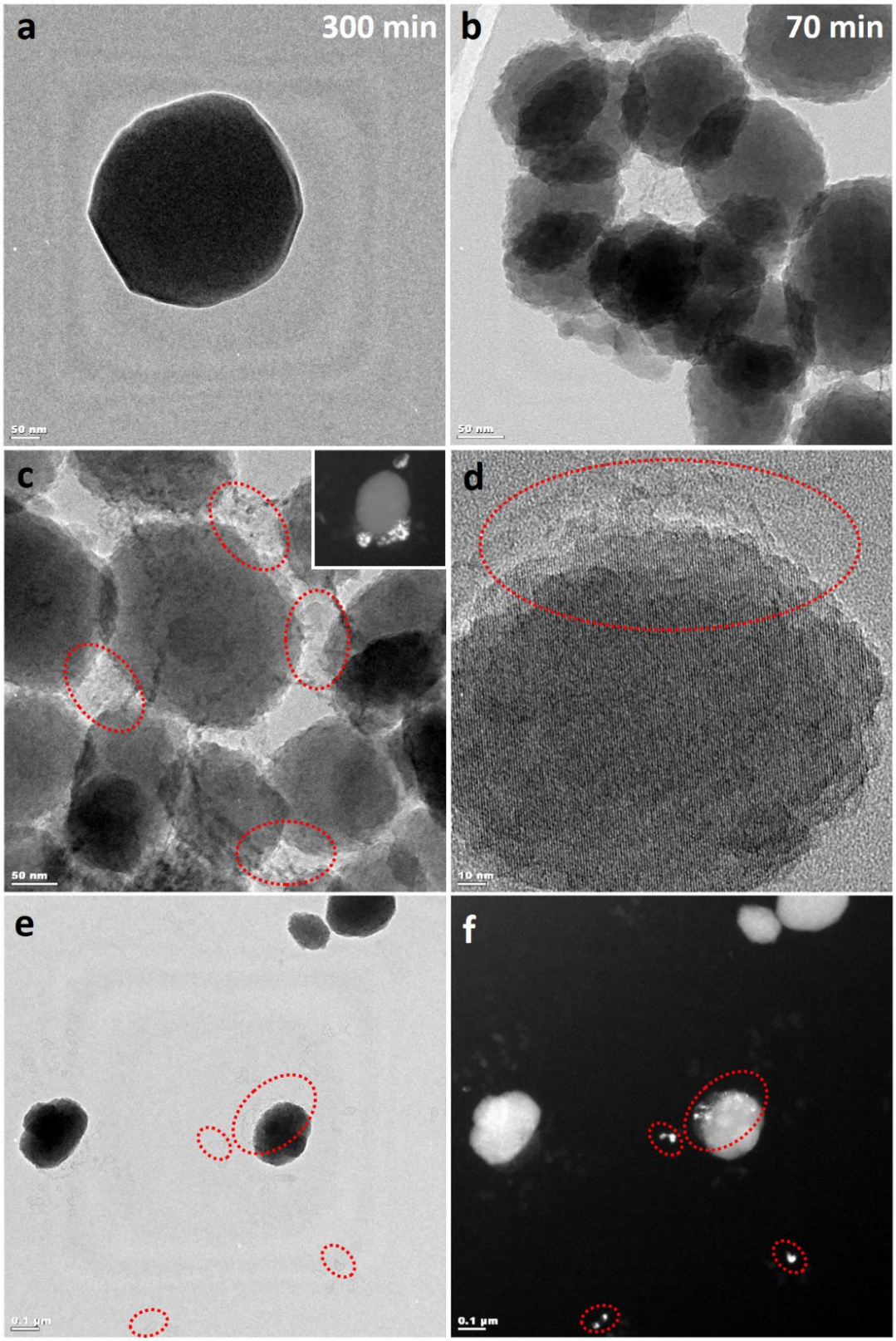

Figure 39. TEM images of samples synthesized via the laser-assisted method with (a) reaction time of 300 min; (b), (c) reaction time of 70 min; (d) HR-TEM image of sample synthesized via the laser-assisted method with a reaction time of 70 min; (e) bright-field (BF) and (f) dark field (DF) images of the same spot for 70 min-sample.

4.5.4 Avrami – Erofeev Equation and Crystallization Process

Growth and nucleation mechanism of TPA – Silicalite-1 zeolite synthesized via laser-assisted method investigated through Avrami - Erofeev equation. The formation of zeolite crystals from source chemicals is described in Figure 40. The induction time covers relaxation, nucleation, and growth stages of the crystallization process and is defined as the elapsed time between the saturation of solution with source nuclei and observation of first crystals.[99] The induction time is divided into three periods: t_r is the relaxation time, required for the systems to achieve a quasi-steady-state distribution of molecular clusters; t_n is the time required for the formation of a nucleus, and t_g is the time required for the nucleus to grow to a detectable size, then induction time is $t_i = t_r + t_n + t_g$.[99] From observations and analyses (XRD, FTIR, TEM), induction time was found to be 70 minutes for the laser-assisted reaction of 80 µl precursor suspension with M1 molar formula. As the color of suspension starts to change (i.e., light milky white), the crystal growth period begins and lasts until saturation.

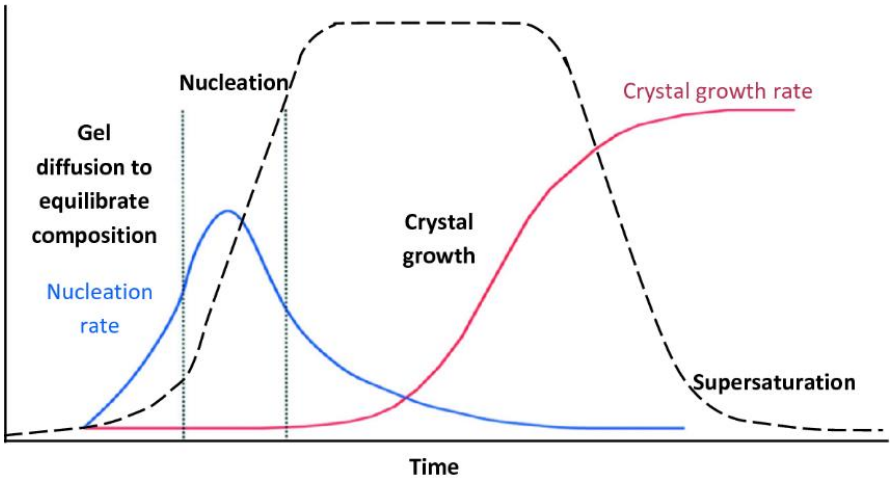

Figure 40. Schematic representation of the nucleation and crystal growth processes and the supersaturation of the system in zeolite synthesis. Adapted from ref [100].

The linear portion of the crystal growth curve is analyzed through Avrami - Erofeev equation.[65] Two points from the linear portion of the crystallization curve (Figure 33) were selected and their crystallinity values were used in the equation. Then, to find n, Avrami – Eroffev equation is solved:

$$\alpha = 1 - \exp(-k \cdot t^n) \qquad (2)$$

where α is the crystallinity percentage, t is time, k is rate constant, and n is Avrami index. Rearranging this equation to find constants:

$$\exp(-k \cdot t^n) = 1 - \alpha$$

$$\exp(k \cdot t^n) = \frac{1}{1 - \alpha}$$

Then natural logarithm of both sides taken twice:

$$k \cdot t^n = -\ln(1 - \alpha)$$

$$\ln(k) + n \cdot \ln(t) = \ln(-\ln(1 - \alpha))$$

For reaction time and crystallinity, values from Table 13 are used for the determination of the n – Avrami index. The crystallinity values chosen for this purpose are 90 min sample (α = 55%) and 180 min sample (α = 78%).

$$n \cdot (\ln(180) - \ln(90)) = \ln(-\ln(1 - 0.78)) - \ln(-\ln(1 - 0.55))$$

$$n \cdot (5.193 - 4.500) = 0.415 + 0.225$$

$$n \cdot 0.693 = 0.64$$

$$\boldsymbol{n = 0.93}$$

The Avrami index is called also as geometric factor since it represents number of mechanism and dimensionality of the growth stage.[99,101,102] The index can be expressed as summation of two other integer indices representing both the mechanism and the dimensionality of growth. Since value of n is the summation of two other integers, i.e. the calculated value of 0.93 should be rounded to the closest integer which is 1.[99,101,102] For simplicity, the index representing mechanism of growth is denoted as n_1 while dimensionality of growth is denoted as n_2. The value of n_1 may be zero or 1 according to the formation of nuclei cores. If the nuclei cores form within the solution during the growth as well, the value of is 1. Otherwise, if nuclei formation ceases during growth, which is the case in zeolite synthesis, the nuclei cores form during the aging step prior to the growth, then n_1 equals zero. The value of n_2 should be one of the integers of 1, 2, 3 or 4, indicating the formation model of a zeolite crystal which can be linear (one dimensional), surface (two dimensional) or three-dimensional.[99,102] In the case of laser-assisted synthesis of TPA – Silicalite-1, the value of n_2 equals 1 which indicates linear growth of zeolites on the crystal surface. This result is complementary to observations through TEM analyses (Figure 39).

The growth part of TPA – Silicalite-1 zeolite is analyzed from XRD powder pattern crystallinity calculation for years. However, analyzing the nucleation part of the crystallization process through XRD is not straightforward because the size of the synthesized clusters in the nucleation stage cannot be detected and collected readily. In the current thesis, the growth stage (i.e., between reaction times of 70 min. – 240 min.) was analyzed based on crystallinity calculations using XRD powder patterns. For the nucleation stage (i.e., between reaction times of 20 min. - 70 min.), the shift of the characteristic absorption band in the IR spectrum (see section 4.5.2) is transcribed into the nucleation period of the crystal growth.

4.6 Effect of Femtosecond Laser Parameters on Synthesis of TPA – Silicalite-1

The possible effects of different laser parameters along with synthesis parameters such as reaction time, volume, and type of molar formula of precursor suspension, are also studied. Average laser power on the sample and repetition rate of laser pulses altered and their effects on crystallinity, yield, and crystal size were investigated. For better comparison, 80 µl precursor suspension of M1 molar formula was used in all trials. Reaction times were set to 3 hours. When the incident laser power was set to 0.67 W, no powder particle could be obtained and solution color remained transparent at the end of 3 hours of laser treatment. Table 15 summarizes the results of laser parameter changes.

The repetition rate of laser pulses was set to 200 kHz for all of the experiments previously mentioned in the thesis. An increase in repetition rate to 1 MHz (5 times) led to zeolite crystals with similar average particle sizes for both 0.90 W and 1.12 W average laser powers (Table 15).

Pulse fluence is the energy delivered per area that is hit by a laser pulse (*Fluence = Pulse Energy / Area*). Peak power is the maximum optical power that a laser pulse would attain. The rise in the repetition rate while keeping average laser power the same, results in laser pulses with lower energy and hence lower pulse fluence and peak power. For the current system, change in these two parameters seems not to affect the final result significantly. The results indicate that a change in laser power affects the result considerably in terms of yield and average crystal size. For the same reaction times, as average laser power decreases, the amount of total energy absorbed by reaction suspension decreases which leads to relatively lower yield (wt. %) and smaller crystals.

Table 15. Experiments with varying laser parameters and characteristics of the corresponding TPA – Silicalite-1 samples. SD indicates standard deviation. Sample size (N) for particle size distribution analyses was set to 100.

Exp. Code	Avg. Power (W)	Repetition Rate (kHz)	Molar Formula	Reaction Time (h)	Pulse Fluence (Jcm^{-2})	Peak power (MW)	Avg. Crystal Size ± SD (nm)	Yield (wt %)	Energy Absorbed ($MJ/moleSiO_2$)
C12	1.12	200	M1	3	8.84	18.67	333.8 ± 30.0	69.7	201.7
C56	1.12	1000	M1	3	1.77	3.73	300.6 ± 25.2	60.5	201.7
C57	0.90	1000	M1	3	1.41	3.00	309.0 ± 28.0	53.5	161.7
C48	0.90	200	M1	3	7.07	15.00	246.9 ± 27.1	39.6	161.7
C49*****	0.67	200	M1	3	5.31	11.33	-	-	120.0

***** Initial transparent color of the suspension did not change at the end of 3 hours of reaction time. Powder sample could not be collected for further analysis

4.7 Femtosecond Laser-assisted Syntheses of Template-free Nanosized Zeolite Y and Mesoporogen-free Hierarchical ZSM-5

4.7.1 Nanosized Zeolite Y

The new laser-assisted synthesis method of zeolites has been tested on template-free nanosized zeolite Y as well. The molar formula and synthesis procedure were obtained from the reference 103.[103] Prepared transparent precursor suspension was used both for hydrothermal and laser-assisted syntheses. The first color change for the laser-assisted synthesis was observed after 20 minutes of laser treatment when 400 µl of precursor suspension was used. XRD patterns of both samples are provided in the figure below.

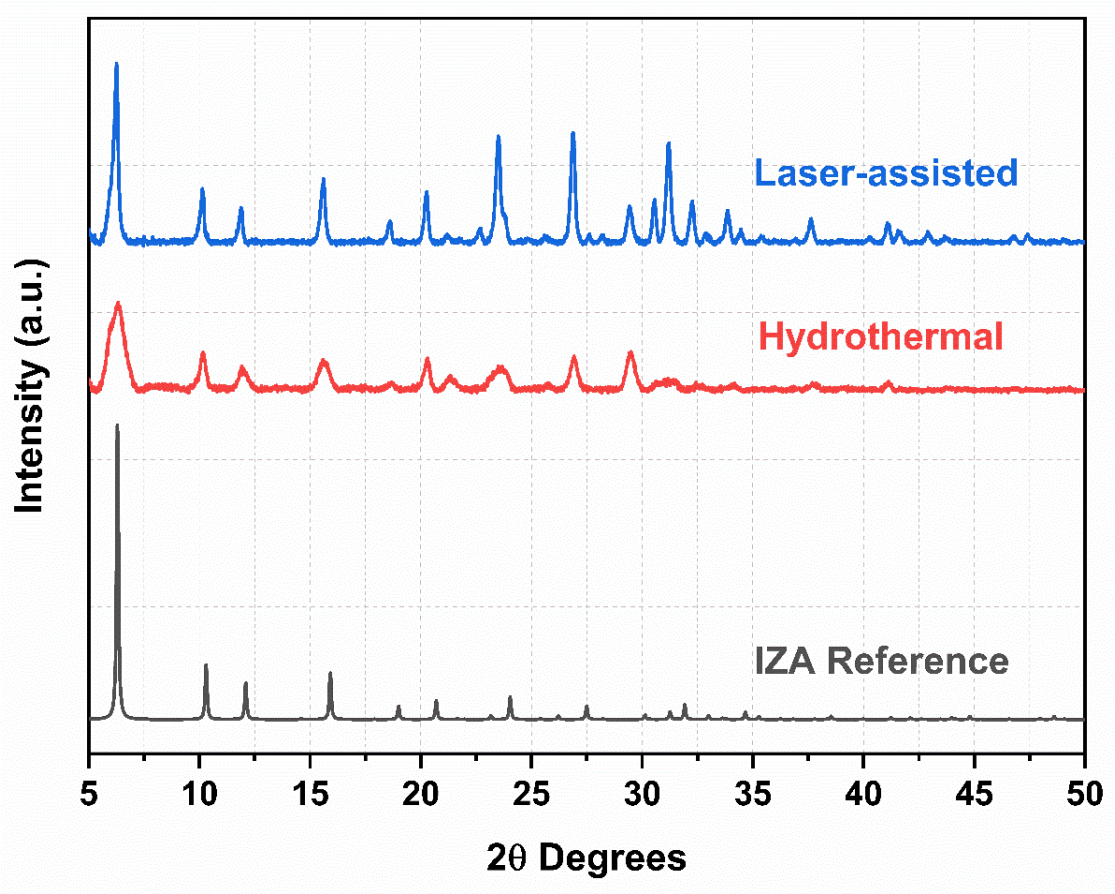

Figure 41. XRD patterns of nanosized zeolite Y synthesized via laser-assisted (blue), hydrothermal (red) methods, and reference pattern (grey) obtained from the IZA web page.

The sample synthesized via the laser-assisted method with 30 minutes of reaction time analyzed through TEM. The average size of the synthesized crystals is expected to be ~10 nm in size.[103] Therefore, the synthesized crystals were tent to agglomerate (Figure 42-a). During HR-TEM analyses of the sample, rapid transition from crystalline into amorphous phase under high voltage of TEM electron beam (200 kV) was observed. HR-TEM image in Figure 42-b shows lattice fringes indicating the crystalline phase of the zeolite just before this transition.

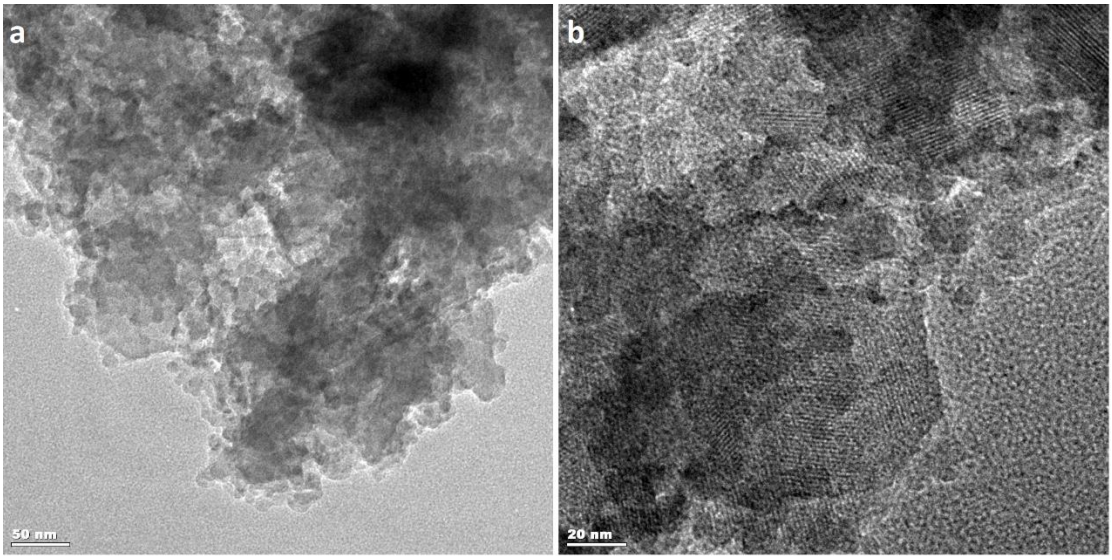

Figure 42. (a) TEM and (b) HR-TEM images of nanosized zeolite Y synthesized via the laser-assisted method. Analysis was performed for the sample with 30 minutes of reaction time.

Crystallinity (%) and yield (wt. %) values were determined for the zeolite Y sample synthesized via the laser-assisted method with 1.5 hours reaction time and compared to the sample synthesized via the hydrothermal method with a reaction time of 45 hours. Crystallinities calculated from XRD patterns for the peaks corresponding to characteristic planes of zeolite Y structure, which are at 6.28, 15.78, 24.0, 26.88, 31.14 2θ degrees.[104,105] From calculations, the sample synthesized via laser-assisted method appears to be more crystalline, so its crystallinity is taken as 100%. The yield (wt. %) values were calculated by dividing the weight of the final product (after

subtracting zeolitic water determined through TGA) by the weight of the initial SiO_2 and Al_2O_3. TGA graphs for zeolite Y synthesized via laser-assisted and hydrothermal methods are provided in Appendix D.

Table 16. Comparison of nanosized zeolite Y samples synthesized via laser-assisted and hydrothermal methods. The laser-assisted sample is taken as a reference in crystallinity calculation. Yield values were calculated after subtracting zeolitic water content (found through TGA) from weighed amounts.

Synthesis Method	Reaction Time (h)	Crystallinity (%)	Yield (wt. %)
Hydrothermal	45	77	21.05
Laser-assisted	1.5	100	56.86

4.7.2 Hierarchical Mesoporogen-free ZSM-5

Another trial for testing the new synthesis method was the synthesis of hierarchical ZSM-5 zeolite. The method proposed by Zhu et al.[63] was adapted to obtain hierarchical ZSM-5 by using a femtosecond laser (Figure 43). A two-step procedure was applied to obtain hierarchical structures. In the first step, the amount of water in the initial precursor was limited to a certain amount to hinder ZSM-5 crystal growth (i.e., sub-nanocrystal size < 50 nm). As known from the literature, when the same molar formulas are used decreased water amount hinders crystal growth.[34] In the second step, additional water is added and assembly of sub-nanocrystals was achieved by applying hydrothermal and laser-assisted synthesis methods.

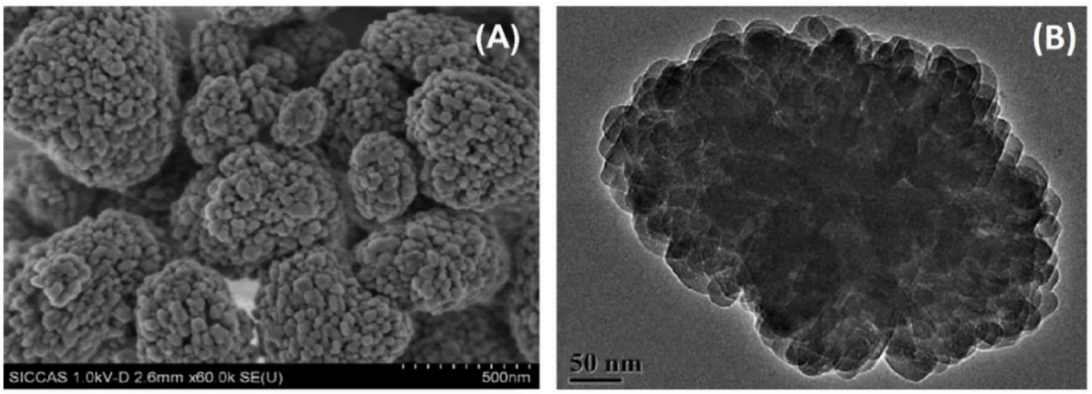

Figure 43. SEM (A) and TEM (B) images of hierarchical nanosized zeolite assemblies synthesized by aging the precursor at 100 °C for 48 h followed by hydrothermal treatments at 150 °C for 24 h without using any template.[63]

As a control experiment, the same precursor suspension was used to synthesize hierarchical zeolites by applying the hydrothermal method in our laboratory as well. SEM images of the structures show that there is no morphological difference between the crystals synthesized by the conventional hydrothermal method (Figure 44 - top) and the laser-assisted method (Figure 44 - bottom). The average crystal sizes were around ~ 300 - 600 nm. The morphology of the structures (SEM images) suggests that assembly of sub-nanocrystals was achieved after hydrothermal and laser-assisted syntheses. Intermesoporosity was achieved in between sub-nanocrystals without using any mesoporogen. However, it was shown that in the literature,[63] hierarchical porous ZSM-5 zeolites showed noticeably higher catalytic activity in the chemoselective esterification between itaconic acid and n-butyl alcohol than traditional ZSM-5 zeolites (i.e., microporous) and other homogeneous catalysts. [63]

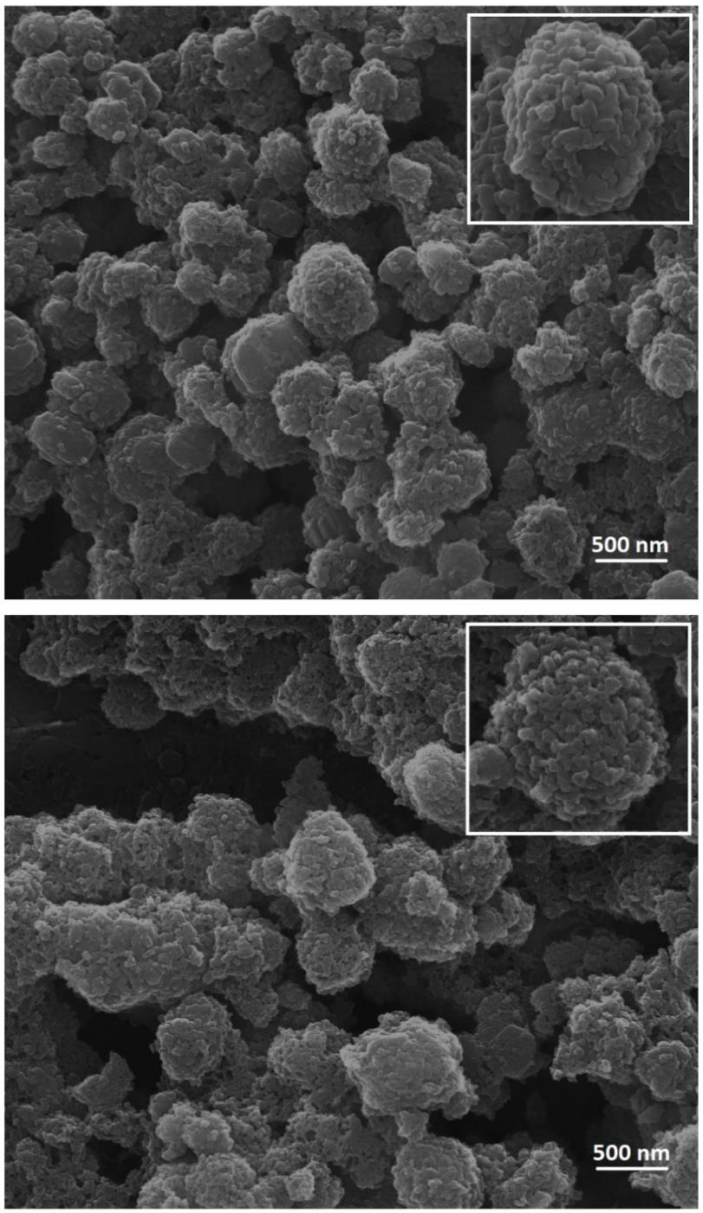

Figure 44. SEM images of hierarchical zeolites obtained by no template (mesoporogen) method (different magnification), (top) conventional hydrothermal method at 150 °C for 24 h, and (bottom) laser-assisted method (reaction time = 5h).

TEM images of the hierarchical zeolites obtained by applying the no template method show that each ~ 300 - 600 nm crystal has sub-nanocrystals aggregated on top of each other (Figure 45). Sub-nanocrystal aggregation can be seen clearly from the contrast difference (Figure 45 top left).

The selected area electron diffraction (SAED) patterns of the hierarchical zeolites obtained by applying the no template method suggest the polycrystalline nature of the structures (i.e., rings and bright diffraction spots) (Figure 45 and 46 top right). Moreover, lattice fringes were observed in HR-TEM images of the structures showing crystallinity of the structure.

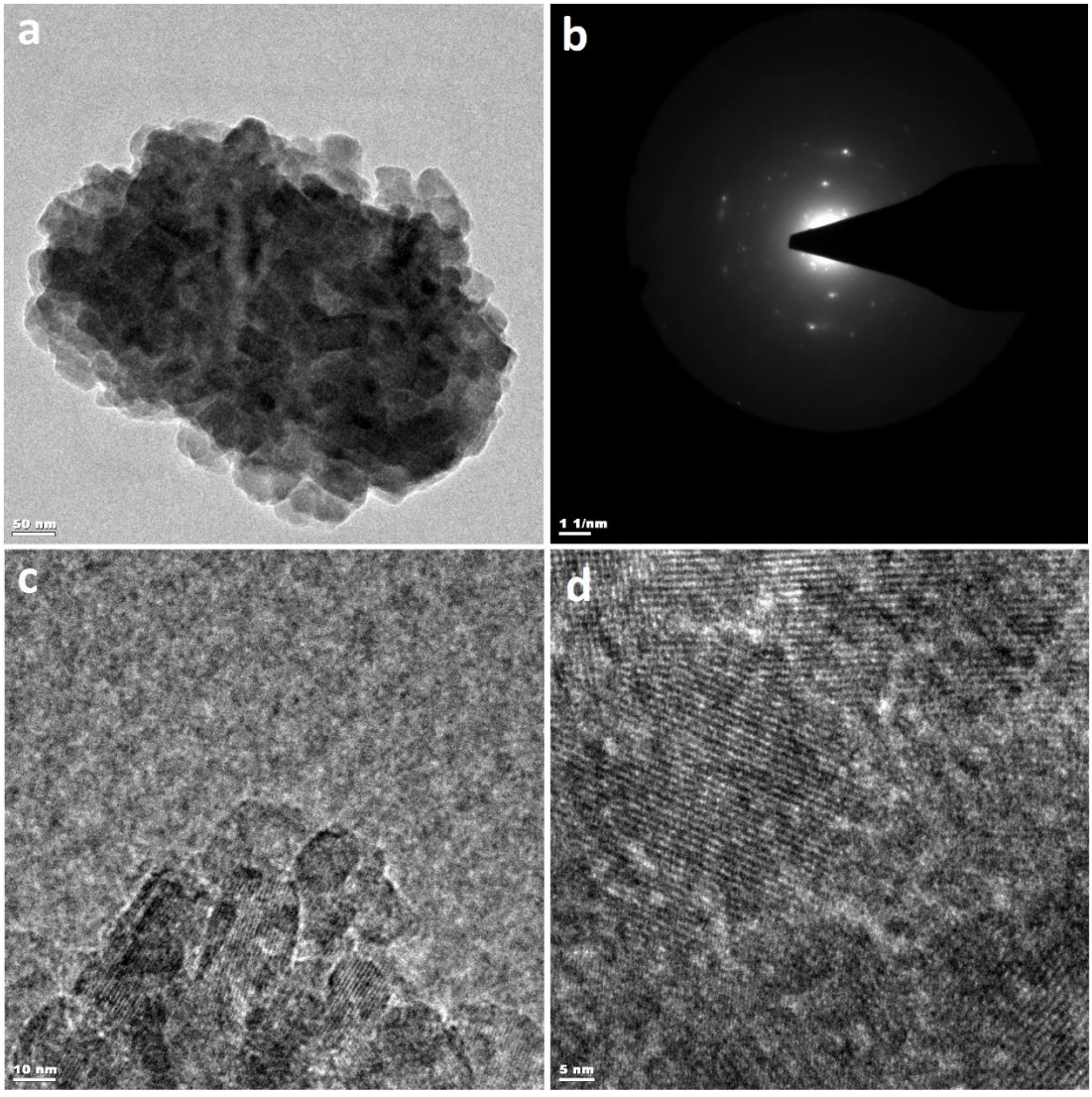

Figure 45. TEM images and SAED pattern of hierarchical zeolites obtained by applying the no template (mesoporogen) method (laser-assisted synthesis).

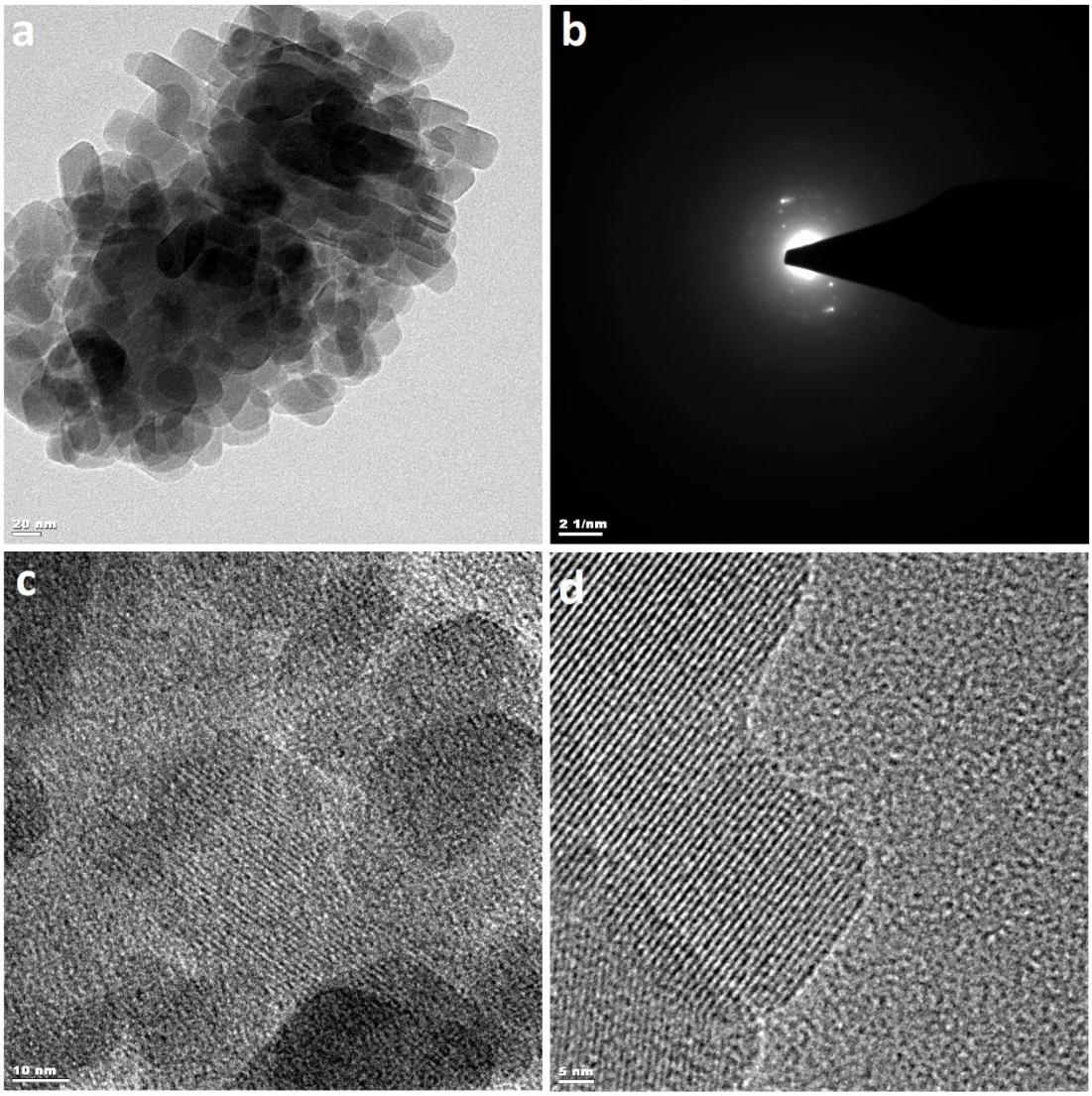

Figure 46. TEM images and SAED pattern of hierarchical zeolites obtained by applying the no template (mesoporogen) method (hydrothermal synthesis).

XRD patterns of the samples proved that the synthesized structures were ZSM-5 zeolites (MFI framework type zeolite) (Figure 47). Because the hierarchical ZSM-5 crystals were synthesized by assembly of sub-nanocrystals, their morphologies were not as sharp as traditional crystals. To examine it further, the precursors aged at 100 °C for 1 day and 2 days were characterized as well. As explained in the method part in detail, before hydrothermal and laser syntheses, the precursor suspension was placed in an oil bath to stir at 100 °C for 44h. The amount of water in the initial precursor was limited to a certain amount to hinder ZSM-5 crystal growth (i.e., sub-nanocrystal size

< 50 nm). XRD patterns of the precursors aged at 100 °C for 1 day and 2 days show highly crystalline features as shown in HR-TEM images as well (Figures 45 and 46). However, SEM images of the precursor suspensions proved that assembly of the sub-nanocrystals was obtained only after laser-assisted and hydrothermal syntheses (Figure 48).

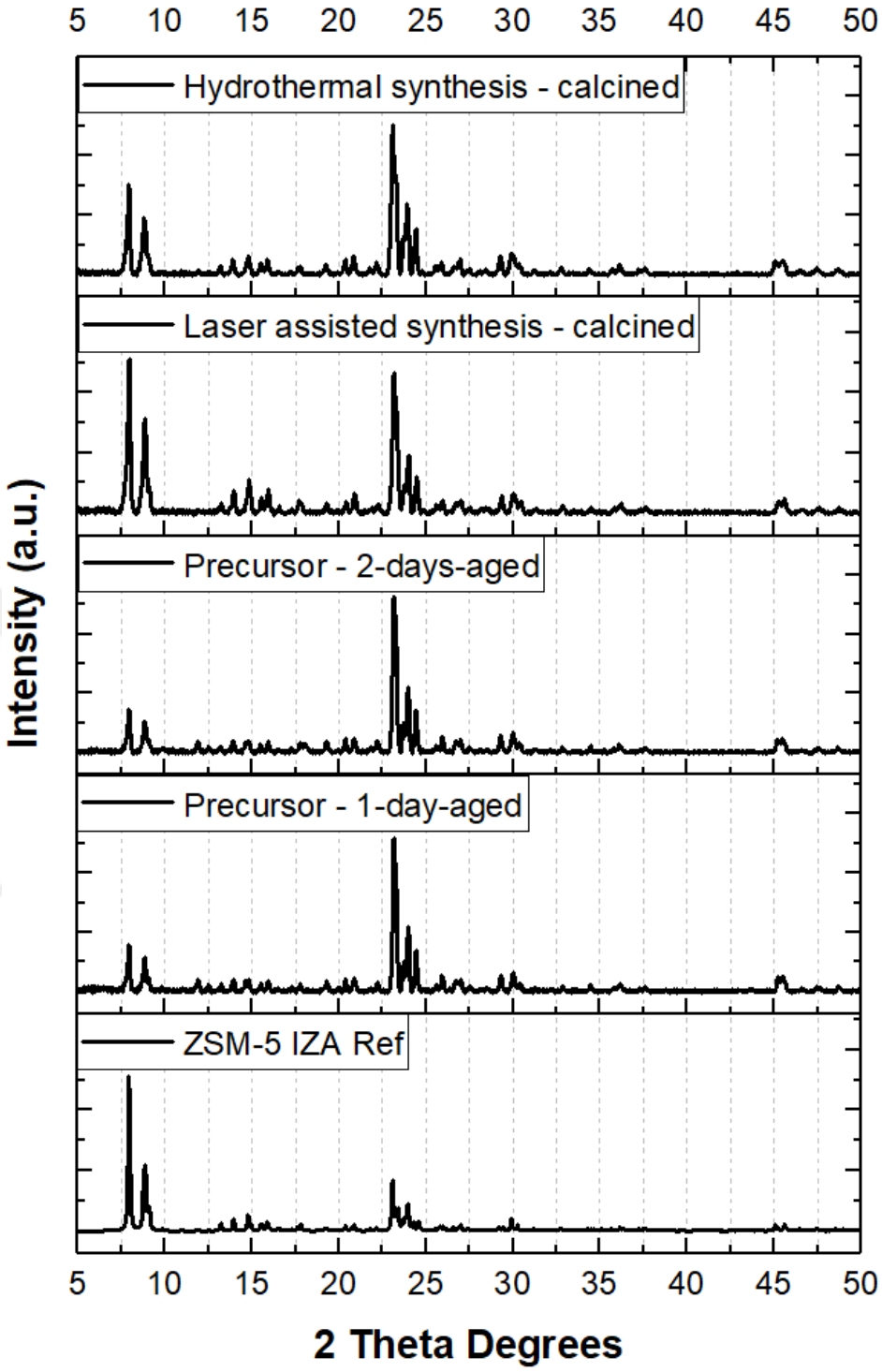

Figure 47. XRD patterns of precursor and hierarchical zeolites by applying the no template (mesoporogen) method. At the bottom, the ZSM-5 reference pattern of the International Zeolite Association (IZA) can be found.

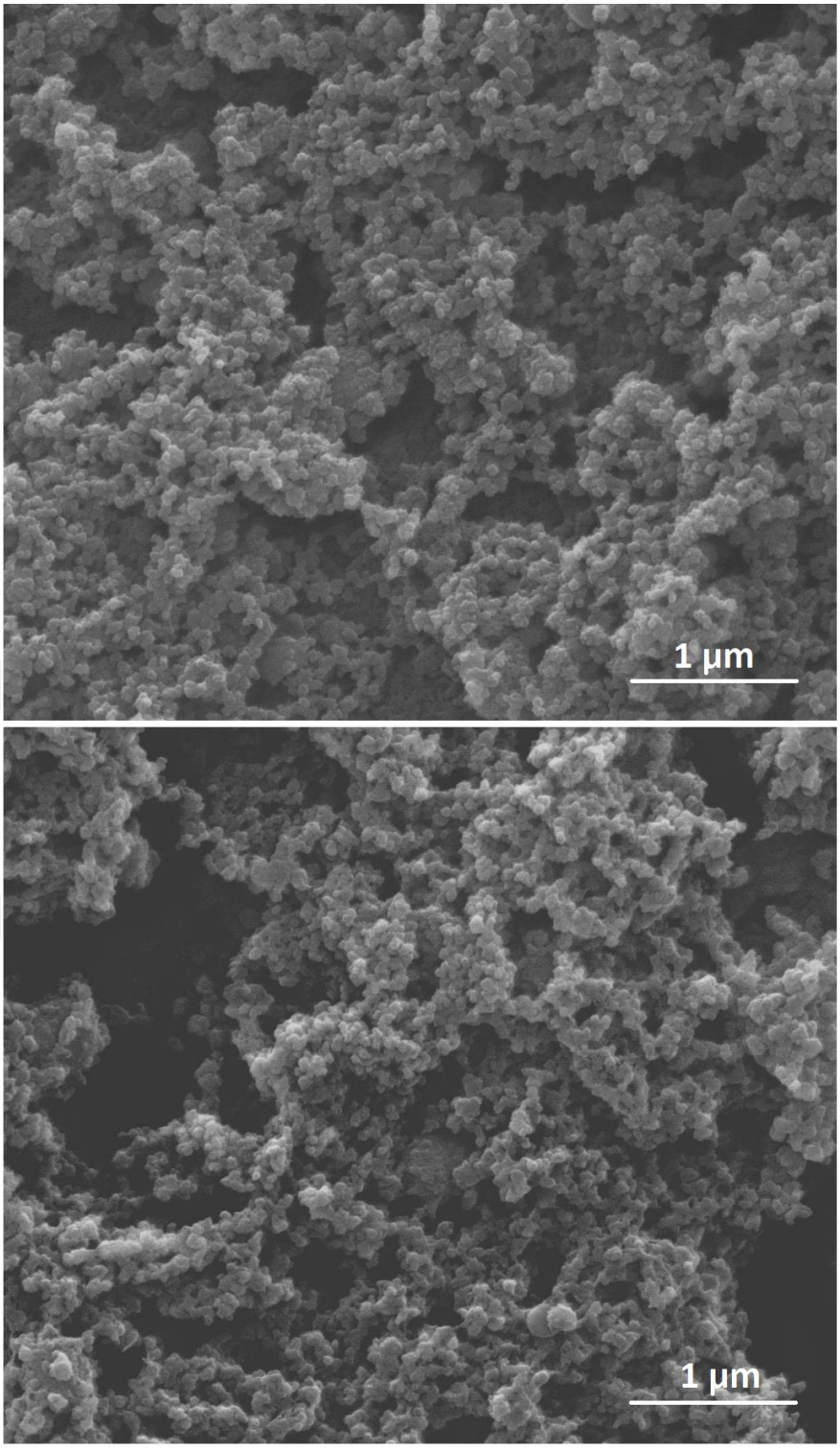

Figure 48. SEM images of centrifuged and dried powder precursor (top) aged 1-day and (bottom) aged 2-days at 100 °C in an oil bath.

Table 17 shows a summary of peak analyses of laser-assisted and hydrothermal syntheses (Figure 49 and 50). A slight shift (~ 0.05) in 2 theta degrees is due to measurement errors (e.g, slight height difference of the powder sample) although 3 mg powder samples were weighed in the balance before XRD measurements. The crystallinity of the sample synthesized via laser-assisted method relative to the reference sample (i.e., synthesized by applying the hydrothermal method in our laboratory) was calculated to be 72 %. The crystallinity of the zeolite is calculated by dividing the sum of area integrated of characteristic peaks in XRD patterns for laser-assisted synthesis to the sum of area integrated of hydrothermal synthesis (reference).

Table 17. Peak analyses of hierarchical zeolites obtained by applying the no template (mesoporogen) method. (2θ = 2 Theta degrees, FWHM = full width half maximum).

2θ	**FWHM**		**Area Integrated (%)**	
	Laser-assisted	Hydrothermal	Laser-assisted	Hydrothermal
23.17	0.22	0.22	48.84	46.07
23.35	0.15	0.15	18.97	17.87
23.78	0.20	0.18	8.44	9.24
24.00	0.15	0.17	14.07	16.26
24.47	0.17	0.17	9.69	10.55

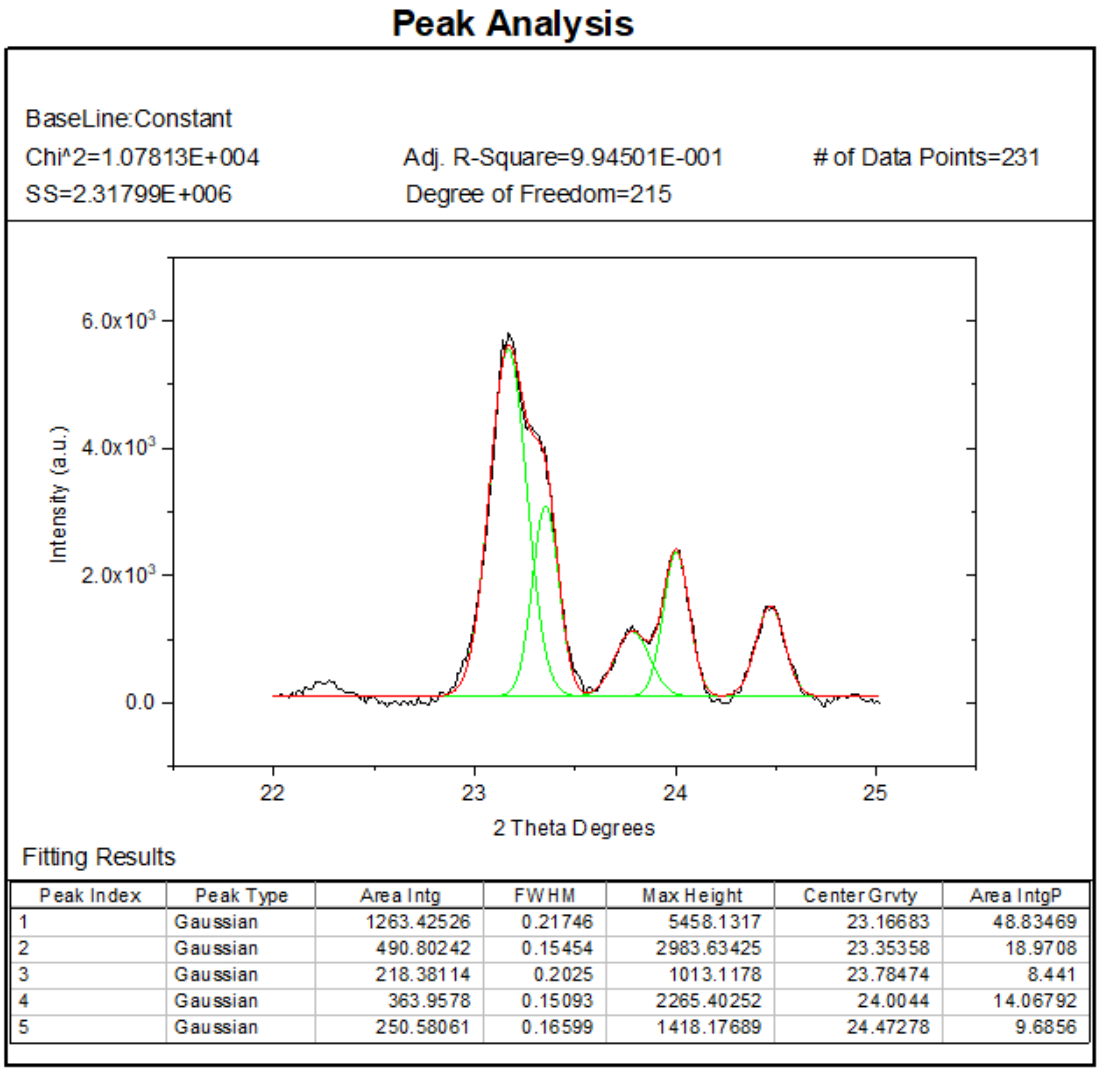

Fitting Results

Peak Index	Peak Type	Area Intg	FWHM	Max Height	Center Grvty	Area IntgP
1	Gaussian	1263.42526	0.21746	5458.1317	23.16683	48.83469
2	Gaussian	490.80242	0.15454	2983.63425	23.35358	18.9708
3	Gaussian	218.38114	0.2025	1013.1178	23.78474	8.441
4	Gaussian	363.9578	0.15093	2265.40252	24.0044	14.06792
5	Gaussian	250.58061	0.16599	1418.17689	24.47278	9.6856

Figure 49. XRD peak analysis of hierarchical zeolite obtained by applying no template method (laser-assisted synthesis, calcined sample).

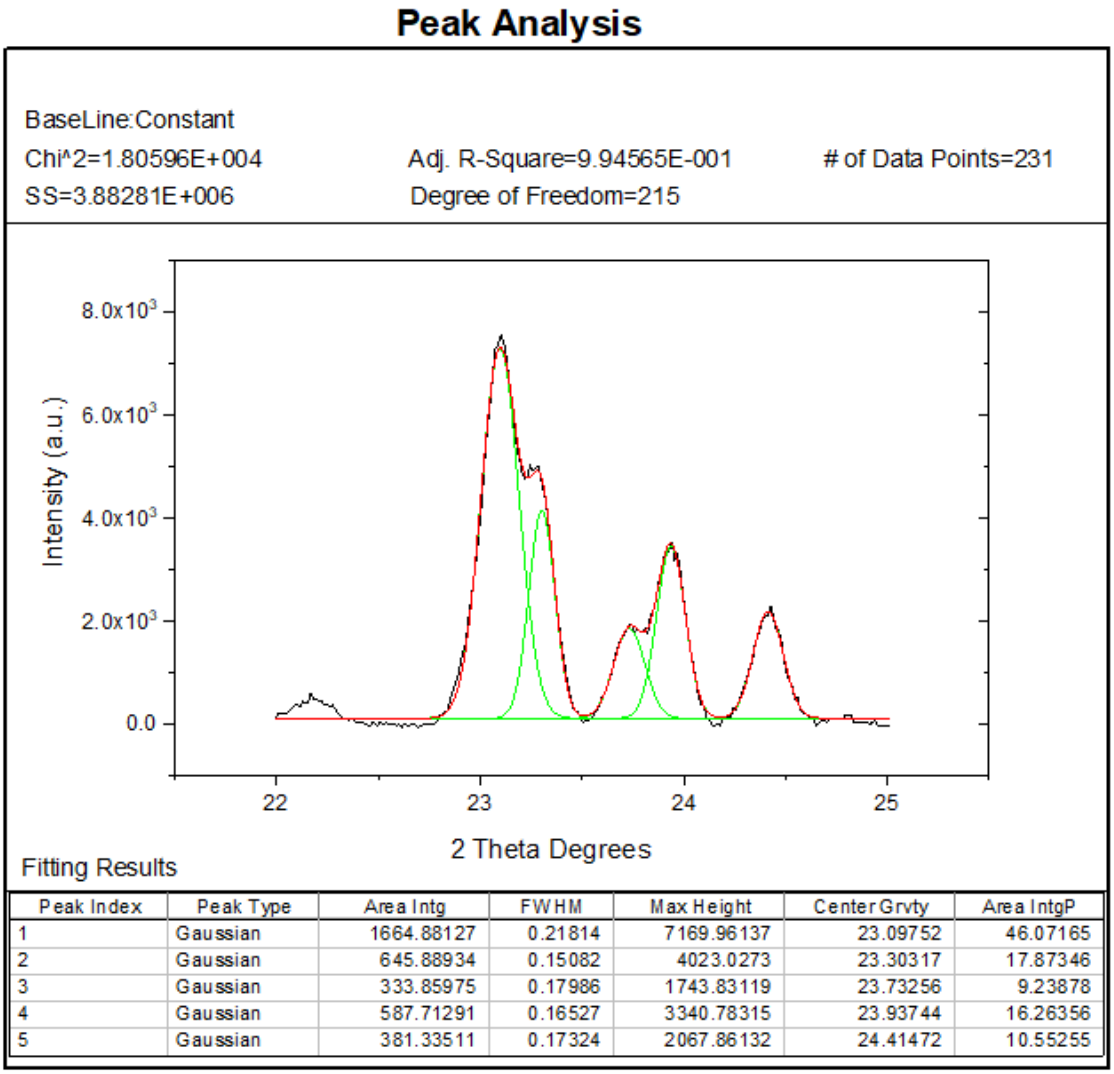

Fitting Results

Peak Index	Peak Type	Area Intg	FWHM	Max Height	Center Grvty	Area IntgP
1	Gaussian	1664.88127	0.21814	7169.96137	23.09752	46.07165
2	Gaussian	645.88934	0.15082	4023.0273	23.30317	17.87346
3	Gaussian	333.85975	0.17986	1743.83119	23.73256	9.23878
4	Gaussian	587.71291	0.16527	3340.78315	23.93744	16.26356
5	Gaussian	381.33511	0.17324	2067.86132	24.41472	10.55255

Figure 50. XRD peak analysis of hierarchical zeolite obtained by applying no template method (hydrothermal synthesis, calcined sample).

Characterizations of the template-free zeolite Y and mesoporogen-free hierarchical ZSM-5 showed that laser-assisted synthesis is applicable for the synthesis of other types of zeolites as well.

CHAPTER 5

CONCLUSION and FURTHER SUGGESTIONS

This thesis reports a novel synthesis mechanism of zeolites through femtosecond laser pulses. The interaction of ultrafast laser pulses with an optically transparent fluidic medium introduced by S. Ilday *et.al*[60,61] applied to the precursor suspensions used in the syntheses of TPA – Silicalite-1, nanosized microporous zeolite Y and hierarchical template-free ZSM-5. All these zeolites have been synthesized within much shorter time scales compared to the hydrothermal synthesis method. In general, reaction times are reduced from days to several hours.

The energy delivered by ultrafast laser pulses is absorbed by the precursor suspension used for zeolite synthesis, in the glass - liquid interface of the proposed reaction setup which is designed in the scope of this thesis. The ultrafast laser pulses drive the system to far from equilibrium through spatiotemporal gradient. The appropriate environment for zeolite synthesis, such as local high temperature and local high pressure (shock waves) is achieved. Each pulse delivers a precise amount of energy, which some portion of it is absorbed by the precursor suspension and spent for the formation of zeolite building blocks. The clusters formed by each laser pulse are distributed evenly to the full volume of the reaction suspension by the laser-induced flows and this phenomena reduces the induction period in zeolite synthesis significantly. The size distribution profile of zeolite crystals synthesized via the laser-assisted method is much uniform compared to conventional synthesis methods such as hydrothermal, microwave etc.

The synthesized TPA – Silicalite-1 zeolites are characterized through several characterization techniques. XRD powder patterns, SEM, HR-TEM images were obtained and compared to the same zeolites synthesized via the hydrothermal method. Striking advantages of the laser-assisted method are shortened reaction time (from 24 hours to ~5 hours), much uniform particle size distribution, and higher crystallinity relative to the sample synthesized via the hydrothermal method. BET analyses showed that available surface area for adsorption and pore size distribution values are similar to the sample synthesized via the hydrothermal method. For all characterization studies of TPA – Silicalite-1 synthesized via the laser-assisted method, results compared to literature examples of the same zeolite synthesized via hydrothermal method. The first observation from the comparison was an increase in the average particle size for the laser-assisted method when the same molar formulas were employed. Different molar formulas were used for the laser-assisted synthesis method to decrease average particle size and a similar phenomenon was observed; while average particle size decreased, particle sizes were bigger compared to the hydrothermal method. The second striking observation was the uniformity of synthesized particles in terms of size. Even synthesized particles are bigger for the laser-assisted method, they are much uniform in size compared to samples via the hydrothermal method. Scale-up trials for TPA – Silicalite-1 showed that if there is no linear correlation between the volume of precursor suspension and necessary reaction time to obtain zeolite with similar properties, i.e. if volume increased 5 times, reaction time increase ~2 times. For the next step of scale-up of the laser-assisted synthesis, multiple laser beams can be directed to several reaction bottles with the use of proper equipment. Crystallization kinetics of TPA – Silicalite-1 synthesized via laser-assisted method has been examined through XRD (crystallinity), HR-TEM and ATR-FTIR analyses, and Avrami index calculations. The

overall characterizations suggest that, in the growth stage, the non-classical pathway of zeolites, attachment of crystalline nanosized aggregates to crystal surface is dominated. The nucleation stage was analyzed through ATR-FTIR, where the evolution of zeolite building blocks starting from primary building units to 3-dimensional channels was observed.

The main characterization studies have been carried out for TPA – Silicalite-1 zeolite. The hydrothermal syntheses to obtain reference samples for characterization studies were prepared from same precursor suspensions to synthesize a zeolite via laser-assisted synthesis method. For comparison purposes, same volumes of precursor suspensions have been used for both conventional and newly developed methods. Further comparison in terms of energy efficiency can be done through wall-plug efficiencies. Lasers have considerably higher wall-plug efficiencies compared to conventional ovens, since an oven spend great part of the drawn electrical energy to stay at a desired temperature of the zeolite reaction. Considering also decreased reaction times through newly developed laser-assisted synthesis method of zeolites, which decrease reaction times almost in an order of magnitude (from 24 - 48 hours to 3-5 hours), the new method promise high energy efficiency as well.

The new laser-assisted synthesis method of zeolites has been tested on template-free nanosized template-free zeolite Y and mesoporogen-free hierarchical ZSM-5. Characterizations of them showed that laser-assisted synthesis is applicable for the synthesis of other types of zeolites as well.

There is an enormous number of potential applications for the newly developed laser-assisted method of zeolite synthesis. The precursor suspensions employed for the synthesis of zeolites in the current thesis were transparent to ensure multiphoton absorption. So, a greater number of transparent precursor suspensions can be employed

for the laser-assisted synthesis of other types of zeolites including the ones with high industrial importance. The precision assured by the laser pulses can be implemented on kinetic studies of other kind of zeolites. The developed method was successfully applied to the synthesis of template free zeolite Y, which demonstrated the potential of the laser-assisted method to be used in green zeolite syntheses.

REFERENCES

1. Vercaemst, C. Isomeric Olefinic Periodic Mesoporous Organosilicas : An Emerging Class of Versatile Nanomaterials. (Universiteit GENT, 2009).
2. Aurebach, S. M., Carrado, K. & Dutta, P. K. *Handbook of Zeolite Science and Technology*. (CRC Press, 2003).
3. Yu, J. & Xu, R. Insight into the construction of open-framework aluminophosphates. *Chem. Soc. Rev.* **35**, 593–604 (2006).
4. Moshoeshoe, M., Silas Nadiye-Tabbiruka, M. & Obuseng, V. A Review of the Chemistry, Structure, Properties and Applications of Zeolites. *Am. J. Mater. Sci.* **2017**, 196–221 (2017).
5. For IZA website please visit: http://www.iza-structure.org (2021).
6. Tosheva, L. & Valtchev, V. P. Nanozeolites: Synthesis, Crystallization Mechanism, and Applications. *Chem. Mater.* **17**, 2494–2513 (2005).
7. Koohsaryan, E. & Anbia, M. Nanosized and hierarchical zeolites: A short review. *Cuihua Xuebao/Chinese J. Catal.* **37**, 447–467 (2016).
8. Mintova, S., Gilson, J. P. & Valtchev, V. Advances in nanosized zeolites. *Nanoscale* **5**, (2013).
9. Mintova, S., Grand, J. & Valtchev, V. Nanosized zeolites: Quo Vadis? *Comptes Rendus Chim.* **19**, 183–191 (2016).
10. Wen, J., Dong, H. & Zeng, G. Application of zeolite in removing salinity/sodicity from wastewater: A review of mechanisms, challenges and opportunities. *J. Clean. Prod.* **197**, 1435–1446 (2018).
11. Lee, K. P., Arnot, T. C. & Mattia, D. A review of reverse osmosis membrane materials for desalination-Development to date and future potential. *J. Memb. Sci.* **370**, 1–22 (2011).
12. Caro, J., Noack, M., Kölsch, P. & Schäfer, R. Zeolite membranes - state of their development and perspective. *Microporous Mesoporous Mater.* **38**, 3–24 (2000).
13. Smith, J. V. (R.M.) Barrer. Zeolites and clay minerals as sorbents and molecular sieves. *Mineral. Mag.* **43**, 829–830 (1980).
14. Yilmaz, B. & Müller, U. Catalytic applications of zeolites in chemical industry. *Top. Catal.* **52**, 888–895 (2009).

15. Chidanand, Mittal, N. & Prasad, E. *Catalyst Market by Type (Zeolites, Metals, Chemical Compounds, Enzymes, and Organometallic Materials), Process (Recycling, Regeneration, and Rejuvenation), and Application (Petroleum Refining, Chemical Synthesis, Polymer Catalysis, and Environmental): Glo*. https://www.alliedmarketresearch.com/catalysts-market (2021).
16. Blatov, V. A., Ilyushin, G. D. & Proserpio, D. M. The zeolite conundrum: Why are there so many hypothetical zeolites and so few observed? A possible answer from the zeolite-type frameworks perceived as packings of tiles. *Chem. Mater.* **25**, 412–424 (2013).
17. Zhang, X. Q., Trinh, T. T., Van Santen, R. A. & Jansen, A. P. J. Mechanism of the initial stage of silicate oligomerization. *J. Am. Chem. Soc.* **133**, 6613–6625 (2011).
18. Kumar, S., Penn, R. L. & Tsapatsis, M. On the nucleation and crystallization of silicalite-1 from a dilute clear sol. *Microporous Mesoporous Mater.* **144**, 74–81 (2011).
19. Grand, J., Awala, H. & Mintova, S. Mechanism of zeolites crystal growth: New findings and open questions. *CrystEngComm* **18**, (2016).
20. Davis, M. E. Ordered porous materials for emerging applications. *Nature* **417**, 813–821 (2002).
21. Bacakova, L., Vandrovcova, M., Kopova, I. & Jirka, I. Applications of zeolites in biotechnology and medicine: A review. *Biomater. Sci.* **6**, 974–989 (2018).
22. Parlett, C. M. A., Wilson, K. & Lee, A. F. Hierarchical porous materials: Catalytic applications. *Chem. Soc. Rev.* **42**, 3876–3893 (2013).
23. Wang, Z., Yu, J. & Xu, R. Needs and trends in rational synthesis of zeolitic materials. *Chem. Soc. Rev.* **41**, 1729–1741 (2012).
24. Hedström, A. Ion Exchange of Ammonium in Zeolites: A Literature Review. *J. Environ. Engieering* **127**, (2001).
25. Li, J. R., Kuppler, R. J. & Zhou, H. C. Selective gas adsorption and separation in metal-organic frameworks. *Chem. Soc. Rev.* **38**, 1477–1504 (2009).
26. Horike, S., Shimomura, S. & Kitagawa, S. Soft porous crystals. *Nat. Chem.* **1**, 695–704 (2009).
27. Mintova, S., Jaber, M. & Valtchev, V. Nanosized microporous crystals: Emerging applications. *Chem. Soc. Rev.* **44**, 7207–7233 (2015).
28. Zhang, H. *et al.* Rational synthesis of Beta zeolite with improved quality by

decreasing crystallization temperature in organotemplate-free route. *Microporous Mesoporous Mater.* **180**, 123–129 (2013).

29. Li, Y., Sun, H., Wang, Y., Xu, B. & Yan, Z. Green routes for synthesis of zeolites. *Prog. Chem.* **27**, 503–510 (2015).
30. Warner, J. C. Green Chemistry and Innovation. *ACS Symp. Ser.* **1205**, 79–85 (2015).
31. Liu, B. *et al.* Synthesis of low-silica CHA zeolite chabazite in fluoride media without organic structural directing agents and zeolites. *Microporous Mesoporous Mater.* **196**, 270–276 (2014).
32. Mohamed, R. M., Aly, H. M., El-Shahat, M. F. & Ibrahim, I. A. Effect of the silica sources on the crystallinity of nanosized ZSM-5 zeolite. *Microporous Mesoporous Mater.* **79**, 7–12 (2005).
33. Cundy, C. S. & Cox, P. A. The hydrothermal synthesis of zeolites: Precursors, intermediates and reaction mechanism. *Microporous Mesoporous Mater.* **82**, 1–78 (2005).
34. Schoeman, B. J., Sterte, J. & Otterstedt, J. E. The Synthesis of Discrete Colloidal Zeolite Particles. *Stud. Surf. Sci. Catal.* **83**, 49–56 (1994).
35. Kirschhock, C. E. A., Feijen, E. J. P., Jacobs, P. A. & Martens, J. A. Hydrothermal Zeolite Synthesis. in *Handbook of Heterogenous Catalysis* (2008).
36. Zeng, X. *et al.* Microwave synthesis of zeolites and their related applications. *Microporous Mesoporous Mater.* **323**, 111262 (2021).
37. Khan, N. A. & Jhung, S. H. Synthesis of metal-organic frameworks (MOFs) with microwave or ultrasound: Rapid reaction, phase-selectivity, and size reduction. *Coord. Chem. Rev.* **285**, 11–23 (2015).
38. Slangen, P. M., Jansen, J. C. & Van Bekkum, H. MICROPOROUS MATERIALS ELSEVIER The effect of ageing on the microwave synthesis of zeolite NaA. *Microporous Mater.* **9**, 259–265 (1997).
39. Tsai, T., Shih, H., Liao, S. & Chao, K. Well-aligned SAPO-5 membrane : preparation and characterization 1. *Microporous Mesoporous Mater.* **22**, 333–341 (1998).
40. Nüchter, M., Ondruschka, B., Bonrath, W. & Gum, A. Microwave assisted synthesis – a critical technology overview. *Green Chem.* **6**, 128–141 (2004).
41. Tompsett, G. A., Conner, W. C. & Yngvesson, K. S. Microwave synthesis of

nanoporous materials. *ChemPhysChem* **7**, 296–319 (2006).

42. Motuzas, J. *et al.* Rapid synthesis of silicalite-1 seeds by microwave assisted hydrothermal treatment. *Microporous Mesoporous Mater.* **80**, 73–83 (2005).
43. Chen, X. *et al.* Morphology control of self-stacked silicalite-1 crystals using microwave-assisted solvothermal synthesis. *Microporous Mesoporous Mater.* **104**, 296–304 (2007).
44. Priecel, P. & Lopez-Sanchez, J. A. Advantages and Limitations of Microwave Reactors: From Chemical Synthesis to the Catalytic Valorization of Biobased Chemicals. *ACS Sustain. Chem. Eng.* **7**, 3–21 (2019).
45. Li, Y. & Yang, W. Microwave synthesis of zeolite membranes: A review. *J. Memb. Sci.* **316**, 3–17 (2008).
46. Rao, K. J., Vaidhyanathan, B., Ganguli, M. & Ramakrishnan, P. A. Synthesis of inorganic solids using microwaves. *Chem. Mater.* **11**, 882–895 (1999).
47. Madhusoodana, C. D., Das, R. N., Kameshima, Y. & Okada, K. Microwave-assisted hydrothermal synthesis of zeolite films on ceramic supports. *J. Mater. Sci.* **41**, 1481–1487 (2006).
48. Li, Y., Liu, J. & Yang, W. Formation mechanism of microwave synthesized LTA zeolite membranes. *J. Memb. Sci.* **281**, 646–657 (2006).
49. Parnham, E. R. & Morris, R. E. Ionothermal synthesis of zeolites, metal-organic frameworks, and inorganic-organic hybrids. *Acc. Chem. Res.* **40**, 1005–1013 (2007).
50. Askari, S., Miar Alipour, S., Halladj, R. & Davood Abadi Farahani, M. H. Effects of ultrasound on the synthesis of zeolites: A review. *J. Porous Mater.* **20**, 285–302 (2013).
51. Valtchev, V. P., Tosheva, L. & Bozhilov, K. N. Synthesis of zeolite nanocrystals at room temperature. *Langmuir* **21**, (2005).
52. Cheng, J. *et al.* A review of ultrafast laser materials micromachining. *Opt. Laser Technol.* **46**, 88–102 (2013).
53. Shugaev, M. V. *et al.* Fundamentals of ultrafast laser-material interaction. *MRS Bull.* **41**, 960–968 (2016).
54. Kerse, C. *et al.* Ablation-cooled material removal with ultrafast bursts of pulses. *Nature* **537**, 84–88 (2016).
55. Phillips, K. C., Gandhi, H. H., Mazur, E. & Sundaram, S. K. Ultrafast laser processing of materials: a review. *Adv. Opt. Photonics* **7**, 684 (2015).

56. Zhang, Y., Tzou, D. Y. & Chen, J. K. Micro-and nanoscale heat transfer in femtosecond laser processing of metals. *High-Power Femtosecond Lasers Prop. Mater. Appl.* 159–206 (2009).
57. Chowdhury, I. H. & Xu, X. Heat transfer in femtosecond laser processing of metal. *Numer. Heat Transf. Part A Appl.* **44**, 219–232 (2003).
58. Yu, J. *Synthesis of zeolites*. *Studies in Surface Science and Catalysis* vol. 168 (Elsevier B.V., 2007).
59. Ito, Y., Shinomoto, R., Otsu, A., Nagato, K. & Sugita, N. Dynamics of pressure waves during femtosecond laser processing of glass. *Opt. Express* **27**, 29158 (2019).
60. Ilday, S. *et al.* Rich complex behaviour of self-assembled nanoparticles far from equilibrium. *Nat. Commun.* **8**, (2017).
61. Makey, G. *et al.* Universality of dissipative self-assembly from quantum dots to human cells. *Nat. Phys.* **16**, 795–801 (2020).
62. Hedlund, J., Mintova, S. & Sterte, J. Controlling the preferred orientation in silicalite-1 films synthesized by seeding. *Microporous Mesoporous Mater.* **28**, 185–194 (1999).
63. Zhu, Y. *et al.* Highly chemoselective esterification for the synthesis of monobutyl itaconate catalyzed by hierarchical porous zeolites. *J. Catal.* **299**, 20–29 (2013).
64. Alda, J., Alda, J., Alda, J. & Alda, J. Encyclopedia of Optical Engineering. *Encycl. Opt. Eng.* (2011) doi:10.1081/e-eoe.
65. Mintova, S., Valtchev, V., Vultcheva, E. & Veleva, S. Crystallization kinetics of zeolite ZSM-5. *Zeolites* **12**, 210–215 (1992).
66. Rayalu, S., Udhoji, J., Meshram, S., Naidu, R. & Devotta, S. Estimation of crystallinity in flyash-based zeolite-A using XRD and IR spectroscopy. *Curr. Sci. Assoc.* **89**, 2147–2151 (2005).
67. Qi, J., Zhao, T., Xu, X., Li, F. & Sun, G. Hydrothermal synthesis of size-controlled silicalite-1 crystals. *J. Porous Mater.* **18**, 509–515 (2011).
68. Liang, D. *et al.* TEM observation of aggregation steps in room-temperature silicalite-1 zeolite formation. *J. Phys. Chem. C* **111**, 14283–14285 (2007).
69. Radoor, S., Karayil, J., Jayakumar, A., Parameswaranpillai, J. & Siengchin, S. Release of toxic methylene blue from water by mesoporous silicalite-1: characterization, kinetics and isotherm studies. *Appl. Water Sci.* **11**, 1–12

(2021).

70. Wang, B. *et al.* Cobalt oxide encapsulated hydrophilic hierarchical Silicalite-1 for highly efficient conversion of cyclohexyl hydroperoxide. *Microporous Mesoporous Mater.* **302**, 110186 (2020).
71. Groen, J. C., Peffer, L. A. A. & Pérez-Ramírez, J. Pore size determination in modified micro- and mesoporous materials. Pitfalls and limitations in gas adsorption data analysis. *Microporous Mesoporous Mater.* **60**, 1–17 (2003).
72. Bae, Y. S., Yazaydın, A. Ö. & Snurr, R. Q. Evaluation of the BET method for determining surface areas of MOFs and zeolites that contain Ultra-Micropores. *Langmuir* **26**, 5475–5483 (2010).
73. Ravishankar, R. *et al.* Physicochemical characterization of silicalite-1 nanophase material. *J. Phys. Chem. B* **102**, 2633–2639 (1998).
74. Thommes, M. *et al.* Physisorption of gases, with special reference to the evaluation of surface area and pore size distribution (IUPAC Technical Report). *Pure Appl. Chem.* **87**, 1051–1069 (2015).
75. Rezaei, E., Soltan, J. & Chen, N. Catalytic oxidation of toluene by ozone over alumina supported manganese oxides: Effect of catalyst loading. *Appl. Catal. B Environ.* **136**–**137**, 239–247 (2013).
76. Naik, S. P., Chiang, A. S. T., Thompson, R. W. & Huang, F. C. Formation of silicalite-1 hollow spheres by the self-assembly of nanocrystals. *Chem. Mater.* **15**, 787–792 (2003).
77. Malhis, A. A., Arar, S. H., Fayyad, M. K. & Hodali, H. A. Amino- and thiol-modified microporous silicalite-1 and mesoporous MCM-48 materials as potential effective adsorbents for Pb(II) in polluted aquatic systems. *Adsorpt. Sci. Technol.* **36**, 270–286 (2018).
78. Fujii, S. *et al.* Design of zeolite boiler in thermochemical energy storage and transport system utilizing unused heat from sugar mill. *Appl. Energy* **238**, 561–571 (2019).
79. Tokay, B., Somer, M., Erdem-Şenatalar, A., Schüth, F. & Thompson, R. W. Nanoparticle silicalite-1 crystallization from clear solutions: Nucleation. *Microporous Mesoporous Mater.* **118**, 143–151 (2009).
80. Mintova, S., Gilson, J. P. & Valtchev, V. Advances in nanosized zeolites. *Nanoscale* **5**, 6693–6703 (2013).
81. Lutz, W. Zeolite Y: Synthesis, Modification, and Properties—A Case

Revisited. *Adv. Mater. Sci. Eng.* **2014**, 20 (2014).

82. Mousavi, S. F., Jafari, M., Kazemimoghadam, M. & Mohammadi, T. Template free crystallization of zeolite Rho via Hydrothermal synthesis: Effects of synthesis time, synthesis temperature, water content and alkalinity. *Ceram. Int.* **39**, 7149–7158 (2013).
83. Grifoni, E. *et al.* Confinement effects and acid strength in zeolites. *Nat. Commun.* **12**, (2021).
84. Lupulescu, A. I. & Rimer, J. D. In situ imaging of silicalite-1 surface growth reveals the mechanism of crystallization. *Science (80-.).* **344**, 729–732 (2014).
85. Choudhary, M. K., Jain, R. & Rimer, J. D. In situ imaging of two-dimensional surface growth reveals the prevalence and role of defects in zeolite crystallization. *Proc. Natl. Acad. Sci. U. S. A.* **117**, 28632–28639 (2020).
86. Zhang, X. *et al.* Synthesis of self-pillared zeolite nanosheets by repetitive branching. *Science (80-.).* **336**, 1684–1687 (2012).
87. Lewis, D. W., Willock, D. J., Catlow, C. R. A., Thomas, J. M. & Hutchings, G. J. De novo design of structure-directing agents for the synthesis of microporous solids. *Nature* **382**, (1996).
88. Subotič, B., Bronic, J. & Antonic Jelic, T. *Theoretical and Practical Aspects of Zeolite Nucleation*. *Ordered Porous Solids* (2009). doi:10.1016/B978-0-444-53189-6.00006-8.
89. Grand, J., Awala, H. & Mintova, S. Mechanism of zeolites crystal growth: New findings and open questions. *CrystEngComm* **18**, 650–664 (2016).
90. Mintova, S., Olson, N. H., Valtchev, V. & Bein, T. Mechanism of zeolite a nanocrystal growth from colloids at room temperature. *Science (80-.).* **283**, 958–960 (1999).
91. Feng, G. *et al.* Accelerated crystallization of zeolites via hydroxyl free radicals. *Science (80-.).* **351**, 1188–1191 (2016).
92. Yeong, Y. F., Abdullah, A. Z., Ahmad, A. L. & Bhatia, S. Synthesis, structure and acid characteristics of partially crystalline silicalite-1 based materials. *Microporous Mesoporous Mater.* **123**, 129–139 (2009).
93. Kirschhock, C. E. A. *et al.* Identification of precursor species in the formation of MFI zeolite in the TPAOH-TEOS-H2O system. *J. Phys. Chem. B* **103**, 4965–4971 (1999).
94. Lesthaeghe, D. *et al.* MFI fingerprint: How pentasil-induced IR bands shift

during zeolite nanogrowth. *J. Phys. Chem. C* **112**, 9186–9191 (2008).

95. Mojet, B. L., Ebbesen, S. D. & Lefferts, L. Light at the interface: The potential of attenuated total reflection infrared spectroscopy for understanding heterogeneous catalysis in water. *Chem. Soc. Rev.* **39**, 4643–4655 (2010).
96. Shih, H. K., Chu, Y. L., Chang, F. C., Zhu, C. Y. & Kuo, S. W. A cross-linkable triphenylamine derivative as a hole injection/transporting material in organic light-emitting diodes. *Polym. Chem.* **6**, 6227–6237 (2015).
97. Patis, A., Dracopoulos, V. & Nikolakis, V. Investigation of silicalite-1 crystallization using attenuated total reflection/fourier transform infrared spectroscopy. *J. Phys. Chem. C* **111**, 17478–17484 (2007).
98. Fultz, B. & Howe, J. M. Diffraction Contrast in TEM Images. *Transm. Electron Microsc. Diffractometry Mater.* 339–422 (2002) doi:10.1007/978-3-662-04901-3_7.
99. Cubillas, P. & Anderson, M. W. *Synthesis Mechanism: Crystal Growth and Nucleation*. *Zeolites and Catalysis: Synthesis, Reactions and Applications* vol. 1 (2010).
100. Chaves Lima, R., Bieseki, L., Vinaches Melguizo, P. & Castellã Pergher, S. B. *Environmentally Friendly Zeolites*. (Springer, 2019). doi:10.1007/978-3-030-19970-8.
101. Chen, C. & Cheng, T. Application of avrami equation to kinetics analysis of fly ash based linde F (K) zeolite. *Asian J. Chem.* **25**, 1811–1813 (2013).
102. Heireche, L., Heireche, M. & Belhadji, M. Kinetic Study of Non-Isothermal Crystallization in $Se_{90-x}Zn_{10}Sb_x$ (x = 0, 2, 4, 6) Chalcogenide Glasses. *J. Cryst. Process Technol.* **04**, 111–120 (2014).
103. Awala, H. *et al.* Template-free nanosized faujasite-type zeolites. *Nat. Mater.* **14**, 447–451 (2015).
104. Travkina, O. S. *et al.* Template-free synthesis of high degree crystallinity zeolite y with micro-meso-macroporous structure. *RSC Adv.* **7**, 32581–32590 (2017).
105. Li, Q., Zhang, Y., Cao, Z., Gao, W. & Cui, L. Influence of synthesis parameters on the crystallinity and Si/Al ratio of NaY zeolite synthesized from kaolin. *Pet. Sci.* **7**, 403–409 (2010).

Appendices

Appendix A - Molarity and mass compositions for M2 and M3 molar formulas.

Batch Composition of M2 Molar Formula

25 SiO_2: 9 TPAOH: 480 H_2O: 100 EtOH

Table A1. Molar composition of reagents necessary to form TPA-Silicalite-1 zeolite synthesis (M2 molar formula).

	25 SiO_2	9 TPAOH	480 H_2O
25 TEOS	25 mol -25 mol		
9 (TPAOH · 44.92 H_2O)	0	9 TPAOH -9 TPAOH	480 H_2O -404.28
75.72 H_2O		0	75.72 -75.72
			0

Table A2. Mass composition of reagents necessary to form TPA-Silicalite-1 zeolite precursor suspension (M2 molar formula).

Compound formula	**# of moles**	**FW (g/mol)**	**Mass [a] (g)**	**Solution density (g/ml)**	**Volume [b] (ml)**	**Volume (%)**
TEOS	25	208.33	5208.25	0.94	5540.7	**34.84**
(TPAOH · 44.92 H_2O)	9	1011.92	9107.28	1.012 [c]	8999.29	**56.59**
H_2O	75.72	18	1362.96	1	1362.96	**8.57**

[a] Mass = Number of moles x FW

[b] Volume = Mass / density

[c] Solution density of 1M TPAOH

Table A3. Molarities of compounds in precursor solution for M2 molar formula.

Compound formula	Number of moles	MW (g/mol)	Mass (g) [a]	Molarity (mol/l solution) [b]
SiO_2	25	208.33	5208.25	**1.57**
TPAOH	9	203.36	1830.24	**0.57**
H_2O	75.72 + 404.28 = 480	18	26100	**30.2**

[a] Mass = Number of moles x MW

[b] Molarity = mole / liter of solution. The total volume of the solution is 15902.95 ml (Table A2).

Batch Composition of M3 Molar Formula

25 SiO_2: 9 TPAOH: 411 H_2O: 100 EtOH

Table A4. Mole composition of reagents necessary to form TPA-Silicalite-1 zeolite synthesis mixture (M3 molar formula).

	25 SiO_2	9 TPAOH	411 H_2O
25 TEOS	25 mol -25 mol		
9 (TPAOH · 44.92 H_2O)	0	9 TPAOH -9 TPAOH	411 H_2O -404.28
6.72 H_2O		0	6.72 -6.72
			0

Table A5. Mass composition of reagents necessary to form TPA-Silicalite-1 zeolite precursor suspension (M3 molar formula).

Compound formula	# of moles	FW (g/mol)	Mass [a] (g)	Solution density (g/ml)	Volume [b] (ml)	Volume (%)
TEOS	25	208.33	5208.25	0.94	5540.7	**37.79**
(TPAOH · 44.92 H_2O)	9	1011.92	9107.28	1.012 [c]	8999.29	**61.38**
H_2O	6.72	18	120.96	1	120.96	**0.83**

[a] Mass = Number of moles x FW

[b] Volume = Mass / density

[c] Solution density of 1M TPAOH

Table A6. Molarities of compounds in precursor solution for M3 molar formula.

Compound formula	Number of moles	MW (g/mol)	Mass (g) [a]	Molarity (mol/l solution) [b]
SiO_2	25	208.33	5208.25	**1.71**
TPAOH	9	203.36	1830.24	**0.61**
H_2O	6.72 + 404.28 = 411	18	7398	**28.03**

[a] Mass = Number of moles x MW

[b] Molarity = mole / liter of solution. The total volume of the solution is 14660.95 ml (Table A5).

Appendix B - Energy loss and absorption measurements to determine the portion of average laser power absorbed by precursor suspension for TPA – Silicalite-1 synthesis via the laser-assisted method

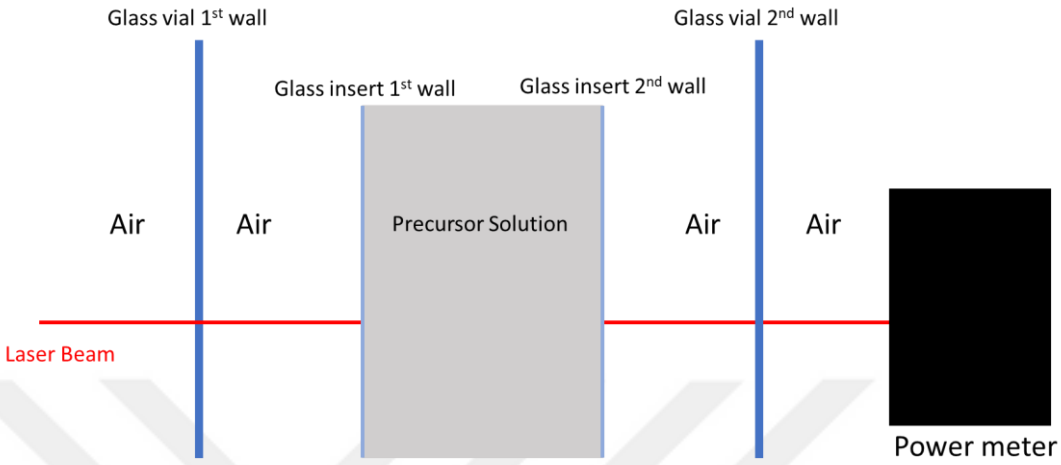

Figure B1. Schematic description of traveling laser beam through zeolite reaction bottle.

For such a system, power losses due to interfaces which beam passes through are calculated. To consider losses due to each interface, three different measurements were carried out. For all measurements, average laser power has been set to 5.3 W. This power value was measured at a point just before the laser beam hits the first wall of the glass vial (or glass insert for the second and third measurements). Then second power measurement was made just after the beam leaving second wall of the glass vial (or glass insert for the second and third measurements). For a system as described in Figure B1, unknowns are:

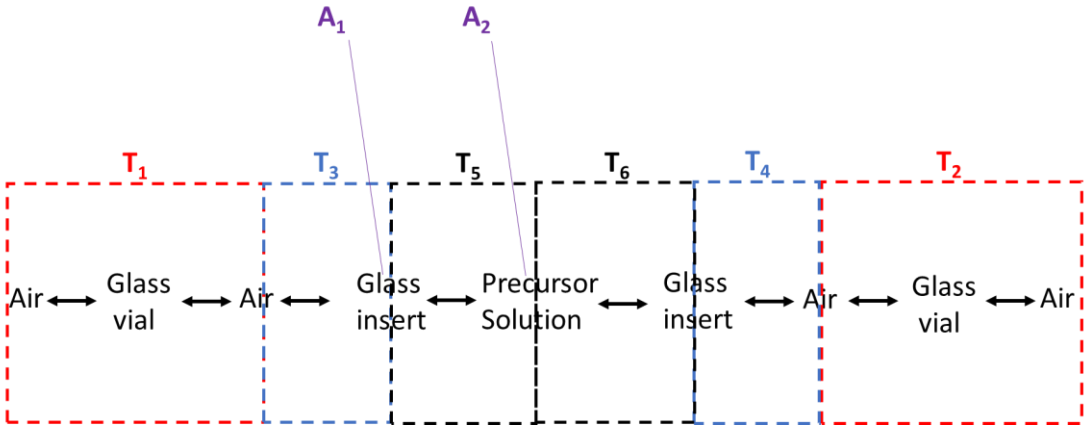

T_1 – (or T_2, they are identical) is the transmittance of light when passing from Air – Glass vial – Air interfaces; T_3 – (or T_4, they are identical) is the transmittance of light when passing from Air – Glass insert interface; T_5 – (or T_6, they are identical) is the transmittance of light when passing from Glass insert – Precursor Solution interface; A_1 – absorbed portion of laser light by 1st wall of glass insert; A_2 – absorbed portion of laser light by precursor suspension.

First measurement (to find T_1)

In the first measurement, a glass vial with no insert and no precursor solution was placed and power loss was measured (Figure B2).

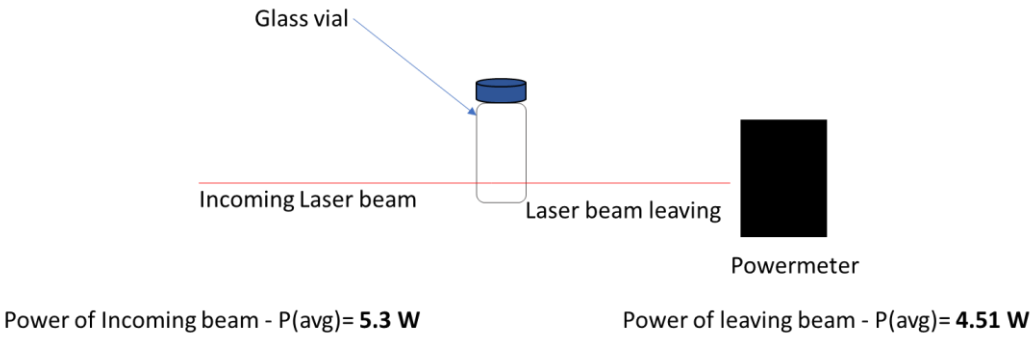

Figure B2. Schematic description of 1st measurement setup.

The recording of the power meter indicates that transmittance (T) for the 1st measurement is:

$$T = \frac{4.51\,W}{5.3W} = 0.851$$

Having a look at the travel path of the laser beam, we will see two identical sources of power loss which are Air – Glass vial – Air interfaces, I will denote them as T_1 and T_2 where $T_1 = T_2$:

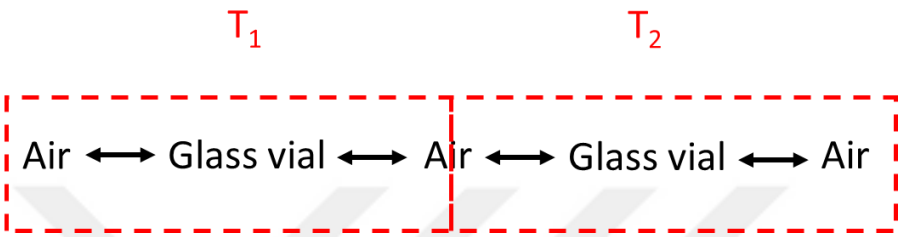

Then T_1 (or T_2) is found as:

$$5.3 \cdot (T_1) \cdot (T_2) = 4.51$$

$$T1 = \sqrt{\frac{4.51}{5.3}} = \sqrt{0.851} = 0.922$$

So, the loss due to Air – Glass vial – Air interfaces is **0.078** or **7.8%.**

Second measurement (to find T3 and A1)

For the second measurement, an empty glass insert with no precursor solution was placed in front of the beam (Figure B3).

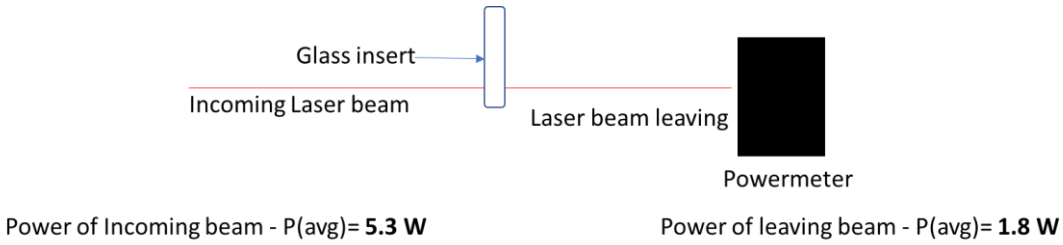

Figure B3. Schematic description of 2nd measurement setup.

The recording of the power meter indicates that transmittance (T) for the 2nd measurement is:

$$T = \frac{1.8\,W}{5.3W} = 0.34$$

Having a look at the travel path of the laser beam, we will see four identical sources of power loss which are Air – Glass insert interfaces. Transmittance from Air – Glass insert is denoted as T_3.

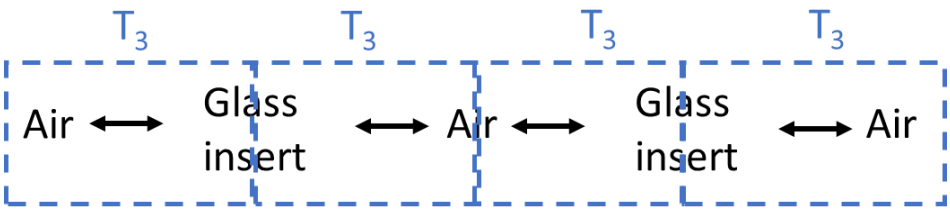

To find T_3, the Fresnel equation is used. Glass insert is made of chromatographic glass with a refractive index of 1.5 and refractive index of air is 1. Then reflectance of Air – Glass insert interface can be calculated from Fresnel's equation, assuming the angle of incidence to be 0, reflectance (R) equals:

$$R = \left|\frac{n_1 - n_2}{n_1 + n_2}\right|^2$$

$$R = \left|\frac{1.5 - 1}{1.5 + 1}\right|^2 = 0.04$$

Since R, Reflectance is equal to 1 – Transmittance, T3 equals 0.96. However, when putting this value and check the results of 2nd measurement, they don't comply with each other. If the power loss was due to reflectance of optical media, measured power would be:

$$5.3\ W\ \cdot T_3 \cdot T_3 \cdot T_3 \cdot T_3 = 4.5\ W$$

Measured power is 1.8 W. So, there is the absorption of laser light by glass insert. Including absorption by Glass insert into the calculation:

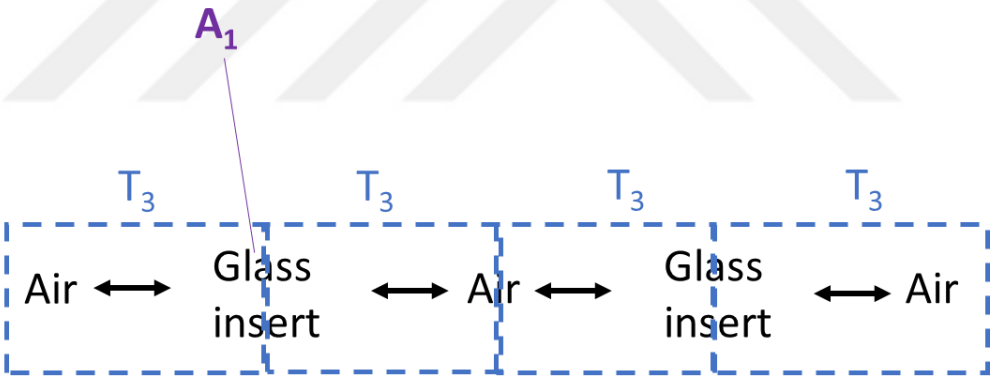

$$5.3\ W \cdot (1 - A_1) \cdot T_3 \cdot T_3 \cdot T_3 \cdot T_3 = 1.8\ W$$

$$A_1 = 0.6$$

So, the glass insert absorbs 60% of incident laser power and transmits only 40%.

Third measurement (to find T_5 and A_2)

This time, precursor solution to obtain zeolite was filled to glass insert, which is then irradiated by laser (Figure B4). Please note that incident power on the glass insert

was set to 5.3 W again, as it was the same for previous measurements. The measurement setup is provided below:

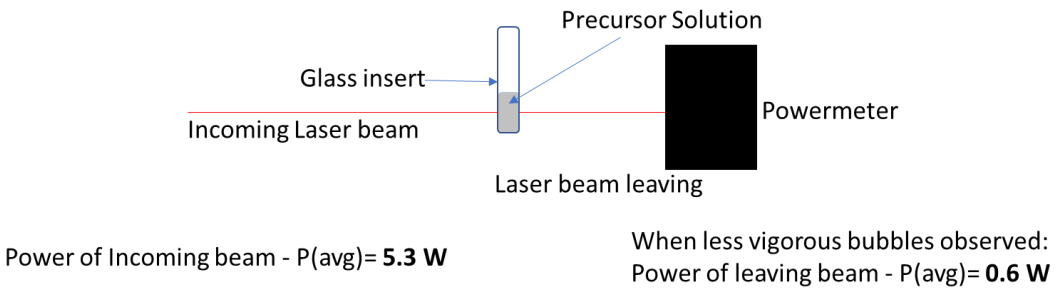

Figure B4. Schematic description of 3rd measurement setup.

From previous measurements, values of T_1 (T_2), T_3 (T_4) and A_1 are known. Unknowns left are T5 (T6) and A2, which are transmittance from Glass insert – Precursor Solution interface and Absorption by precursor solution.

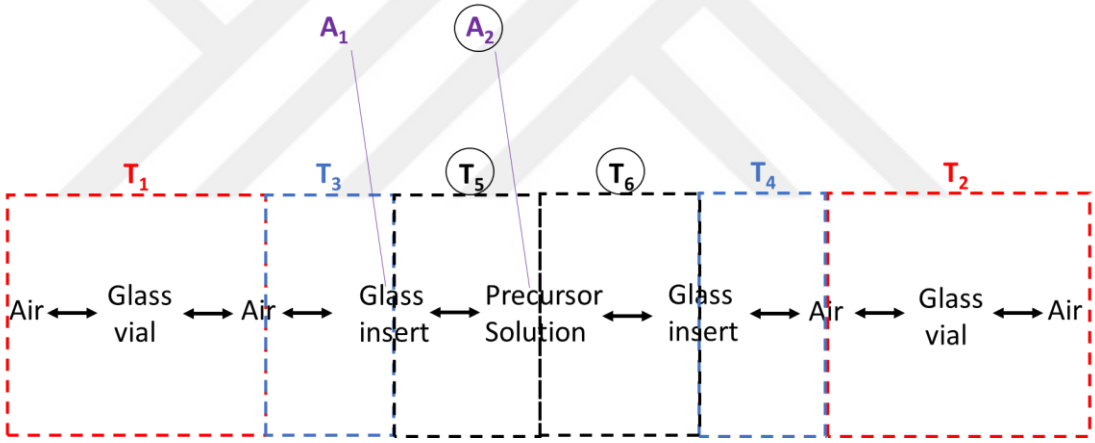

The average power of incident laser light is 5.3W. Until the beam reaches a power meter, some part of it is lost due to interfaces, and some part is absorbed by precursor suspension. To find an absorbed portion of laser power by precursor suspension, let's simplify the system to:

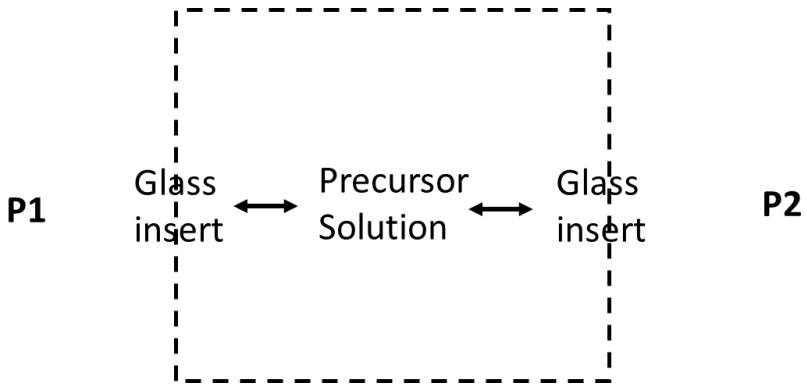

Where P_1 is average laser power just before glass insert – precursor solution interface, and P_2 is average laser power just after precursor solution – glass insert interface. So, P_1 and P_2 are:

$$P_1 = 5.3 \cdot 0.922 \cdot 0.96 \cdot 0.4 = 1.88\,W$$

$$P_2 = \frac{0.6}{0.922 \cdot 0.96} = 0.68\,W$$

Assuming refractive index of precursor solution similar to water (1.33) and glass insert to be 1.5, similar to common glass, power loss due to reflectance from glass insert – precursor solution interface can be calculated:

$$R = \left|\frac{n_1 - n_2}{n_1 + n_2}\right|^2$$

$$R = \left|\frac{1.5 - 1.33}{1.5 + 1.33}\right|^2 = 0.004$$

So, the portion of laser power that is lost due to the glass insert – precursor Solution interface is 0.004 (transmittance is 0.996). To find power absorbed by precursor suspension:

$$(P1 \cdot 0.996) - \frac{P2}{0.996} = Power\ absorbed\ by\ Precursor\ Solution$$

$$Power\ absorbed\ by\ Precursor\ Solution = 1.87 - 0.68 = 1.19\ W$$

$$\frac{1.19\ W}{5.3\ W} \cdot 100\% = 22.5\%$$

As a result, **22.5%** of the average laser power used on zeolite synthesis is absorbed by precursor solution.

Appendix C - Characteristic XRD peak areas of TPA – Silicalite-1 synthesized via the laser-assisted method with varying reaction times.

Table C1. Crystallinity calculations of TPA – Silicalite-1 synthesized via the laser-assisted method. 70_{Total}, 90_{Total}, 120-, 150-, 180 -, 200-, 220-, 240-, 260-,280- and 300 min indicate independent experiments with different laser treatment times. AVG and PA are the abbreviations of average and peak area, respectively. The sample synthesized via the hydrothermal method is taken as a reference for crystallinity calculations.

Peak No	**Bragg Angle**	**Peak Area**										
		70_{Total}*	**90_{Total}***	**120 min**	**150 min**	**180 min**	**200 min**	**220 min**	**240 min**	**260 min**	**280 min**	**300 min**
1	22.2	748.75	685.30	1087.29	953.69	1301.59	1289.98	1365.51	1338.91	1480.2	1438.37	1593.28
2	23.2	247.27	496.36	190.26	449.13	306.89	573.89	616.39	796.8	571.52	712.72	560.69
3	23.7	128.41	190.69	176.28	197.74	216.06	253.7	296.43	292.39	290.81	268.15	292.63
4	24.0	248.51	296.81	343.12	379.88	422.15	499.71	542.7	568.82	537.18	580.66	588.68
5	24.4	283.55	209.38	249.12	270.68	297.97	347.61	386.37	406.25	361.61	396.25	420.08
$\sum_{n=1}^{5} PA_{n,s}$		1656.49	1878.54	2046.07	2251.12	2544.66	2964.89	3207.4	3403.17	3241.32	3396.15	3455.36
Crystallinity (%)		**48**	**55**	**61**	**66**	**75**	**87**	**95**	**99**	**98**	**99**	**100**

***** - Because the yields of 70 min and 90 min reactions are too low (~ 0.3 mg), to collect enough amount (2 mg), 7 samples mixed per each.

Appendix D - TGA plots for TPA – Silicalite-1 synthesized via the laser-assisted method for the batch with M2 (Figure D1) and M3 (Figure D2) molar formulas, nanosized zeolite Y synthesized via hydrothermal (Figure D3), and laser-assisted (Figure D4) methods.

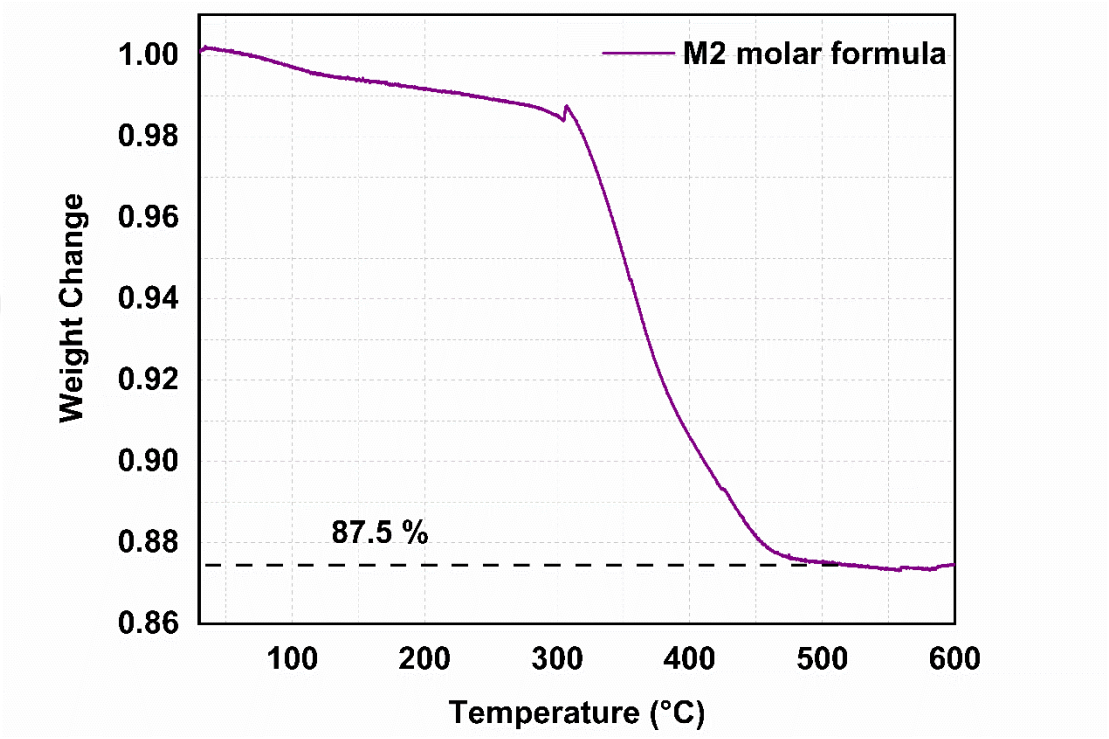

Figure D1. TGA plot of TPA – Silicalite-1 zeolite synthesized via the laser-assisted method for the batch with M2 molar formula.

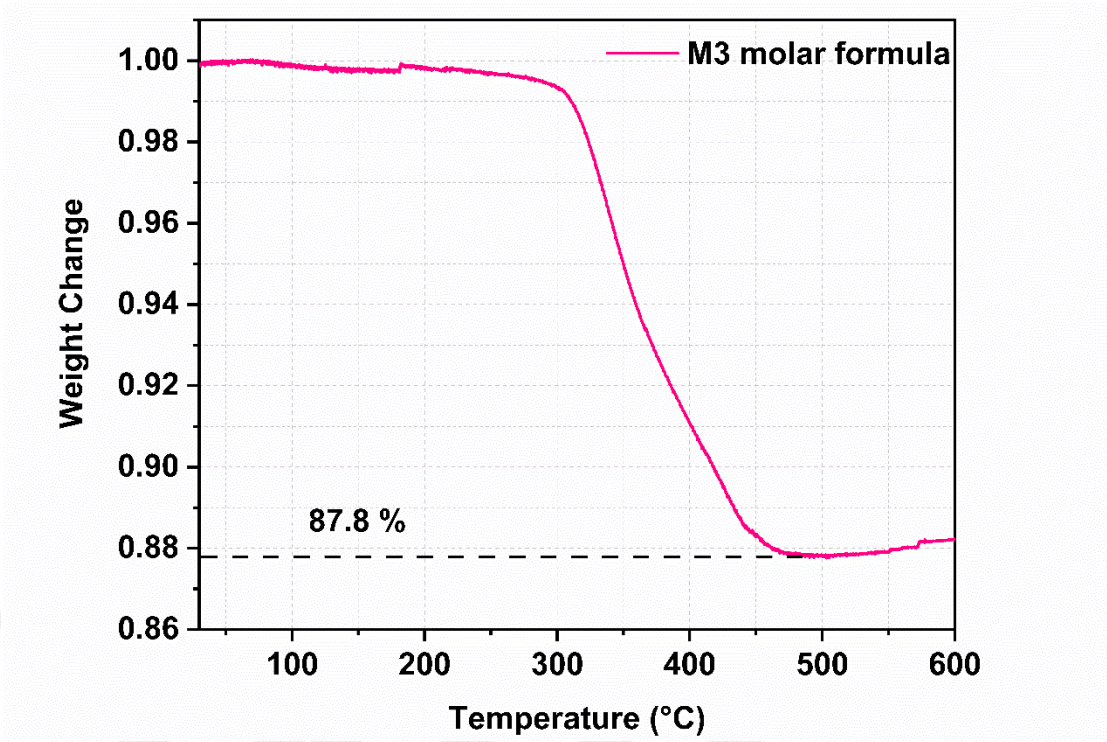

Figure D2. TGA plot of TPA – Silicalite-1 zeolite synthesized via the laser-assisted method for the batch with M3 molar formula.

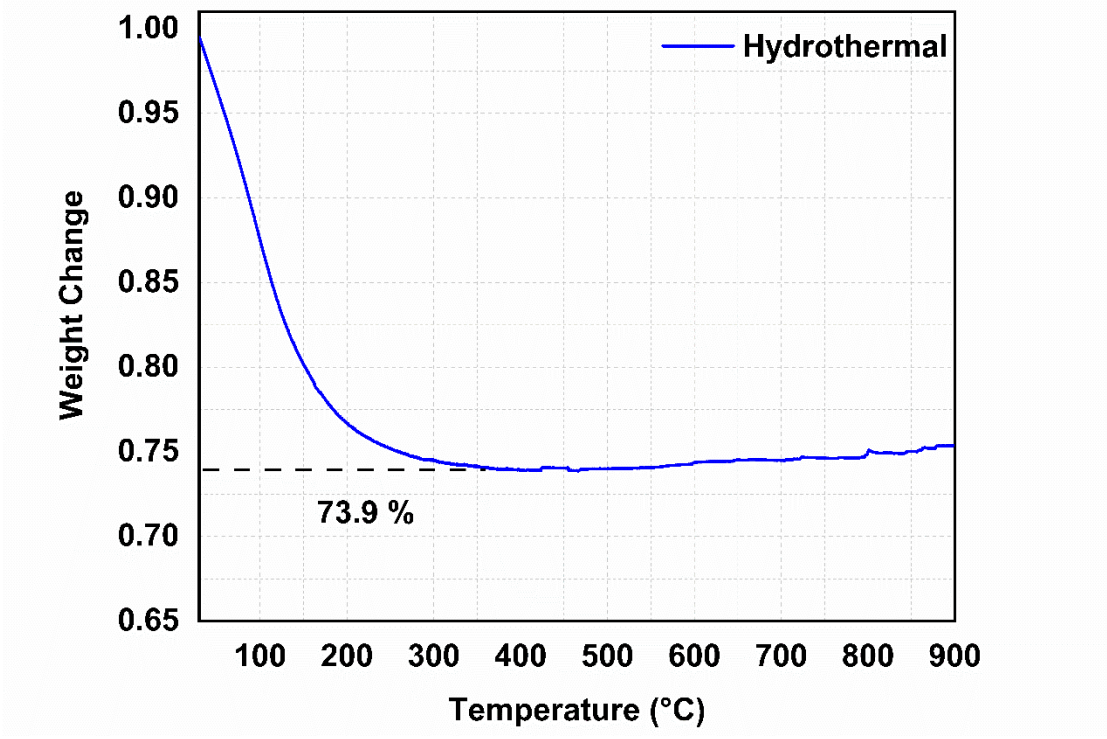

Figure D3. TGA plot of nanosized zeolite Y synthesized via hydrothermal method.

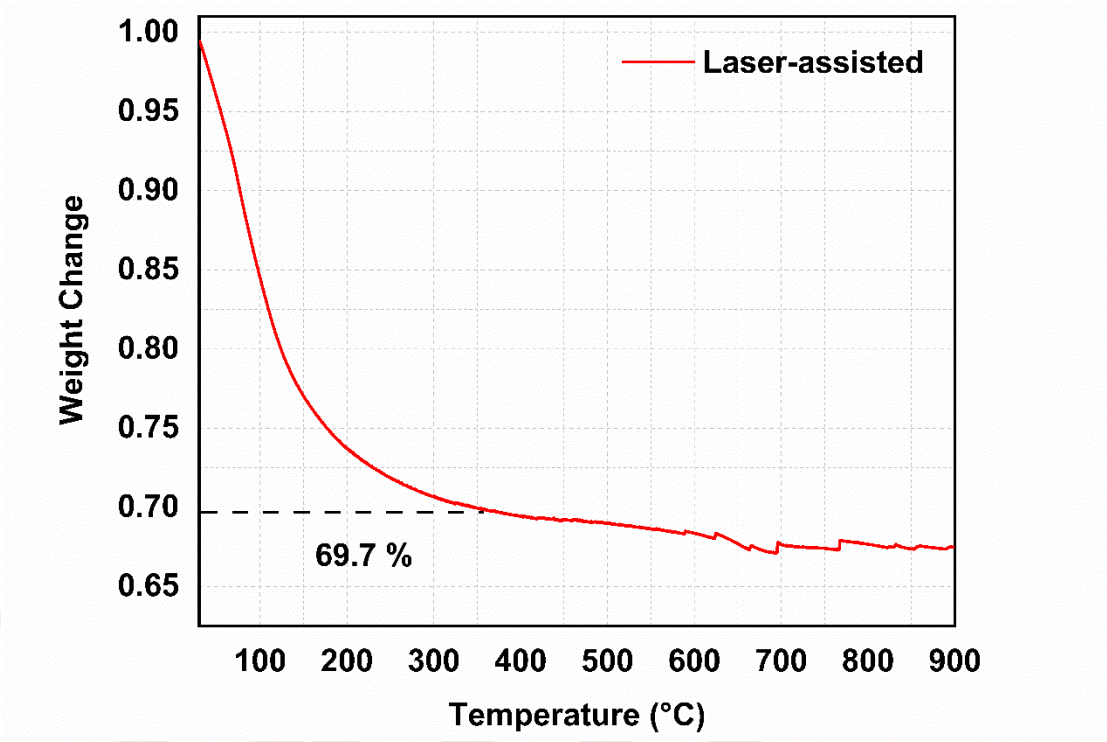

Figure D4. TGA plot of nanosized zeolite Y synthesized via the laser-assisted method

Appendix E - Energy Dispersive X-ray Spectroscopy (EDS) analysis of Silicalite-1 synthesized via the laser-assisted method

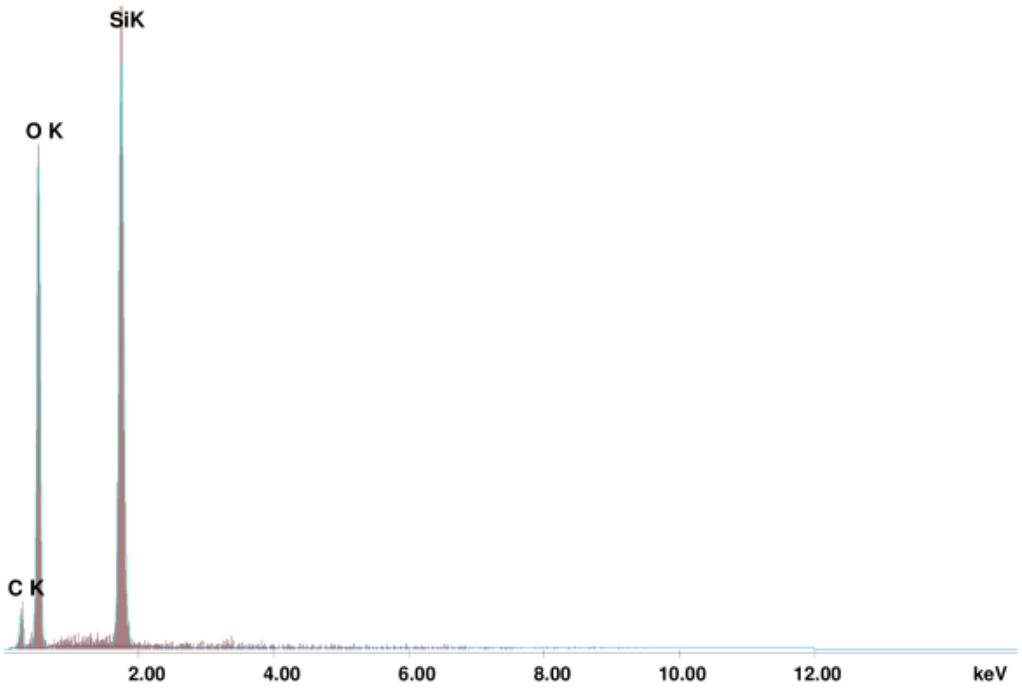

Weight % by Element

Filename	C K	O K	SiK
genspc.spc	12.17	46.21	41.62

Atomic % by Element

Filename	C K	O K	SiK
genspc.spc	18.82	53.66	27.52

K-Ratio

Filename	C K	O K	SiK
genspc.spc	0.0204	0.1874	0.3648

Figure E1. Energy Dispersive X-ray Spectroscopy (EDS) analysis for calcined Silicalite-1 zeolite synthesized via the laser-assisted method.